Unlocking the Benefits of Spaceborne Imaging Spectroscopy for Sustainable Agriculture

Dissertation zur Erlangung des Doktorgrades an der Fakultät für Geowissenschaften der Ludwig-Maximilians-Universität München

vorgelegt von

Matthias Wocher

eingereicht am 5. September 2022, München

Supervisor: PD Dr. Tobias Hank

2nd Supervisor: Prof. Dr. Wolfram Mauser

Day of the oral exam: 14. December 2022

Spruch mit kurzem o

ssso

- Ernst Jandl

ACKNOWLEDGEMENTS

While Munich held the European Championships 2022, I held my very own personal marathon, called *Thesis August 2022,* which probably was even far less thrilling and fortunately was not caught on camera although there were some highly emotional moments. As I write these last lines of this thesis, I think of many people who have accompanied me on this very exciting, varied, and sometimes challenging journey and without whom this thesis would not have been possible. First and foremost, I would like to express my deepest gratitude to my supervisor PD Dr. Tobias Hank. Thank you for always listening, your everlasting support, your driving passion for science, and your ever insightful and accurate view of the big picture.

I am also indebted to my co-supervisor Prof. Dr. Wolfram Mauser, who gave me the chance to work on this PhD in the first place and whom I would also deeply like to thank for unreservedly giving me the opportunity to be part of the teaching staff at the Department of Geography of the LMU Munich which I very much enjoy.

I would also like to sincerely thank the other members of the EnMAP Team Agriculture, especially Dr. Katja Berger, for her unstinting support, her expertise and cheerfulness, and her unmatched focus and skill to putting thoughts on paper. Special thanks are also to Dr. Martin Danner, my best possible PhD predecessor, for always sharing his Python coding skills in my early days and beyond, and for the great teamwork on developing the EnMAP-Box Agricultural Applications.

Further big thanks go to Dr. Jochem Verrelst for introducing me to the powerful ARTMO toolbox and the opportunity to come to Valencia, which was unfortunately cancelled at short notice due to the pandemic.

I further want to thank Jonas Meier for the close sharing of thoughts and all my other colleagues for inspiring discussions, balcony beers, even more beers on summer and Christmas parties, and for the pleasant working environment, to Andrea Ebner who patiently helped me with countless contracts and other bureaucratic matters.

Many thanks also to all the Hiwis who helped to steadily build up the now widely known Munich-North-Isar validation dataset during five years of field campaigns: to Marie P., Mona R., Alexander W., Lisa K., Manou H., Lukas G., Johannes H., Werner H., Christian M., Luzie S., Katharina W., Matthias S., Adrian J., Katharina A., Elin G., Stefanie W., Luis G., Marlis H., Miriam L., Markus S., Sarah M., Anja L., Joshua P., Stefanie S., Simon S., Tassilo H., Jana L., Ben H., Marco M., Karin G., Julian S., and Lukas B.

A warm thank you also belongs to Chico who largely maintained my physical well-being and kept my brain running (except when there was pasta but that's my fault).

To my family and friends for listening to absurd science topics and especially to my dear Sarah: thank you for always being there for me, even in hard times.

Summary

With the Environmental Mapping and Analysis Program (EnMAP) mission, launched on April 1st 2022, new opportunities unfold for precision farming and agricultural monitoring. The recurring acquisition of spectrometric imagery from space, contiguously resolving the electromagnetic spectrum in the optical domain (400—2500 nm) within close narrow bands, provides unprecedented data about the interaction of radiation with biophysical and biochemical crop constituents. These interactions manifest in spectral reflectance, carrying important information about crop status and health. This information may be incorporated in agricultural management systems to support necessary efforts to maximize yields against the backdrop of an increased food demand by a growing world population. At the same time, it enables the effective optimization of fertilization and pest control to minimize environmental impacts of agriculture.

Deriving biophysical and biochemical crop traits from hyperspectral reflectance thereby always relies on a model. These models are categorized into (1) parametric, (2) nonparametric, (3) physically-based, and (4) hybrid retrieval schemes. Parametric methods define an explicit parameterized expression, relating a number of spectral bands or derivates thereof with a crop trait of interest. Nonparametric methods comprise linear techniques, such as principal component analysis (PCA) which addresses collinearity issues between adjacent bands and enables compression of full spectral information into dimensionality reduced, maximal informative principal components (PCs). Nonparametric nonlinear methods, i.e., machine learning (ML) algorithms apply nonlinear transformations to imaging spectroscopy data and are therefore capable of capturing nonlinear relationships within the contained spectral features. Physically-based methods represent an umbrella term for radiative transfer models (RTMs) and related retrieval schemes, such as look-up-table (LUT) inversion. A simple, easily invertible and specific RTM is the Beer-Lambert law which may be used to directly infer plant water content. The most widely used general and invertible RTM is the one-dimensional canopy RTM PROSAIL, which is coupling the *Leaf Optical Properties Spectra* model PROSPECT and the canopy reflectance model 4SAIL: *Scattering by Arbitrarily Inclined Leaves*. Hybrid methods make use of synthetic data sets created by RTMs to calibrate parametric methods or to train nonparametric ML algorithms. Due to the ill-posed nature of RTM inversion, potentially unrealistic and redundant samples in a LUT need to be removed by either implementing physiological constraints or by applying active learning (AL) heuristics.

This cumulative thesis presents three different hybrid approaches, demonstrated within three scientific research papers, to derive agricultural relevant crop traits from spectrometric imagery.

In paper I the Beer-Lambert law is applied to directly infer the thickness of the optically active water layer (i.e., EWT) from the liquid water absorption feature at 970 nm. The

model is calibrated with 50,000 PROSPECT spectra and validated over *in situ* data. Due to separate water content measurements of leaves, stalks, and fruits during the Munich-North-Isar (MNI) campaigns, findings indicate that depending on the crop type and its structure, different parts of the canopy are observed with optical sensors. For winter wheat, correlation between measured and modelled water content was most promising for ears and leaves, reaching coefficients of determination (R^2) up to 0.72 and relative RMSE (rRMSE) of 26%, and in the case of corn for the leaf fraction only ($R^2 = 0.86$, rRMSE = 23%). These results led to the general recommendation to collect destructive area-based plant organ specific EWT measurements instead of the common practice to upscale leaf-based EWT measurements to canopy water content (CWC) by multiplication of the leaf area index (LAI). The developed and calibrated plant water retrieval (PWR) model proved to be transferable in space and time and is ready to be applied to upcoming EnMAP data and any other hyperspectral imagery.

In paper II the parametric concept of spectral integral ratios (SIR) is introduced to retrieve leaf chlorophyll a and b content (C_{ab}), leaf carotenoid content (C_{cx}) and leaf water content (C_w) simultaneously from imaging spectroscopy data in the wavelength range 460—1100 nm. The SIR concept is based on automatic separation of respective absorption features through local peak and intercept analysis between log-transformed reflectance and convex hulls. The approach was validated over a physiologically constrained PROSAIL simulated database, considering natural C_{cx}-C_{ab} relations and green peak locations. Validation on airborne spectrometric HyMAP data achieved satisfactory results for C_{ab} ($R^2 = 0.84$; RMSE = 9.06 µg cm^{-2}) and CWC ($R^2 = 0.70$; RMSE = 0.05 cm). Retrieved C_{cx} values were reasonable according to C_{ab}-C_{cx}-dependence plausibility analysis. Mapping of the SIR results as multiband images (3-segment SIR) allows for an intuitive visualization of dominant absorptions with respect to the three considered biochemical variables. Hence, the presented SIR algorithm allows for computationally efficient and RTM supported robust retrievals of the two most important vegetation pigments as well as of water content and is applicable on satellite imaging spectroscopy data.

In paper III a hybrid workflow is presented, combining RTM with ML for inferring crop carbon content (C_{area}) and aboveground dry and fresh biomass (AGB_{dry}, AGB_{fresh}). The concept involves the establishment of a PROSAIL training database, dimensionality reduction using PCA, optimization in the sampling domain using AL against the 4-year MNI campaign dataset, and training of Gaussian process regression (GPR) ML algorithms. Internal validation of the GPR-C_{area} and GPR-AGB models achieved R^2 of 0.80 for C_{area}, and R^2 of 0.80 and 0.71 for AGB_{dry} and AGB_{fresh}, respectively. Validation with an independent dataset, comprising airborne AVIRIS-NG imagery (spectrally resampled to EnMAP) and *in situ* measurements, successfully demonstrated mapping capabilities for both bare and green fields and generated reliable estimates over winter wheat fields at low associated model uncertainties (< 40%). Overall, the proposed carbon and biomass models

demonstrate a promising path toward the inference of these crucial variables over cultivated areas from upcoming spaceborne hyperspectral acquisitions, such as from EnMAP.

As conclusions, the following important findings arise regarding parametric and nonparametric hybrid methods as well as in view of the importance of *in situ* data collection.

(1) Uncertainties within the RTM PROSAIL should always be considered. A possible reduction of these uncertainties is thereby opposed to the invertibility of the model and its intended simplicity.

(2) Both physiological constraints and AL heuristics should be applied to reduce unrealistic parameter combinations in a PROSAIL calibration or training database.

(3) State-of-the-art hybrid ML approaches with the ability to provide uncertainty intervals are anticipated as most promising approach for solving inference problems from hyperspectral Earth observation data due to their synergistic use of RTMs and the high flexibility, accuracy and consistency of nonlinear nonparametric methods.

(4) Parametric hybrid approaches, due to their algorithmic transparency, enable deeper insights into fundamental physical limitations of optical remote sensing as compared to ML approaches.

(5) Integration-based indices that make full use of available hyperspectral information may serve as physics-aware dimensionality reduced input for ML algorithms to either improve estimations or to serve as endmember for crop type discrimination when additional time series information is available.

(6) The validation of quantitative model-based estimations is crucial to evaluate and improve their performance in terms of the underlying assumptions, model parameterizations, and input data.

(7) In the face of soon-to-be-available EnMAP data, collection of *in situ* data for validation of retrieval methods should aim at high variability of measured crop types, high temporal variability over the whole growing season, as well as include area- and biomass-based destructive measurements instead of LAI-upscaled leaf measurements.

Provided the perfect functionality of the payload instruments, the success of the EnMAP mission and the here presented methods depend critically on a low-noise, accurate atmospherically corrected reflectance product. High-level outputs of the retrieval methods presented in this thesis may be incorporated into agricultural decision support systems for fertilization and irrigation planning, yield estimation, or estimation of the soil carbon sequestration potential to enable a sustainable intensive agriculture in the future.

ZUSAMMENFASSUNG

Mit der am 1. April 2022 gestarteten Satellitenmission Environmental Mapping and Analysis Program (EnMAP) eröffnen sich neue Möglichkeiten für die Präzisionslandwirtschaft und das landwirtschaftliche Monitoring. Die wiederkehrende Erfassung spektrometrischer Bilder aus dem Weltraum, welche das elektromagnetische Spektrum im optischen Bereich (400—2500 nm) innerhalb von engen, schmalen Bändern zusammenhängend auflösen, liefert nie dagewesene Daten über die Interaktionen von Strahlung und biophysikalischen und biochemischen Pflanzenbestandteilen. Diese Wechselwirkungen manifestieren sich in der spektralen Reflektanz, die wichtige Informationen über den Zustand und die Gesundheit der Pflanzen enthält. Vor dem Hintergrund einer steigenden Nachfrage nach Nahrungsmitteln durch eine wachsende Weltbevölkerung können diese Informationen in landwirtschaftliche Managementsysteme einfließen, um eine notwendige Ertragsmaximierung zu unterstützen. Gleichzeitig können sie eine effiziente Optimierung der Düngung und Schädlingsbekämpfung ermöglichen, um die Umweltauswirkungen der Landwirtschaft zu minimieren.

Die Ableitung biophysikalischer und biochemischer Pflanzeneigenschaften aus hyperspektralen Reflektanzdaten ist dabei immer von einem Modell abhängig. Diese Modelle werden in (1) parametrische, (2) nichtparametrische, (3) physikalisch basierte und (4) hybride Ableitungsmethoden kategorisiert. Parametrische Methoden definieren einen expliziten parametrisierten Ausdruck, der eine Reihe von Spektralkanälen oder deren Ableitungen mit einem Pflanzenmerkmal von Interesse in Beziehung setzt. Nichtparametrische Methoden umfassen lineare Techniken wie die Hauptkomponentenanalyse (PCA). Diese adressieren Kollinearitätsprobleme zwischen benachbarten Kanälen und komprimieren die gesamte Spektralinformation in dimensionsreduzierte, maximal informative Hauptkomponenten (PCs). Nichtparametrische nichtlineare Methoden, d. h. Algorithmen des maschinellen Lernens (ML), wenden nichtlineare Transformationen auf bildgebende Spektroskopiedaten an und sind daher in der Lage, nichtlineare Beziehungen innerhalb der enthaltenen spektralen Merkmale zu erfassen. Physikalisch basierte Methoden sind ein Oberbegriff für Strahlungstransfermodelle (RTM) und damit verbundene Ableitungsschemata, d. h. Invertierungsverfahren wie z. B. die Invertierung mittels Look-up-Table (LUT). Ein einfaches, leicht invertierbares und spezifisches RTM stellt das Lambert-Beer'sche Gesetz dar, das zur direkten Ableitung des Wassergehalts von Pflanzen verwendet werden kann. Das am weitesten verbreitete, allgemeine und invertierbare RTM ist das eindimensionale Bestandsmodell PROSAIL, eine Kopplung des Blattmodells *Leaf Optical Properties Spectra* (PROSPECT) mit dem Bestandsreflexionsmodell 4SAIL (*Scattering by Arbitrarily Inclined Leaves*). Bei hybriden Methoden werden von RTMs generierte, synthetische Datenbanken entweder zur Kalibrierung parametrischer Methoden oder zum Training nichtparametrischer ML-Algorithmen verwendet. Aufgrund der Äquifinalitätsproblematik bei der RTM-Invertierung,

müssen potenziell unrealistische und redundante Simulationen in einer solchen Datenbank durch die Implementierung natürlicher physiologischer Beschränkungen oder durch die Anwendung von Active Learning (AL) Heuristiken entfernt werden.

In dieser kumulativen Dissertation werden drei verschiedene hybride Ansätze zur Ableitung landwirtschaftlich relevanter Pflanzenmerkmale aus spektrometrischen Bilddaten vorgestellt, die anhand von drei wissenschaftlichen Publikationen demonstriert werden.

In Paper I wird das Lambert-Beer'sche Gesetz angewandt, um die Dicke der optisch aktiven Wasserschicht (bzw. EWT) direkt aus dem Absorptionsmerkmal von flüssigem Wasser bei 970 nm abzuleiten. Das Modell wird mit 50.000 PROSPECT-Spektren kalibriert und anhand von In-situ-Daten validiert. Aufgrund separater Messungen des Wassergehalts von Blättern, Stängeln und Früchten während der München-Nord-Isar (MNI)-Kampagnen, zeigen die Ergebnisse, dass je nach Kulturart und -struktur, unterschiedliche Teile des Bestandes mit optischen Sensoren beobachtet werden können. Bei Winterweizen wurde die höchste Korrelation zwischen gemessenem und modelliertem Wassergehalt für Ähren und Blätter erzielt und sie erreichte Bestimmtheitsmaße (R^2) von bis zu 0,72 bei einem relativen RMSE (rRMSE) von 26%, bei Mais entsprechend nur für die Blattfraktion (R^2 = 0,86, rRMSE = 23%). Diese Ergebnisse führten zu der allgemeinen Empfehlung, Kompartiment-spezifische EWT-Bestandsmessungen zu erheben, anstatt der üblichen Praxis, blattbasierte EWT-Messungen durch Multiplikation mit dem Blattflächenindex (LAI) auf den Bestandswassergehalt (CWC) hochzurechnen. Das entwickelte und kalibrierte Modell zur Ableitung des Pflanzenwassergehalts (PWR) erwies sich als räumlich und zeitlich übertragbar und kann auf bald verfügbare EnMAP-Daten und andere hyperspektrale Bilddaten angewendet werden.

In Paper II wird das parametrische Konzept der spektralen Integralratios (SIR) eingeführt, um den Chlorophyll a- und b-Gehalt (C_{ab}), den Karotinoidgehalt (C_{cx}) und den Wassergehalt (C_w) simultan aus bildgebenden Spektroskopiedaten im Wellenlängenbereich 460-1100 nm zu ermitteln. Das SIR-Konzept basiert auf der automatischen Separierung der jeweiligen Absorptionsmerkmale durch lokale Maxima- und Schnittpunkt-Analyse zwischen log-transformierter Reflektanz und konvexen Hüllen. Der Ansatz wurde anhand einer physiologisch eingeschränkten PROSAIL-Datenbank unter Berücksichtigung natürlicher C_{cx}-C_{ab}-Beziehungen und Positionen der Maxima im grünen Wellenlängenbereich validiert. Die Validierung mit flugzeuggestützten spektrometrischen HyMAP-Daten ergab zufriedenstellende Ergebnisse für C_{ab} (R^2 = 0,84; RMSE = 9,06 µg cm^{-2}) und CWC (R^2 = 0,70; RMSE = 0,05 cm). Die ermittelten C_{cx}-Werte wurden anhand einer Plausibilitätsanalyse entsprechend der C_{ab}-C_{cx}-Abhängigkeit als sinnvoll bewertet. Die Darstellung der SIR-Ergebnisse als mehrkanalige Bilder (3-segment SIR) ermöglicht zudem eine auf die drei betrachteten biochemischen Variablen bezogene, intuitive Visualisierung der dominanten Absorptionen. Der vorgestellte SIR-Algorithmus ermöglicht somit wenig rechenintensive und RTM-gestützte robuste Ableitungen der beiden wichtigsten Pigmente

sowie des Wassergehalts und kann in auf jegliche zukünftig verfügbare Hyperspektraldaten angewendet werden.

In Paper III wird ein hybrider Ansatz vorgestellt, der RTM mit ML kombiniert, um den Kohlenstoffgehalt (C_{area}) sowie die oberirdische trockene und frische Biomasse (AGB_{dry}, AGB_{fresh}) abzuschätzen. Das Konzept umfasst die Erstellung einer PROSAIL-Trainingsdatenbank, die Dimensionsreduzierung mittels PCA, die Reduzierung der Stichprobenanzahl mittels AL anhand des vier Jahre umspannenden MNI-Kampagnendatensatzes und das Training von Gaussian Process Regression (GPR) ML-Algorithmen. Die interne Validierung der GPR-C_{area}- und GPR-AGB-Modelle ergab einen R^2 von 0,80 für C_{area} und einen R^2 von 0,80 bzw. 0,71 für AGB_{dry} und AGB_{fresh}. Die Validierung auf einem unabhängigen Datensatz, der flugzeuggestützte AVIRIS-NG-Bilder (spektral auf EnMAP umgerechnet) und In-situ-Messungen umfasste, zeigte erfolgreich die Kartierungsfähigkeiten sowohl für offene Böden als auch für grüne Felder und führte zu zuverlässigen Schätzungen auf Winterweizenfeldern bei geringen Modellunsicherheiten ($< 40\%$). Insgesamt zeigen die vorgeschlagenen Kohlenstoff- und Biomassemodelle einen vielversprechenden Ansatz auf, der zur Ableitung dieser wichtigen Variablen über Anbauflächen aus künftigen weltraumgestützten Hyperspektralaufnahmen wie jenen von EnMAP genutzt werden kann.

Als Schlussfolgerungen ergeben sich die folgenden wichtigen Erkenntnisse in Bezug auf parametrische und nichtparametrische Hybridmethoden sowie bezogen auf die Bedeutung der In-situ-Datenerfassung.

(1) Unsicherheiten innerhalb des RTM PROSAIL sollten immer berücksichtigt werden. Eine mögliche Verringerung dieser Unsicherheiten steht dabei der Invertierbarkeit des Modells und dessen beabsichtigter Einfachheit entgegen.

(2) Sowohl physiologische Einschränkungen als auch AL-Heuristiken sollten angewendet werden, um unrealistische Parameterkombinationen in einer PROSAIL-Kalibrierungs- oder Trainingsdatenbank zu reduzieren.

(3) Modernste ML-Ansätze mit der Fähigkeit, Unsicherheitsintervalle bereitzustellen, werden als vielversprechendster Ansatz für die Lösung von Inferenzproblemen aus hyperspektralen Erdbeobachtungsdaten aufgrund ihrer synergetischen Nutzung von RTMs und der hohen Flexibilität, Genauigkeit und Konsistenz nichtlinearer nichtparametrischer Methoden angesehen.

(4) Parametrische hybride Ansätze ermöglichen aufgrund ihrer algorithmischen Transparenz im Vergleich zu ML-Ansätzen tiefere Einblicke in die grundlegenden physikalischen Grenzen der optischen Fernerkundung.

(5) Integralbasierte Indizes, die die verfügbare hyperspektrale Information voll ausschöpfen, können als physikalisch-basierte dimensionsreduzierte Inputs für ML-Algorithmen dienen, um entweder Schätzungen zu verbessern oder um als Eingangsdaten die verbesserte Unterscheidung von Kulturpflanzen zu

ermöglichen, sobald zusätzliche Zeitreiheninformationen verfügbar sind.

(6) Die Validierung quantitativer modellbasierter Schätzungen ist von entscheidender Bedeutung für die Bewertung und Verbesserung ihrer Leistungsfähigkeit in Bezug auf die zugrunde liegenden Annahmen, Modellparametrisierungen und Eingabedaten.

(7) Angesichts der bald verfügbaren EnMAP-Daten sollte die Erhebung von In-situ-Daten zur Validierung von Ableitungsmethoden auf eine hohe Variabilität der gemessenen Pflanzentypen und eine hohe zeitliche Variabilität über die gesamte Vegetationsperiode abzielen sowie flächen- und biomassebasierte destruktive Messungen anstelle von LAI-skalierten Blattmessungen umfassen.

Unter der Voraussetzung, dass die Messinstrumente perfekt funktionieren, hängt der Erfolg der EnMAP-Mission und der hier vorgestellten Methoden entscheidend von einem rauscharmen, präzise atmosphärisch korrigierten Reflektanzprodukt ab. Die Ergebnisse der in dieser Arbeit vorgestellten Methoden können in landwirtschaftliche Entscheidungsunterstützungssysteme für die Dünge- oder Bewässerungsplanung, die Ertragsabschätzung oder die Schätzung des Potenzials der Kohlenstoffbindung im Boden integriert werden, um eine nachhaltige Intensivlandwirtschaft in der Zukunft zu ermöglichen.

Contents

List of Figures

List of Tables

List of Abbreviations

Abbreviation	Description
ARTMO	**A**utomated **R**adiative **T**ransfer **M**odel **O**perator
AGB	**A**bove**g**round **B**iomass
ANN	**A**rtificial **N**eural **N**etwork
ARD	**A**utomatic **R**elevance **D**etermination
ASI	**A**nalyze **S**pectral **I**ntegral
BRDF	**B**idirectional **R**eflectance **D**istribution **F**unction
CHIME	**C**opernicus **H**yperspectral **I**maging **M**ission for the **E**nvironment
DESIS	**D**LR **E**arth **S**ensing **I**maging **S**pectrometer
EBD	**E**uclidian-**b**ased **D**istance
ECV	**E**ssential **C**limate **V**ariable
EnMAP	**En**vironmental **M**apping and **A**nalysis **P**rogram
ESU	**E**lementary **S**ampling **U**nit
FAO	**F**ood and **A**griculture **O**rganization of the United Nations
FAST	**F**ourier **A**mplitude **S**ensitivity **T**est
FWHM	**F**ull-**W**idth-**H**alf-**M**aximum
GCOS	**G**lobal **C**limate **O**bserving **S**ystem
GPR	**G**aussian **P**rocess **R**egression
GSA	**G**lobal **S**ensitivity **A**nalysis
GSD	**G**round **S**ampling **D**istance
LIDF	**L**eaf **I**nclination **D**istribution **F**unction
LUT	**L**ook-**U**p-**T**able
ML	**M**achine **L**earning
MLRA	**M**achine **L**earning **R**egression **A**lgorithm
MNI	**M**unich-**N**orth-**I**sar (campaigns)
MSI	**M**ulti**S**pectral **I**nstrument
NDVI	**N**ormalized-**D**ifference-**V**egetation-**I**ndex
NDWI	**N**ormalized-**D**ifference-**W**ater-**I**ndex
NIR	**N**ear-**I**nfrared
PAL	**P**ool-**A**ctive **L**earning
PCA	**P**rincipal **C**omponent **A**nalysis
PCR	**P**rincipal **C**omponent **R**egression
PLS	**P**artial **L**east **S**quares
PLSR	**P**artial **L**east **S**quares **R**egression
PRISMA	**PR**ecursore **I**per**S**pettrale della **M**issione **A**pplicativa
PROSAIL	Coupling of PROSPECT and 4SAIL models
PROSPECT	leaf optical **PRO**perties **SPECT**ra (model)

PWR	**P**lant **W**ater **R**etrieval
REIP	**R**ed **E**dge **I**nflection **P**oint
RFR	**R**andom **F**orest **R**egression
RGB	**R**ed-**G**reen-**B**lue
RTM	**R**adiative **T**ransfer **M**odel
4SAIL	**S**cattering by **A**rbitrarily **I**nclined **L**eaves (model)
SBG	**S**urface **B**iology and **G**eology (mission)
SIR	**S**pectral **I**ntegral **R**atio
SNR	**S**ignal-to-**N**oise **R**atio
SVR	**S**upport **V**ector **R**egression
SWIR	**S**hort**W**ave **I**nfra-**R**ed
TOA	**T**op-**O**f-**A**tmosphere
TOC	**T**op-**O**f-**C**anopy
VIS	**VIS**ible light
VNIR	**V**isible to **N**ear-**I**nfra**R**ed
WI	**W**ater **I**ndex

List of Symbols

Symbol	Description	Unit
AGB	Aboveground Biomass	[g m^{-2}]
ALA	Average leaf angle	[deg]
C_{ab}	Chlorophyll a + b content	[µg cm^{-2}]
C_{anth}	Anthocyanin content	[µg cm^{-2}]
C_{area}	Area-based carbon content	[g m^{-2}]
CBC	Carbon-based constituents	[g cm^{-2}]
C_{brown}	Brown Pigments	[-]
C_{cx}	Carotenoid content	[µg cm^{-2}]
C_m	Dry matter content	[g cm^{-2}]
C_{mass}	Mass-based carbon concentration	[%]
C_p	Protein content	[g cm^{-2}]
C_w	Water content	[g cm^{-2}] or [cm]
CV	Coefficient of variation	[%]
CWC	Canopy water content	[g cm^{-2}] or [cm]
d	Path length	[cm]
EWT	Equivalent water thickness	[g cm^{-2}] or [cm]
FMC	Fuel moisture content	[%]
h_{spot}	Hotspot size parameter	[-]
LAI	Leaf Area Index	[m^2 m^{-2}]
N	Mesophyll structure parameter	[-]
OZA	Observer zenith angle	[deg]
p_{soil}	Soil brightness parameter	[-]
PWC	Plant water concentration	[%]
R^2	Coefficient of determination	[-]
rAA	Relative azimuth angle	[deg]
R'	d-dependent reflectance	[-]
R_0	Measured reflectance	[-]
RMSE	Root-mean-square-error	[input]
rRMSE	Relative root-mean-square-error	[%]
nRMSE	Normalized root-mean-square-error	[%]
SAC	Specific absorption coefficient	[cm^2 $µg^{-1}$]
S_{Ti}	FAST first-order sensitivity coefficient	[-]
SZA	Solar zenith angle	[deg]
VMR	Variance-to-mean-ratio	[-]
$\alpha(\lambda)$	Wavelength-dependent absorption coefficient	[cm^2 $µg^{-1}$]
Φ_0	Incident radiation intensity	[-]

1 Introduction

Agriculture in the 21st century faces a multitude of challenges that are linked to ongoing global changes and trends. With global population expected to reach 9.7 billion by 2050 (UN 2022), world food demand is estimated to increase by 30-62% according to a recent synthesis of earlier projections by van Dijk et al. (2021). Today, agricultural areas globally cover almost 40% of the terrestrial land surface, with one-third used as cropland, and two-thirds consisting of grasslands and pastures for grazing livestock (FAO 2021). While further cropland expansion among other implications reduces biodiversity and releases greenhouse gas emissions (Mauser et al. 2015), intensification is the preferred option to meet future demand and has also been the main driver of unprecedented yield gains since the 1960s (Burney et al. 2010). However, evidence is clear that a focused intensification approach based on the excessive use of fertilizers and pest control has negative effects on ecosystems and climate (Emmerson et al. 2016; Balafoutis et al. 2017; Carlson et al. 2017). Hence, along with impacts of climate change, unsustainable farming practices negatively affect primary means of agricultural production, i.e., environmental factors, characterized by soil fertility, water availability, temperature conditions (Hank et al. 2019), and biodiversity (FAO 2019). Consequently, the concept of sustainable intensification emerged as a major farming perspective, which is based on the idea to increase yields while at the same time minimize environmental impacts (Garnett et al. 2013). A cornerstone for a large-scale implementation of this principle is seen in other ongoing global trends: technological change and digitalization. Part of these trends is the concept of precision farming (Blackmore 1994) based on site-specific data, where all means of production are spatially optimized to increase yields on limited land while at the same time preventing emissions and environmental degradation (Hank et al. 2019). Key data provider for precision farming are remotely sensed measurements of the land surface using sensors on land vehicles, drones, airplanes, or satellites. The acquired information then contributes to a spatially customized crop demand-driven management of fertilization, irrigation, plant protection, seeding and harvesting (Mulla 2013). While the spatial coverage of sensing techniques from e.g., tractors and airborne measurements is limited to a small number of fields, satellite observations cover large areas within regular revisit times. Crop monitoring based on satellite remote sensing therefore is a rapidly growing field of interest both in terms of practical management applications (Erickson and Lowenberg-DeBoer 2021) and scientific literature (Weiss et al. 2020). In the past, this development has largely been driven by free of charge multispectral imagery (Hank et al. 2019) of the ESA Copernicus Sentinel-2 and the NASA Landsat Earth observation programs. With the launch of the hyperspectral Environmental Mapping and Analysis Program (EnMAP) (Guanter et al. 2015) mission on 1st April 2022 new possibilities unfold for agricultural monitoring. This thesis explains and demonstrates these new opportunities based on diverse novel physically-based approaches to derive crop traits from spaceborne imaging spectroscopy data.

1.1 Earth Observation for Agriculture

In the agricultural context, Earth observation primarily refers to measuring the reflected electromagnetic radiation of the terrestrial surface in the optical domain (400—2500 nm) from the visible (VIS, 400—700 nm) via the near-infrared (NIR, 700—1300 nm) to the shortwave infrared (SWIR, 1300—2500 nm) wavelength regions where light interactions with plant material predominantly occur (Knipling 1970). Agricultural relevant information about the state, dynamics and composition of crop traits is then inferred in a spatial way based on the relationship between wavelength-specific absorption characteristics of vegetation and spectral reflectance (Mauser et al. 2012). The crop traits of interest for agricultural monitoring comprise canopy biophysical variables (e.g., leaf area index, biomass, etc.) and biochemical variables (e.g., chlorophyll content, water content, etc.) on leaf and canopy level (Mariotto et al. 2013). To be useful for precision agricultural management practices, enabling accurate crop status mapping of within and between farm field variations (Cohen and Alchanatis 2018), the following criteria must be met: derived variables must be (1) described in physical units (Schaepman et al. 2005), the retrieval methods must be (2) generally applicable to diverse crop types (Kimes et al. 2000), must be (3) transferable to other locations and times (Verrelst et al. 2013b), and must come (4) at a reasonable computational effort to provide fast mapping speeds (Verrelst et al. 2019). Also, the derived information must be (5) directly observable in the spectral signal (Hank et al. 2019). Inferring biophysical and biochemical variables from Earth observation data thereby always relies on models, enabling the interpretation of measured reflectance and its translation into quantitative measures of a variable of interest (Verrelst et al. 2015b).

Since the advent of spaceborne Earth observation in the 1970s, satellites orbiting the globe were equipped with multispectral instruments, recording radiation in the optical domain within few broad discrete bands. For decades, quantitative estimations of crop traits from multispectral observations were mostly based on simple regression models established over *in situ* measurements and the broadband spectral information of single bands or combinations thereof. These statistical approaches primarily consisted of establishing a vegetation index (VI) between two or more bands to enhance features in reflectance sensitive to crop properties (Glenn et al. 2008). Although such models enabled the expression of results in physical units, they lack fundamental generic capacity and transferability (Verrelst et al. 2015b). Nonetheless, these indices are computationally feasible and thus desirable for a recurrent global coverage, as is available with today's public operational systems, e.g., Sentinel-2 and the Landsat series or with commercial systems, such as Planet's PlanetScope fleet or the DigitalGlobe satellites. Although the number of bands in multispectral systems gradually increased, measuring the full optical domain of the electromagnetic spectrum in a spatial way, continuously at a high spectral resolution (i.e., imaging spectroscopy) and signal-to-noise ratio (SNR) was long restricted to airborne instruments. This situation changed with recently launched imaging spectroscopy missions.

With the scientific precursors EnMAP and the Italian PRecursore Iper-Spettrale della Missione Applicativa (PRISMA) (Cogliati et al. 2021), launched on 22nd March 2019, today, two hyperspectral sensors circle the globe. Further operational missions are planned, such as the NASA Surface Biology and Geology (SBG) (National Academies of Sciences 2018) observing system and the ESA Copernicus Hyperspectral Mission for the Environment (CHIME) (Nieke and Rast 2019). These hyperspectral sensors cover the full optical domain within several hundred of narrow bands at a ground sampling distance (GSD) of 30 m. With the prerequisite of an accurate correction of atmospheric effects (Gao et al. 2009), these sensors are able to resolve fine absorption features of plant material at spectral sampling distances ≤ 10 nm.

The information added by the high spectral resolution is seen as a key to accurately estimate and quantify different type combinations of leaf pigments (e.g., chlorophyll a and b, carotenoids, and anthocyanins), plant water content, nitrogen and carbon content, as well as leaf area index (LAI), live and senescent biomass, dry matter content, and others (Ustin and Gamon 2010). The ability of a continuous monitoring of these variables over the whole growth cycle is critical for an effective and sustainable cropland management (Mariotto et al. 2013).

Particular importance in terms of the research of this thesis lies on the following variables: pigment contents provide important information about vegetation photosynthetic potential and activity (Chappelle et al. 1992) and the respective foliar compositions serve es indicators for numerous stresses (Berger et al. 2022). On the other hand, information on water content can be used for irrigation management (Ben-Gal et al. 2009) and crop ripening monitoring (Hank et al. 2019). Furthermore, information about the carbon stored in biomass can improve the knowledge about the potential of carbon farming, i.e. soil carbon sequestration methods as a negative emission strategy (Paustian et al. 2019). For this reason, above-ground biomass has also been defined as one of the Essential Climate Variables (ECV) by the Global Climate Observing System (GCOS 2022).

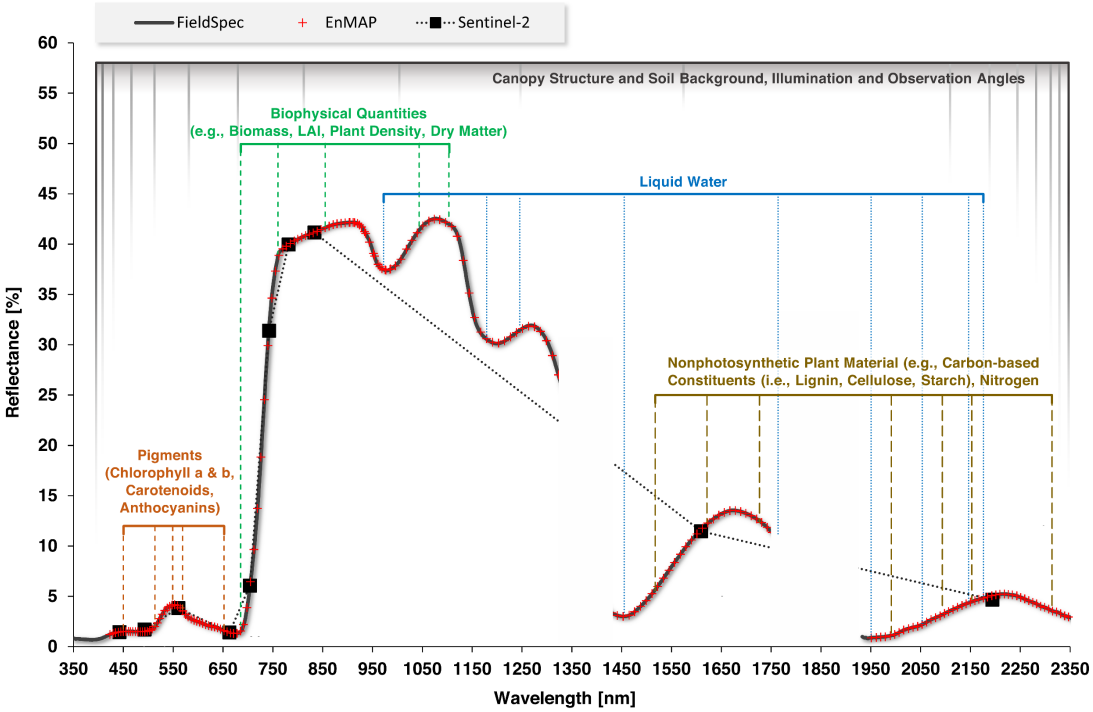

Figure 1.1: Canopy reflectance of vital green winter wheat (*triticum aestivum*) as observed by a field spectrometer @2150 bands (ASD FieldSpec 3 Jr; black line), broadband Sentinel-2 Multispectral Instrument @10 bands (black squares + dotted line) and EnMAP Hyperspectral Imager @242 bands (red crosses). Dominant absorption features of biophysical and biochemical variables are indicated as colored lines according to Thenkabail et al. (2013) and a PROSAIL canopy radiative transfer model (RTM) global sensitivity analysis (GSA). Figure modified after Hank et al. (2019).

The additional exploitable information provided by hyperspectral compared to multispectral remote sensing in the respective absorption regimes is illustrated in Figure 1.1. The importance of complete coverage of the NIR-SWIR absorption regions of liquid water, as well as carbon and nitrogen related absorption regions, should be emphasized. Hyperspectral, high SNR sensors that previously existed in orbit, such as the German DLR Earth Sensing Imaging Spectrometer (DESIS) (Krutz et al. 2018) only cover the VNIR region from 400 to 1000 nm. Figure 1.1 also indicates the apparent difficulty of deriving explicit variable quantities due to the superimposition of whole spectrum, canopy architecture related effects on reflectance, and multiple leaf constituent related absorption features.

Taking the sum of these issues into consideration, it always boils down to a model-based approach to exploit the abundant contained information in the spectrum and to accurately pinpoint the aimed variables. In the past, various approaches of different complexity were developed.

1.2 Hyperspectral Methods for Crop Traits Retrieval

In the following an overview of retrieval approaches for crop traits is given. Exemplary studies are referenced in view of their applicability in agricultural crop monitoring. Approaches to retrieve biochemical and biophysical vegetation traits from remotely sensed data were categorized by Verrelst et al. (2015b); (2019) into (1) parametric regression methods, (2) nonparametric regression methods, (3) physically-based methods, and (4) hybrid methods.

1.2.1 Parametric Regression Methods

Parametric regression methods define an explicit parameterized expression, relating a number of spectral bands or derivates thereof with a crop trait of interest (Verrelst et al. 2015b) in the form of a ratio, a normalized index or other linear equations. Due to its simplicity, the corresponding VI approach has been most widely applied, also to hyperspectral signatures which resulted in a multitude of indices published over the years (see e.g., Zeng et al. (2022) for an overview). Although optimized narrowband VIs may have an improved sensitivity to certain variables, the mentioned issues about generality and transferability remain. These drawbacks are based on the fact that interconnected nonlinear radiative processes between complex canopy architectures and diverse leaf physiologies cannot be uniformly addressed using simple linear mathematical formulations (Verrelst et al. 2019). As one consequence, VIs tend to saturate when leaf and canopy related absorption features superimpose. This, for instance, is the case in the red and NIR spectral regions between chlorophyll content and LAI, as well as leaf inclination with the widely applied Normalized Difference Vegetation Index (NDVI). Additionally, with respect to hyperspectral sampling, selecting only a few bands for the establishment of a VI underexploits the information density of contiguous spectral measurements (Atzberger et al. 2011). Addressing the latter, integration-based methods were proposed (Kokaly and Clark 1999). Integrating over certain areas in the reflectance spectrum allows to more extensively exploit distinct absorption feature spaces, as has been demonstrated for, e.g., leaf chlorophyll content estimations (Oppelt and Mauser 2004; Delegido et al. 2010). Further parametric regression methods include spectral transformation approaches such as continuum removal (Clark and Roush 1984), where reflectance is divided by, e.g., its convex hull, allowing for the analysis of absorption features from a common baseline (e.g., Mutanga et al. 2005), log-inversion of reflectance to mitigate saturation effects (Yoder and Pettigrew-Crosby 1995) and VIs from spectral derivates (e.g., Sims and Gamon 2002). Also direct informative wavebands have been introduced, such as the chlorophyll content related red edge inflection point (REIP) (e.g., Oppelt and Mauser 2004; Hank et al. 2021), inferred from the spectrum's second derivative (the reader is advised that an interactive tool, developed by the author to derive the REIP from hyperspectral data, is available within the open-source software EnMAP-Box 3 (van der Linden et al. 2015) 'Agricultural Applications'

(Appendix A.1)).

Although the continuous refinement of parametric methods often led to a higher information density in the resulting indices, due to limitations regarding transferability and general applicability (Atzberger et al. 2011), their informative value about crop status is of a qualitative nature. Nevertheless, results can be provided almost instantly without high computational requirements and the predictive capabilities of parametric methods can further be largely increased when physically-based approaches are used for calibration (see chapter 1.2.3).

1.2.2 Nonparametric Regression Methods

In recent years, a multitude of nonparametric regression methods have emerged that do not depend on an explicit parameterization. These models use weight factors (coefficients) which are calibrated in a learning process to minimize the prediction errors of the inferred variables (Verrelst et al. 2015b). They are able to digest full-spectrum information, rendering the need for an explicit band selection unnecessary. However, this brings with it the drawback of collinearity (Kumar 1975) or the "curse of dimensionality" (Hughes 1968), meaning that close adjacent narrow bands are highly intercorrelated, which may decrease model performance due to redundant data and possible noise (Verrelst et al. 2019). The issue of collinearity is often tackled using band selection techniques (e.g., Abdel-Rahman et al. 2013; Feilhauer et al. 2015; Verrelst et al. 2016b) or dimensionality reduction algorithms such as principal component analysis (PCA) (Jolliffe and Cadima 2016) or partial least squares (PLS) (Haaland and Thomas 1988). With PCA, reflectance spectra are compressed into principal components (PCs), each of which represents the direction and amount of maximum variance in an uncorrelated lower-dimensional feature space. Similarly, PLS applies dimensionality reduction with the difference that the reduction is supervised, meaning that it makes explicit use of target information (i.e., crop traits) during transformation. It should be noted that PCs are less interpretable since they are constructed as linear combinations of the input bands. Within related retrieval methods, these dimensionality reduction techniques are intrinsically embedded, such as in principal component regression (PCR) (Wold et al. 1987) where a linear regression is fitted over coefficients of the respective PCs, or in partial least squares regression (PLSR) (Geladi and Kowalski 1986), where it is fitted over the weight factors of the PLS components. Among others, PCR and PLSR are associated with the linear subcategory of nonparametric methods. PLSR outperformed PCR when used directly for crop traits retrieval (e.g., Atzberger et al. 2010; Wang et al. 2017a) since it inherently considers the aimed variable. This, however, does not render PCA irrelevant since it can be efficiently applied for dimensionality reduction of imaging spectroscopy data as a preprocessing step for the second subcategory of nonparametric retrieval methods: nonlinear methods.

Nonlinear nonparametric methods, commonly referred to as machine learning (ML) regression algorithms apply nonlinear transformations to imaging spectroscopy data and are

therefore capable of capturing nonlinear relationships within the contained spectral features (Verrelst et al. 2019). The most commonly used algorithms for biophysical and biochemical variables retrieval include decision tree algorithms, such as random forest regression (RFR) (Breiman 2001), artificial neural networks (ANNs) (Haykin 1998), and kernel-based methods, e.g., support vector regression (SVR) (Vapnik et al. 1996), and Gaussian process regression (GPR) (Rasmussen and Williams 2006). These advanced data-driven techniques make no assumptions about the data distribution and are therefore able to integrate data from different sources. To be able to discriminate subtle absorption features in spectrometric data, ML approaches depend on a model training process, which is computationally demanding and requires a vast amount of input data. Although many of these techniques date back to the 1990s, computation demand has been the main reason that application of these methods in hyperspectral Earth observation has only gained popularity in recent years. Moreover, the provision of sufficient training data that typically originates from *in situ* measurements is cost and labor intensive. Using simulated data for training hereby represents a promising alternative (see chapter 1.2.3). Another much discussed downside is that most ML approaches act as black boxes, since recognized patterns in the established models are grounded on a stochastic rather than a physical basis. Therefore, results lack interpretability in physical terms (Liang 2007). In order to bring light into the black box, one strategy is to incorporate ML algorithms themselves to select sensitive bands and later use this pre-selection to build a predictive model. While this approach cannot be followed with the pure black box of ANNs, RFR is inherently able to identify sensitive spectral bands (Abdel-Rahman et al. 2013; Feilhauer et al. 2015). This is also the case for GPR through extracting this knowledge from automatic relevance determination (ARD) kernels (Camps-Valls et al. 2016; Verrelst et al. 2016b; Berger et al. 2020a). However, selected sensitive bands across different methods and datasets are often ambiguous and miss to reflect the actual absorption coefficients of vegetation constituents (see e.g., Feilhauer et al. 2015). Another strategy is using algorithms that handle regression tasks in a Bayesian framework, such as GPR, providing analytical estimates of uncertainty intervals together with the final estimates due to its probabilistic handling of regression tasks. Analyzing these prediction intervals enables useful insights into uncertainties of model parameterization and input data. Moreover, information about uncertainties can be used to assess the transferability of the models to other locations and times (Verrelst et al., 2013a). Apart from the benefit of uncertainty intervals, GPR proved outstanding performances in hyperspectral regression problems (e.g., Verrelst et al. 2011; Camps-Valls et al. 2019; Berger et al. 2021b) and often outperformed other ML algorithms (Verrelst et al. 2012; Caicedo et al. 2014; Angel and McCabe 2022).

1.2.3 Physically-Based Methods

Physically-based (or mechanistic) methods represent an umbrella term for radiative transfer models (RTMs) and related retrieval, i.e., inversion schemes. RTMs

deterministically simulate the radiative transfer within a canopy from a description of its structure and the properties of its constituents using physical laws (Weiss et al. 2020). RTM inversion means simulating a spectrum that ideally matches a measured spectrum to draw conclusions about biophysical and biochemical variables from the underlying parameters of the simulation. Within the field of reflectance spectroscopy, many RTMs of different complexity have been developed, from one-dimensional turbid medium to 3-D ray-tracing representations of a plant canopy. With regard to applicability in crop traits retrieval, here, a trade-off decision has to be made: while 3-D models may be able to describe radiative transfer processes very close to reality, these models are considered noninvertible due to numerous parameters that are not measurable in the real world, leaving many parameters open for calibration. This in turn leads to an unacceptable number of degrees of freedom during the inversion of these models.

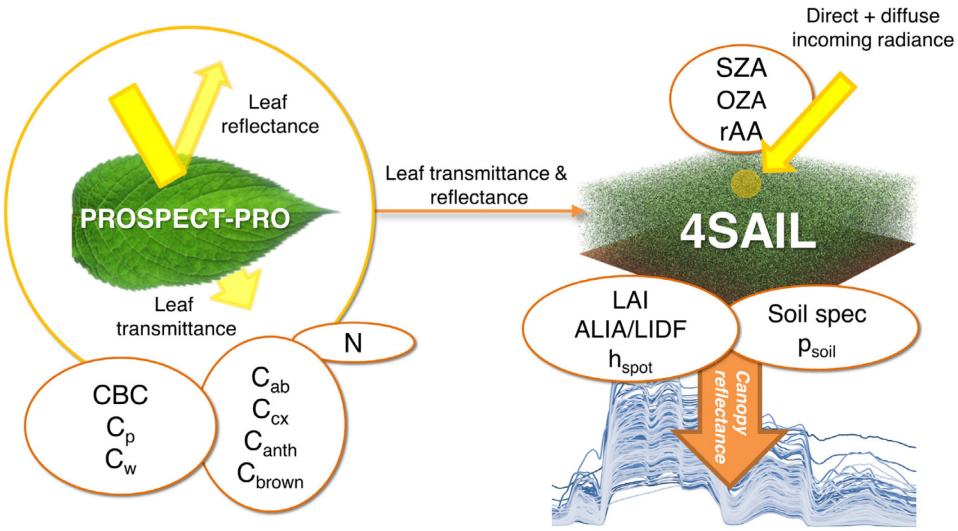

Figure 1.2: Flowchart and parameters of the PROSAIL RTM, coupling the latest version of the leaf RTM PROSPECT-PRO with the 1-D turbid medium canopy RTM 4SAIL. Figure modified after Berger et al. (2018a).

The most widely used invertible model is the 1-D turbid medium RTM PROSAIL (Jacquemoud et al. 2009) (Figure 1.2) which is coupling the constantly evolving *Leaf Optical Properties Spectra* model PROSPECT (Jacquemoud and Baret 1990; Féret et al. 2008; Féret et al. 2017; Féret et al. 2021) and the canopy reflectance model 4SAIL: *Scattering by Arbitrarily Inclined Leaves* (Verhoef and Bach 2007). The latest recalibrated version of the leaf RTM PROSPECT-PRO (Féret et al. 2021) simulates reflectance and transmittance of leaves in the optical domain as a function of leaf pigments, i.e. chlorophyll a and b (C_{ab}), carotenoids (C_{cx}), and anthocyanins (C_{anth}), a leaf mesophyll structure parameter (N), brown pigments (C_{brown}) and equivalent water thickness (EWT/C_w), as well as dry matter content (C_m) as the sum of nitrogen-containing proteins (C_p) and carbon-based constituents (CBC). For upscaling to the canopy level, 4SAIL simulates the bi-directional reflectance factor of a plant turbid medium (Jacquemoud et al. 2009) as a function of LAI, reflectance and

brightness factor (due to moisture) of the underlying soil (soil spec and p_{soil}), average leaf inclination angle (ALA) or optionally, ellipsoidal leaf inclination distribution (LIDF), and hot spot size (h_{spot}) for a given illumination and viewing geometry (observation zenith angle (OZA), relative azimuth angle (rAA) between sun and sensor, and the solar zenith angle (SZA)). Due to its comparatively limited number of parameters, PROSAIL has been successfully inverted by various studies (see review by Berger et al. 2018a) and also constitutes an essential foundation of the inversion schemes presented throughout this thesis.

To directly invert an RTM, the oldest strategy is the iterative approach of numerical optimization (Kimes et al. 2000), where the RTM is run multiple times, optimizing the input parameters until a simulated result best matches the measured spectrum according to a cost function. This approach, however, tends to get trapped in local minima and proved to be unsuitable for image processing, since optimizing a set of parameters to minimize a cost function for thousands of pixels is computationally infeasible even with the comparatively simple RTM PROSAIL. A second inversion strategy is the look-up-table (LUT) inversion (Kimes et al. 2000), where computational load is drastically reduced by selecting a best-fit-ensemble of spectra from a previously established and stored catalog of model runs.

Although these inversion techniques are considered physically sound, a major constraint lies in the ill-posed nature. This equifinality of model inversion means that many different parameter combinations may be equally valid in terms of their ability to reproduce a measured reflectance spectrum (Atzberger and Richter 2012). In addition, an inherent problem of LUTs consists of implausible spectra produced by unrealistic combinations of input parameters (Yebra and Chuvieco 2009; Jurdao et al. 2013; Wang et al. 2018). To establish a LUT, parameters are drawn within specified ranges and distributions based on measured ranges (Houborg et al. 2009) or *a priori* knowledge (Combal et al. 2003). However, this procedure always results in individual parameters being uncorrelated, thus contradicting observations of vegetation parameters in nature (e.g., LAI and EWT or C_{ab} and C_{cx}). Strategies to improve the sampling include the implementation of physiological constraints (e.g., Yebra and Chuvieco 2009; Jurdao et al. 2013) between biophysical and biochemical variables by implementing local boundary conditions during sample drawing based on *in situ* measured relationships. Another approach is using semi-supervised active learning (AL) heuristics (Settles 2009; Berger et al. 2021c), where a LUT is filtered to only include such spectra that add to an improved prediction capability of an inversion scheme.

To circumvent the equifinality problem, also simpler physically-based approaches, such as the Beer-Lambert law have been used to directly infer the path length through optically active water to derive leaf and canopy water content (e.g., Carter 1991; Bach 1995). With given wavelength-specific absorption coefficients of pure liquid water, the attenuation of the incident radiation thereby only depends on the path length through an optically active water

layer, which is described by EWT. However, due to its simplicity, robust and transferable retrieval models based on the Beer-Lambert law need to be calibrated. This in turn can be done within a hybrid retrieval scheme based on RTM-simulated LUTs.

1.2.4 Hybrid Methods

Hybrid methods, as defined by Verrelst et al. (2015b), describe the strategy of using an RTM-simulated database for the training of ML algorithms, combining the generic capacity of physically-based methods with the flexibility and computational efficiency of nonparametric nonlinear ML approaches. While early experimental hybrid approaches were already applied in the 1990s with the advent of ANNs (e.g., Baret et al. 1995), hybrid retrieval methods to derive crop traits from imaging spectroscopy data have only emerged several years later with combinations of PROSAIL and ML regression algorithms, such as with SVR (Durbha et al. 2007), RFR (Doktor et al. 2014), ANN (Fei et al. 2012), or GPR (Verrelst et al. 2016b; Verrelst et al. 2019). However, Rivera-Caicedo et al. (2017) indicated that the direct input of all 2100 available PROSAIL bands at continuous 1 nm sampling severely impairs the training of ML algorithms due to collinearity. Dimensionality reduction methods, such as PCA, can alleviate this issue while at the same time significantly boosting training time (Danner et al. 2021). The conversion of hyperspectral data into PCs, maximizing algorithmic interpretability while minimizing information loss, is particularly attractive for ML algorithms with a high computational load such as GPR with its time complexity of $\mathcal{O}(n^3)$ (Rasmussen and Williams 2006). Nonetheless, reduction in the spectral domain alone may not suffice in view of the huge number of potentially redundant samples generated by RTMs. Therefore, optimization in the sampling domain is required as well using e.g., AL approaches. Hybrid methods in which GPRs are trained over PCA-compressed and AL-optimized RTM-simulated databases recently achieved outstanding performances (e.g., Berger et al. 2021b; Candiani et al. 2022; Pascual-Venteo et al. 2022; Tagliabue et al. 2022) and may soon be considered state-of-the-art for agricultural mapping activities and beyond (Baker et al. 2018; Verrelst et al. 2019; Svendsen et al. 2020; Machwitz et al. 2021). However, implementing these algorithms in a processing chain requires vast expert and domain knowledge and many determining factors are still subject to some trial and error. These comprise e.g., the right number of selected PCs (Morata et al. 2021; Pascual-Venteo et al. 2022) and the choice of the GPR kernel function (Danner et al. 2021; Angel and McCabe 2022).

Therefore, similarly well-performing but simpler methods are still needed, particularly because transparent parametric approaches can provide easily accessible insights into possible fundamental physical limitations of any spectrum-related retrieval method. This can be effectively enabled when RTMs form the physical basis of a parametric approach. In this way, after calibration over an RTM-simulated LUT, these methods can be tested in the "real world", saving valuable *in situ* measurements for its true purpose, which is the validation of estimation results. Accordingly, Abdelbaki and Udelhoven (2022) recently

expanded the definition of hybrid methods to include RTM-calibrated parametric methods. This definition extension also provides a generally valid framework for the methods applied in the three papers of this thesis.

1.3 Thesis Outline

1.3.1 Research Questions

This thesis presents three different hybrid approaches that are categorized into (1) Beer-Lambert law physically-based, (2) parametric, and (3) nonparametric. Each makes use of the PROSPECT or PROSAIL RTMs for calibration or training. In this way, a general physical basis for all methods is established which is, however, only meaningful to the extent of how accurately the RTM is able to reproduce reality despite its simplicity. This ability thereby is not only related to the assumptions made within the model, but also largely to the sampling strategies applied to build the respective calibration or training databases. Although each of the presented retrieval approaches focuses on different crop traits, their individual estimation performance appears to be predetermined in view of their ability to differentiate superimposed nonlinear radiative processes in a canopy (nonparametric nonlinear > parametric linear). Furthermore, all methods were validated and checked for plausibility on various *in situ* datasets. These datasets show varying levels of differentiation in the temporal and spatial domains, as well as in the number of samples, sampled level (leaf or canopy), number of plant types, and growth stages. Thus, the characteristics of these data sets co-determine the quality of the estimations and directly influence the conclusions to be drawn.

With the theoretical background at hand and the above stated, the following overarching research questions are formulated:

- **Q1**: Are PROSAIL-simulated databases suitable for both training and calibration of retrieval algorithms and what are the main sources of uncertainty?

- **Q2**: Can RTM-calibrated parametric methods compete with nonparametric nonlinear ML approaches in terms of retrieval performance, and in view of general applicability and transferability?

- **Q3**: How meaningful is the validation of retrieval methods based on limited *in situ* measurements with varying levels of differentiation?

- **Q4**: What are the opportunities that arise for agricultural monitoring from the soon-to-be-available EnMAP data streams and which developments are to be expected regarding future imaging spectroscopy missions?

Within this thesis questions Q1—Q4 are discussed based on the versatility and results of the applied methods and their respective implications. They are based on the author's gained expertise regarding hyperspectral data processing and analysis as well as many years of field campaign work.

1.3.2 Publications

This cumulative thesis comprises three scientific publications which have all been published in peer-reviewed journals. In the following, these papers are listed chronologically with information about the publishing journal and its impact factor according to the Elsevier's abstract and citation database (Scopus). Furthermore, the respective authors' contributions are indicated in agreement with the Contributor Roles Taxonomy (CRediT). Each study is briefly introduced in an overview page, naming the respective research project frameworks and describing essential methods and results. Each paper deals with approaches to retrieve biophysical or biochemical variables from imaging spectroscopy data. All developed approaches are hybrid approaches, calibrated or trained over PROSPECT and/or PROSAIL simulated databases, validated over *in situ* measurements, and tested for generality and transferability in preparation of the EnMAP mission. An overview about hybrid retrieval methods is given in Figure 1.3., locating the methodological path of each study within the concept of hybrid retrieval schemes.

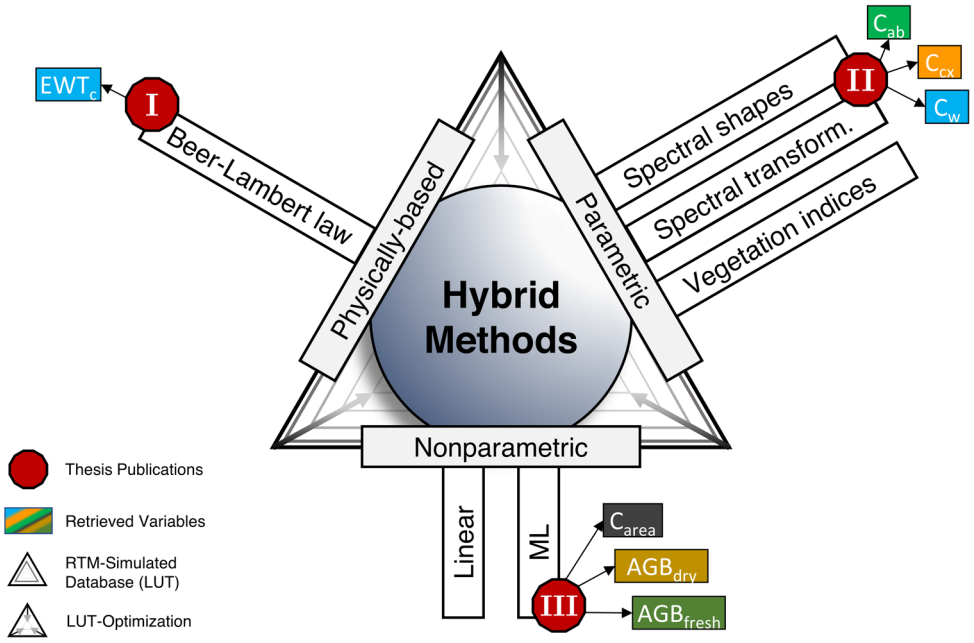

Figure 1.3: Localization of publications in the field of hybrid approaches based on RTM-simulated databases for the retrieval of crop traits from imaging spectroscopy data.

In Paper I, a recursive algorithm was developed to quantify canopy equivalent water thickness (EWT_{canopy}) by extracting the optically active water layer from the Beer-Lambert law using water absorption coefficients of pure liquid water. The model was calibrated over 50,000 PROSPECT simulations, no LUT-optimization technique was applied. Paper II

explored a parametric approach to simultaneously derive C_{ab}, C_{cx}, and C_w from continuous reflectance data using spectral integral ratios, calculated automatically by separating the respective absorption features using peak detection and convex hulls and calibrated using a physiological constrained LUT. Paper III turned to the world of ML. Here, three GPR models were trained over a PCA-reduced, AL-optimized RTM-simulated training database and tuned over the 4-year Munich-North-Isar (MNI) field campaign dataset to derive canopy carbon content (C_{area}) as well as dry and fresh aboveground biomass (AGB_{dry}, AGB_{fresh}). The algorithms developed within Paper I and II are openly accessible for the broad public as easy-to-use tools within the EnMAP-Box 3 Agricultural Applications, available as a plugin for QGIS.

Hence, this thesis presents robust and transferable retrieval methods to derive agricultural relevant crop traits from imaging spectroscopy data and can be applied to atmospherically corrected EnMAP data (and spectrometric imagery of other sensors) as soon as available.

2 Paper I: Physically-Based Retrieval of Canopy Equivalent Water Thickness Using Hyperspectral Data

This study has been published in the journal *Remote Sensing*:

Wocher, M., Berger, K., Danner, M., Mauser, W., & Hank, T. (2018). Physically-Based Retrieval of Canopy Equivalent Water Thickness Using Hyperspectral Data. *Remote Sensing*, 10, 1924. https://doi.org/10.3390/rs10121924.

Journal Impact Factor: 5.45 (2022)

Author Contributions: Conceptualization, M.W., K.B. and T.H.; Data curation, M.W.; Formal analysis, M.W. and K.B.; Funding acquisition, W.M. and T.H.; Investigation, M.W.; Methodology, M.W.; Project administration, W.M. and T.H.; Resources, M.W.; Software, M.W. and M.D.; Supervision, W.M. and T.H.; Validation, M.W. and K.B.; Visualization, M.W.; Writing—original draft, M.W.; Writing—review & editing, M.W., K.B., M.D. and T.H.

Transition to Paper I: Paper I focuses on the development of an algorithm to retrieve canopy water content from imaging spectroscopy data as was set out in the EnMAP Scientific Advisory Group (EnSAG) collaboration project 1.5: "retrieval of canopy liquid water content" between the EnMAP Team Agriculture at LMU and the GeoForschungsZentrum (GFZ) Potsdam during EnSAG Phase III: "Developing the EnMAP Managed Vegetation Scientific Processor". The algorithm presented in this paper served as a benchmark for the coupled retrieval of the three phases of water from simulated EnMAP top-of-atmosphere radiance spectra (Bohn et al. 2020). The novelty of the study lies in the direct inversion of the Beer-Lambert law to derive the thickness of the optically active water layer from measured reflectance at 970 nm using absorption coefficients of pure liquid water in a PROSPECT supported hybrid retrieval scheme. The study furthermore provided auxiliary information about radiation penetration depth into different canopy architectures based on *in situ* winter wheat (*triticum aestivum*) and corn (*zea mays*) water content measurements separated by leaves, stalks, and fruits which were collected during the MNI field campaigns. The developed 'Plant Water Retrieval' model is included as a slim tool within the EnMAP-Box Agricultural Applications (Appendix A.3) and can be applied to any atmospherically corrected spectrometric imagery.

Abstract

Quantitative equivalent water thickness on canopy level (EWT_{canopy}) is an important land surface variable and retrieving EWT_{canopy} from remote sensing has been targeted by many studies. However, the effect of radiative penetration into the canopy has not been fully understood. Therefore, in this study the Beer-Lambert law is applied to inversely determine water content information in the 930 to 1060 nm range of canopy reflectance from measured winter wheat and corn spectra collected in 2015, 2017, and 2018. The spectral model was calibrated using a look-up-table (LUT) of 50,000 PROSPECT spectra. Internal model validation was performed using two leaf optical properties datasets (LOPEX93 and ANGERS). Destructive in-situ measurements of water content were collected separately for leaves, stalks, and fruits. Correlation between measured and modelled water content was most promising for leaves and ears in case of wheat, reaching coefficients of determination (R^2) up to 0.72 and relative RMSE (rRMSE) of 26% and in case of corn for the leaf fraction only ($R^2 = 0.86$, rRMSE = 23%). These findings indicate that, depending on the crop type and its structure, different parts of the canopy are observed by optical sensors. The results from the Munich-North-Isar test sites indicated that plant compartment specific EWT_{canopy} allows us to deduce more information about the physical meaning of model results than from EWT on leaf level which is upscaled to canopy water content (CWC) by multiplication of the leaf area index (LAI). Therefore, it is suggested to collect EWT_{canopy} data and corresponding reflectance for different crop types over the entire growing cycle. Nevertheless, the calibrated model proved to be transferable in time and space and thus can be applied for fast and effective retrieval of EWT_{canopy} in the scope of future hyperspectral satellite missions.

2.1 Introduction

The quantification of water stored in agricultural plants plays an essential role in understanding the impact of cultivated areas on the earth's water cycle. Due to its close association to biochemical factors, such as vegetation transpiration (Running and Gower 1991) and net primary production (Running and Nemani 1991), the knowledge of quantities of water contained within agricultural crops is crucial, particularly for the development of environmental process models (Vohland 2008; Hank et al. 2015). Moreover, quantifying canopy water content is important in regards to the water use efficiency of plants (Clevers et al. 2010), evaluation of plant physiological status and health (Peñuelas et al. 1993; Peñuelas et al. 1997), and crop ripening monitoring (Hank et al. 2019).

Within the optical spectral domain (400 nm–2500 nm), absorption by vegetation liquid water occurs in the near-infrared (NIR) at 970 nm and 1200 nm and in the shortwave infrared (SWIR) at 1450 nm and 1950 nm (Tucker 1980; Danson et al. 1992). Due to a higher absorption coefficient in the SWIR (Kou et al. 1993) most of the early studies

combined those wavelengths with water insensitive wavelengths in the NIR to define empirical narrow-band indices for water content retrieval (Hardisky et al. 1983; Hunt et al. 1987; Hunt and Rock 1989; Gao 1996). However, the strong absorption by water may saturate those bands at high water contents in optically thick canopies (Datt 1999). Moreover, absorption by atmospheric water vapor at 1450 nm and 1900 nm results in noisy measurements which renders these spectral regions unsuitable for further analysis (Tucker 1980), both for top-of-atmosphere (TOA) and top-of-canopy (TOC) spectroscopy. Some vegetation biophysical variables may disturb the signal of water: for instance Jacquemoud et al. (2009) noted that the leaf area index (LAI) masks the water signal between 1000 nm and 1400 nm and advised caution when using such indices for water retrieval. The comparatively low 970 nm water absorption depth is embedded in an area of generally high vegetation reflectance in the NIR. Due to low absorption it is expected that radiation at 970 nm penetrates deeper into the canopy reflecting a larger portion of its total water content without a tendency to saturation (Newton and Blackman 1970; Lillesaeter 1982; Bull 1991; Sims and Gamon 2003; Ghulam et al. 2008). Therefore, Peñuelas et al. (1993; 1997) developed the 970 nm water index (WI) to retrieve relative plant water concentration (PWC). In the following, other studies also focused on the 970 nm absorption to estimate canopy water content (Clevers et al. 2008; Vohland 2008; Clevers et al. 2010; Cernicharo et al. 2013).

Methodologically, the definition of a narrow-band spectral index to retrieve vegetation water content information constitutes the parametric regression type of methods. Their simplicity and thus computational feasibility make them highly desirable for large-scale remote sensing applications. However, a fundamental problem of parametric regression methods is their lack of generality and transferability (Verrelst et al. 2015a). Since indices are not solely influenced by liquid water, but also affected by leaf internal structure and leaf dry matter (Ceccato et al. 2001) or canopy structure, LAI and soil background (Gao 1996; Zarco-Tejada et al. 2003; Yilmaz et al. 2008), the established regression-based relationships and estimated quantities of water stored in a canopy are limited to local conditions (Baret and Guyot 1991). Accordingly, the obtained results are site-, time- and crop-specific (Houborg et al. 2007). Moreover, as more hyperspectral image data with a continuous spectral coverage become accessible, the limited use of a small number of bands does not correspond to the up to date possibilities in view of the available data information density.

For the implications given, physically-based model inversion methods have been introduced as a promising alternative to retrieve biochemical and biophysical vegetation variables. Radiative transfer models (RTM) describe interactions between solar radiation and vegetation constituents using physical laws. Their ability to generate an infinite number of simulated spectra with known input parameters conversely allows their inversion in order to estimate the underlying parameters. For the inversion of RTMs, a variety of strategies have been applied. These include numerical optimization algorithms, look-up table (LUT)

approaches, artificial neural networks (ANN) and other machine learning algorithms (for an overview please refer to Verrelst et al. (2015a); (2019)). Although RTM-based inversion methods are considered to be physically sound, the techniques require profound knowledge, are often computationally demanding and are mathematically highly nonlinear (Jacquemoud et al. 2000; Verrelst et al. 2019). Another limitation of RTM-inversion is the ill-posed nature or equifinality of model inversion. Many different parameter sets may be equally valid in terms of their ability to reproduce a measured reflectance spectrum (for a discussion of this topic see Atzberger and Richter (2012)).

In view of future hyperspectral satellite missions like Italian PRISMA (Labate et al. 2009), US HyspIRI (Lee et al. 2015), Israeli-Italian SHALOM (Feingersh and Ben-Dor 2015), European CHIME (Nieke and Rast 2018b), and German EnMAP (Guanter et al. 2015) fast and efficient retrieval methods for large datasets are required. Mathematically simpler physically-based approaches have been applied before to circumvent the equifinality problem and to reduce the computational effort of RTM-based model inversion. Green*, et al.* (1991; 1993) originally incorporated the Beer-Lambert law to separate liquid water from atmospheric water vapor and determine both to allow the retrieval of surface reflectance from measured AVIRIS radiance. Thereby, the Beer-Lambert law was applied to directly infer the path length through optically active liquid water, i.e., the equivalent water thickness (EWT), from a measured reflectance spectrum using water absorption coefficients for pure liquid water (Ustin et al. 2012; Hunt et al. 2013). Since multiple NIR scattering, and the attendant increase in optical path length at both the leaf and the canopy scale are not accounted for in the simple Beer-Lambert law (Knipling 1970; Carter 1991), absolute quantification of EWT can only be achieved by calibration. Subsequently, validation has to be performed on accurate in-situ measurements. Studies that aimed at separating all three phases of water were not designed to quantify canopy water content in absolute terms and therefore accurate measurements were not carried out (Gao and Goetz 1990, 1995; Green et al. 2006; Thompson et al. 2015). On the other hand, studies which derived water content explicitly by applying the Beer-Lambert law often relied on the assumption that upscaling leaf EWT to canopy water content (CWC) could be done by a simple multiplication with the leaf area index (LAI) (see Clevers et al. 2008, 2010; Yi et al. 2014; Verrelst et al. 2015a; Pasqualotto et al. 2018). In other publications, biomass sampling strategies have not been designed to deduce the single water components of a canopy that an optical sensor can actually detect (e.g. Bach 1995; Ustin et al. 1998; Champagne et al. 2003; Sims and Gamon 2003). Consequently, validation of these approaches could not approve translation into transferable and generally applicable retrieval tools (Hunt et al. 2013).

Therefore, the objective of the present study was to test the performance of the Beer-Lambert law to retrieve crop water content from spectra with a contiguous spectral coverage around 970 nm and perform validation separately for leaves, stalks, and fruits by means of the two very different crop types: corn and winter wheat.

2.2 Materials

2.2.1 Munich-North-Isar Test Site

2.2.1.1 Biomass Sampling and Water Content Determination

Biomass collection was performed in 2015, 2017, and 2018 at three winter wheat fields (*triticum aestivum*) and two corn fields (*zea mays*) of communal farmland 30 km north of Munich (southern Germany) east of the river Isar (Table 2.1, Figure 2.1).

Within the fields, three different sampling points were selected based on long-term biomass distribution pattern observations (TalkingFields Base Map: www.talkingfields.de) representing low, medium, and high persistent relative fertility.

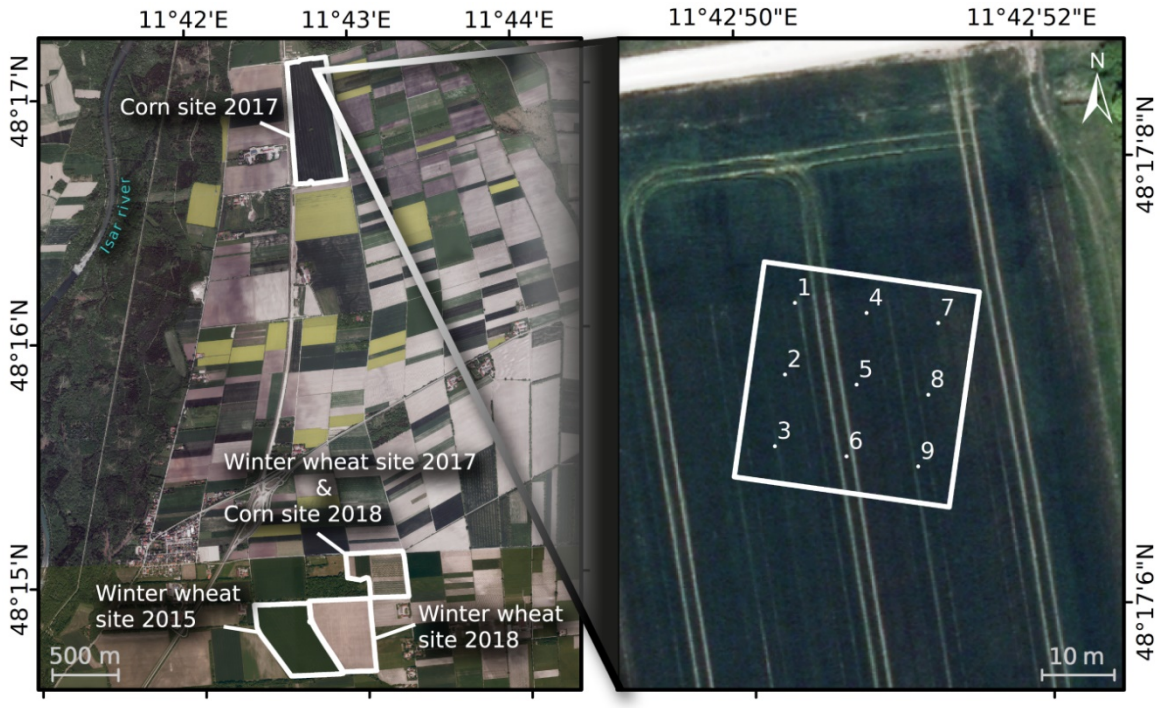

Figure 2.1. Munich-North-Isar test sites overview (left) and exemplary 2017 simulated 30 × 30 m corn EnMap-pixel with 9 ESUs (right).

Table 2.1. Munich-North-Isar winter wheat and corn test sites, locations, periods of sample collection, number of biomass samples, and number of spectral measurements at cloud-free days.

Crop Type	Coordinates	Sampling Period	No. of Samplings	No. of Spectral Measurements
Winter wheat	48°14'51.46''N 11°42'24.10''E	10 April–29 July 2015	17	7
Winter wheat	48°14'56.70''N 11°43'03.60''E	29 March–17 July 2017	16	12
Winter wheat	48°14'52.27''N 11°42'57.06''E	04 April–13 July 2018	12	7
Corn	48°17'06.56''N 11°42'49.98''E	8 June–15 September 2017	11	8
Corn	48°14'56.70''N 11°43'03.60''E	25 May–29 August 2018	13	6

Plant leaf water content is commonly expressed as equivalent water thickness (EWT, Eq. (2.1)) corresponding to a hypothetical thickness of a single layer of water averaged over the whole leaf area (Danson et al. 1992):

$$\mathrm{EWT} = \frac{FW - DW}{A}\ [\mathrm{g\ cm^{-2}}] \text{ or } [\mathrm{cm}],\ [\mathrm{kg\ m^{-2}}] \text{ or } [\mathrm{mm}] \tag{2.1}$$

where FW is the fresh sample weight, DW is the oven dry weight and A is the leaf area. While EWT refers to the water content on leaf level, canopy water content (CWC, Eq. (2.2)) is commonly derived through extrapolation by means of the LAI:

$$\mathrm{CWC} = \mathrm{EWT} * \mathrm{LAI} \tag{2.2}$$

Due to the linkage of LAI to the whole canopy, CWC may be biased towards the leaf fraction. Furthermore, CWC does not allow inferring the actual water detectability of plant components in a canopy from total detected water. Consequently, in this study total $\mathrm{EWT_{canopy}}$ ($\mathrm{EWT_{leaf}}$ + $\mathrm{EWT_{stalk}}$ + $\mathrm{EWT_{fruit}}$) will be defined as the above-ground total equivalent water layer averaged over one square meter of ground surface (Eq. (2.3)).

$$\text{total } \mathrm{EWT_{canopy}} = \sum (FW_{\text{leaves+stalks+fruits}} - DW_{\text{leaves+stalks+fruits}}) * A_g^{-1} \tag{2.3}$$

where A_g denotes the ground area. To monitor the development of total amounts of water stored in the canopy throughout the growing season, biomass samples were collected on a weekly basis. In case of wheat, a minimum transect of 50 cm along a sowing track or an area of 0.25 $\mathrm{m^2}$ was cut at soil level. For corn, 2–3 plants were cut. In-field plant density was obtained by counting plants and rows per meter. The samples were separated into leaf, stalk and fruit compartments, weighed in fresh state and oven-dried until constant weight for 24 h at 105 °C before dry weight was determined. $\mathrm{EWT_{leaf}}$, $\mathrm{EWT_{stalk}}$, $\mathrm{EWT_{fruit}}$ ($\mathrm{EWT_{ear}}$ and $\mathrm{EWT_{cob}}$, respectively) and total $\mathrm{EWT_{canopy}}$ per $\mathrm{cm^2}$ (Table 2.2) were calculated from laboratory results (specific water contents per ground area) and from farm management metadata (plants per meter and row spacing). The phenology was determined according to secondary growth stages of the BBCH-scale (Meier 2018).

Table 2.2. Statistics (range, mean, standard deviation) for in-situ measured EWT_{leaf}, EWT_{stalk}, EWT_{fruit}, total EWT_{canopy} and BBCH-range. Values correspond to measurements with available spectral reflectance data.

Year	**2015**	**2017**		**2018**	
Crop Type	**Winter Wheat**	**Winter Wheat**	**Corn**	**Winter Wheat**	**Corn**
BBCH range [-]	22–87	25–87	30–85	28–87	32–83
EWT_{leaf}: range [cm]	0.007–0.179	0.005–0.182	0.009–0.104	0.045–0.121	0.095–0.161
mean (std) [cm]	0.066 (0.058)	0.082 (0.050)	0.059 (0.035)	0.082 (0.027)	0.132 (0.023)
EWT_{stalk}: range [cm]	0.012–0.256	0.003–0.275	0.008–0.295	0.019–0.268	0.252–0.619
mean (std) [cm]	0.123 (0.084)	0.144 (0.089)	0.161 (0.115)	0.126 (0.099)	0.472 (0.126)
EWT_{fruit}: range [cm]	0.000–0.100	0.000–0.112	0.000–0.248	0.000–0.148	0.000–0.306
mean (std) [cm]	0.044 (0.045)	0.045 (0.045)	0.068 (0.100)	0.048 (0.068)	0.171 (0.123)
Total EWT_{canopy}: range [cm]	0.041–0.417	0.019–0.490	0.017–0.606	0.064–0.503	0.347–1.019
mean (std) [cm]	0.233 (0.141)	0.271 (0.145)	0.289 (0.221)	0.256 (0.170)	0.775 (0.227)

2.2.1.2 Spectroscopic Measurements

At each study site, a 30 × 30 m grid of nine 10 × 10 m squares was marked out delineating the elementary sampling units (ESU). This grid layout was designed to trace the geometric properties of one EnMAP pixel; hence, regarding the viewing geometry and grid location, the sensors descending orbit and inclination angle of 97.96° was accounted for (Figure 2.1).At each sampling date with clear sky conditions (Table 2.1) all nine ESUs were revisited and spectral measurements were taken using an Analytical Spectral Devices Inc. (ASD, Boulder, CO, USA) FieldSpec3 Jr. spectroradiometer with an effective spectral resolution of 3 nm in the VIS (≤700 nm) and 10 nm in the NIR and SWIR (≤2500 nm). Five nadir measurements were conducted per ESU at a height of 25 cm above the canopy, the same height at which the white reference panel (OptoPolymer, Munich, Germany) could be fully observed with the instruments field of view of 25°. Throughout the measurements, the sensor was slightly moved back and forth manually while maintaining the observation angle to obtain a representative spectral sample of the canopy. The five recorded spectra were averaged per ESU and a spatial mean of the nine ESUs was calculated to provide reflectance of the complete 30 × 30 m grid. Further, post-processing included splice-correction, white reference baseline calibration, and slight smoothing using a Savitzky-Golay-Filter with a frame size of 13 nm.

Note that it was not possible to conduct destructive sampling at exactly the same locations where the continuous spectral measurements were taken. However, due to averaging of spectral sampling points over the 30 × 30 m sampling area, it was possible to capture the in-field variability and therefore to represent average field water conditions.

Altogether, the collected dataset comprised destructively measured, plant compartment specific water content samples with corresponding spectral measurements at 26 dates for wheat and 14 dates for corn over three and two years, respectively (see Table 2.1 and Table 2.2).

2.2.2 Leaf Optical Data

Preliminary tests of the EWT_{canopy} retrieval model presented in this study were performed on two different leaf optical datasets. The LOPEX93 database was established in 1993 by the Joint Research Centre (JRC, Ispra, Italy). It associates transmittance and reflectance in the range of 400–2500 nm with biophysical and biochemical measurements of 66 leaf samples from 45 species (Hosgood et al. 1995). In total, the database comprises 330 spectra with corresponding measurements of EWT. Secondly, tests were performed on the ANGERS database containing 276 reflectance spectra and EWT measurements of 43 species (Jacquemoud et al. 2003). While woody species make up the majority of the ANGERS database, both datasets represent a large variety of leaf internal structure and spectra.

2.2.3 Radiative Transfer Models and Look-Up Tables

To check consistency between leaf optical data and modelled spectra, large look-up tables (LUT) using the RTMs PROSPECT and PROSAIL were created. PROSAIL (Jacquemoud et al. 2009) is coupling the *Leaf Optical Properties Spectra* model PROSPECT (Jacquemoud and Baret 1990) and the turbid medium canopy reflectance model 4SAIL (*Scattering by Arbitrary Inclined Leaves*) (Verhoef 1984; Verhoef and Bach 2007). The latest recalibrated version PROSPECT-D (Féret et al. 2008; Féret et al. 2017) simulates bidirectional-hemispherical reflectance and transmittance in the optical domain as a function of leaf pigments (chlorophyll a+b content C_{ab}, carotenoids C_{ar}, and anthocyanins C_{anth}), dry matter C_m, and brown pigments C_{brown} as well as a leaf mesophyll structure parameter N, and EWT (C_w). The canopy model SAIL calculates a bidirectional reflectance factor of 1-D turbid medium plant canopies. With regard to leaf optical properties and reflectance of the underlying soil (p_{soil}), it implements canopy structure (LAI), average leaf inclination angle (ALA) or optionally, ellipsoidal leaf inclination distribution (LIDF), and hot spot size parameter (h_{spot}) for a given illumination and viewing geometry (observation zenith angle (OZA), relative azimuth angle (rAA) between sun and sensor, and the solar zenith angle (SZA)).

Considering the impact of plant foliar water on the 970 nm absorption band, during LUT generation, all parameters with sensitivity in the NIR region were uniformly distributed over a wide value range (Table 2.3). Leaf pigments, having no effect on reflectance in the NIR (Carter 1991; Ceccato et al. 2001), remained constant.

Table 2.3. Parameter ranges for PROSPECT-D and PROSPECT-D + 4SAIL (PROSAIL) LUT. Specified ranges are uniformly distributed, single values are fixed.

PROSPECT-D-Parameters	Range	Notation [Unit]	4SAIL-Parameters	Range	Notation [Unit]
N	1.0–3.0	[-]	LAI	0.5–8.0	[m^2 m^{-2}]
C_{ab}	55	[µg cm^{-2}]	ALA	0–90	[deg]
C_w	0.0002–0.07	[g cm^{-2}]	h_{spot}	0.01–0.5	[-]
C_m	0.001–0.02	[g cm^{-2}]	OZA	0	[deg]
C_{brown}	0.0–1.0	[-]	SZA	35–50	[deg]
C_{ar}	15	[µg cm^{-2}]	rAA	0	[deg]
C_{anth}	5	[µg cm^{-2}]	p_{soil}	0.0–1.0	[-]

2.3 Methods

2.3.1 The Beer-Lambert Law and Retrieval Method Development

The Beer-Lambert law is mathematically formulated as Eq. (2.4):

$$\Phi = \Phi_0 e^{-\alpha(\lambda)d} \tag{2.4}$$

Passing through a medium of thickness d the incident radiation intensity Φ_0 is exponentially attenuated with increasing penetration depth. The absorption characteristics of a medium are defined by its wavelength-dependent absorption coefficients $\alpha(\lambda)$. In this study, due to the accurate spectral resolution in the 970 nm domain (Féret et al. 2008), water absorption coefficients for pure liquid water as determined by Kou et al. (1993) are used. Furthermore, it is assumed that within the absorption band at 970 nm, water is the only quantity-depending, varying active absorber and that variance within absorption of further components is neglectable. Thus, concluding from Eq. (2.4), the absorption depth of measured fresh leaves or canopies at 970 nm is uniquely dependent on the thickness of the optically active water layer (see also discussion in Section 2.3.2). For dry leaves or senescent canopies, absorption by liquid water is neglectable, resulting in a strictly linear reflectance signature at 970 nm. For the retrieval of EWT_{canopy}, Eq. (2.4) is rearranged in accordance with Bach (1995) to Eq. (2.5), where R_0 is the measured reflectance, d is the thickness of the optically active water layer, and R' is the d-dependent reflectance:

$$R' = \frac{R_0}{e^{-\alpha(\lambda)d}} \tag{2.5}$$

Using Eq. (2.5), d is iteratively optimized so that an objective function - the sum of absolute residuals between the modelled reflectance and the linear connection between the descending and ascending vertices of the 970 nm absorption - is minimal (Figure 2.2). The wavelength range considered by the plant water retrieval (PWR) model has been limited to 930–1060 nm based on preliminary minimization of the standard deviation of yielded EWT results from the PROSPECT LUT. Describing the thickness of the optically active water layer, the results can directly be compared to measured EWT on leaf level (Eq. (2.1)), CWC (Eq. (2.2)) and EWT_{canopy} (Eq. (2.3)). The algorithm was implemented in Python, where retrieval of EWT for 50,000 spectra was completed in 69 s on an Intel Core i5-3570K @3.40 GHz.

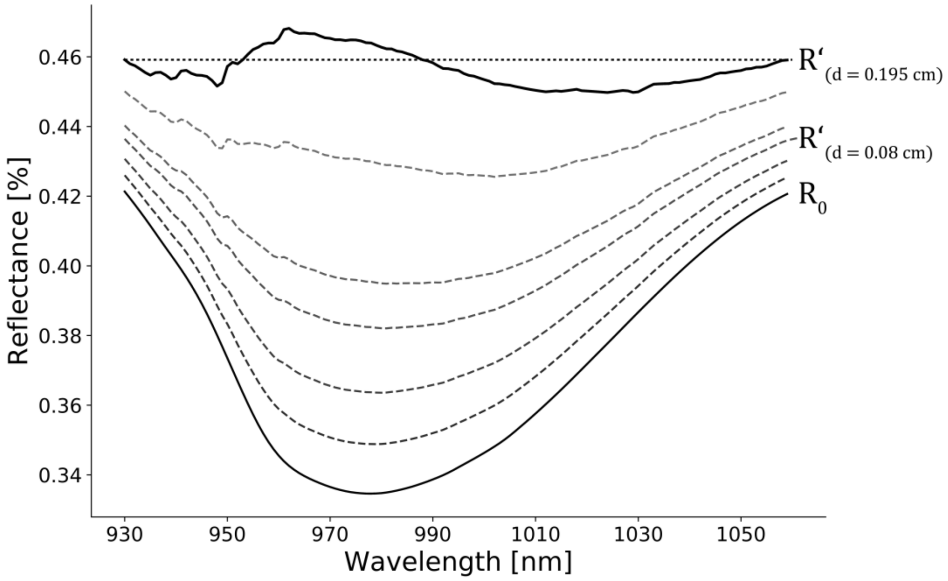

Figure 2.2. Determination of optically active water thickness d from a measured spectrum R_0 through minimization of residuals to assumed dry reflectance line (dotted line).

2.3.2 Global Sensitivity Analysis

The PWR model expects the thickness of optically active water to reflect the vegetation water content detected by a hyperspectral sensor. Both the PROSPECT and PROSAIL LUT were subjected to a global sensitivity analysis (GSA) to identify and evaluate the impact of contributing parameters in the 970 nm domain and to validate the performance of the model. The Fourier amplitude sensitivity test (FAST) identifies the main effects (first-order sensitivity effects), i.e., the contribution (S_{Ti}) to the variance of the model output by each input variable and interactions with other variables (Cannavó 2012). The contribution of parameters to the 970 nm absorption depth and shape is assessed by its distribution width using the variance-to-mean ratio (VMR).

Within PROSPECT (Figure 2.3a) N contributes to 98% of leaf reflectance at the vertices left and right of the 970 nm water absorption band. At 970 nm C_w is the highest contributing parameter in terms of VMR (10^{-2}). Minor influence on the shape of the absorption band is caused by C_{brown} at the descending vertex (VMR = 10^{-3}). C_m and parameter interactions also affect overall reflectance at 970 nm but interference with its shape is smaller by more than two orders of magnitude (10^{-4}). Regarding PROSAIL (Figure 2.3b), C_w likewise is the strongest shape-determining factor at 970 nm in terms of VMR (10^{-2}). However, the 970 nm absorption shape is affected by canopy structural parameters (ALA, LAI, h_{spot}, p_{soil}) and parameter interactions. The sum of influential parameter VMR may exceed C_w VMR, which may result in masking of the water signal when unfavorable parameter combinations occur.

The retrieval method was first tested on all the spectra within both the PROSPECT and the PROSAIL LUT (Figure 2.4). With a coefficient of determination (R^2) of 0.96 the approach indicates a strong correlation between PROSPECT modelled water content C_w

and retrieved optically active water content EWT (Figure 2.4a). However, the high relative root mean square error ($rRMSE = RMSE * mean_{observations}{}^{-1}$) of 286% with an intercept close to zero revealed a strong systematical offset. The growing spread of results towards higher values of C_w suggests a simultaneously increasing influence of other parameters due to the exponential radiative transfer from specific absorption coefficients to transmission and reflectance (Jacquemoud and Baret 1990).

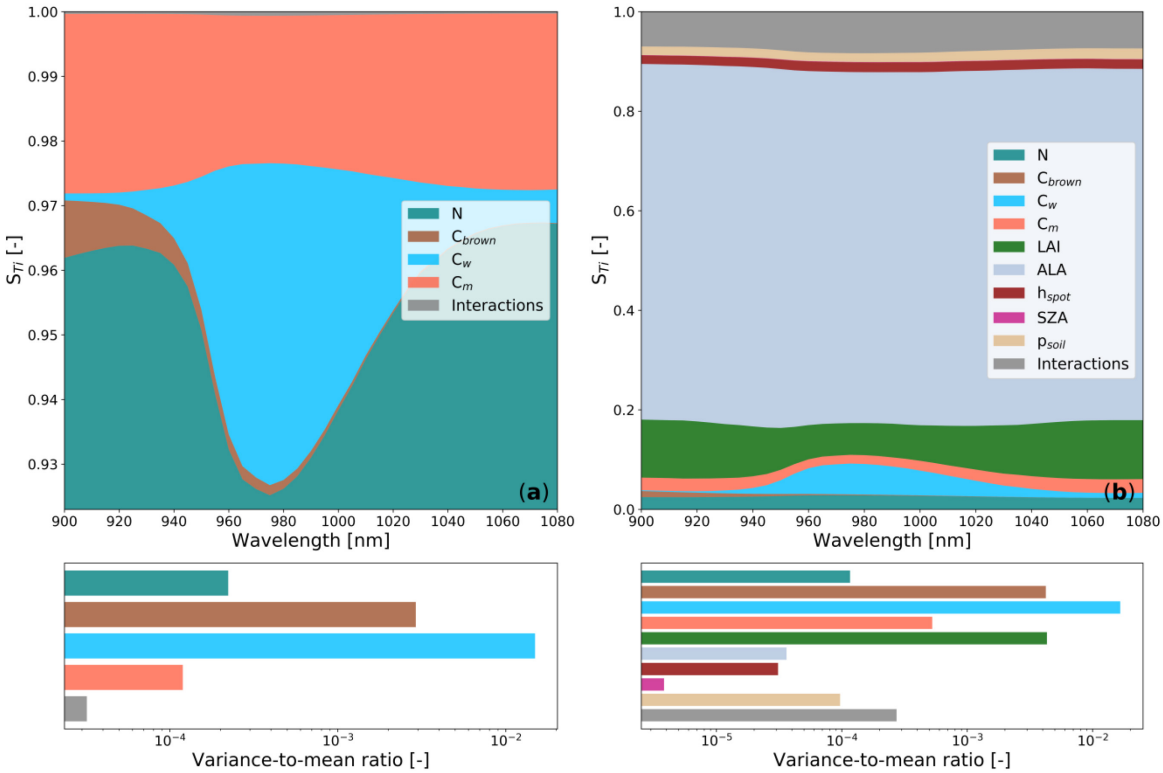

Figure 2.3. FAST first-order sensitivity coefficients and interactions (S_{Ti}) to reflectance (900–1080 nm) for PROSPECT (a) and PROSAIL (b) parameters. Due to high contribution of the leaf structure coefficient N within PROSPECT, only the upper contribution range ≤ is shown. Below, influences of parameters that affect the shape of the water absorption band considered within the PWR model (930–1060 nm) are quantified by the variance-to-mean ratio (VMR).

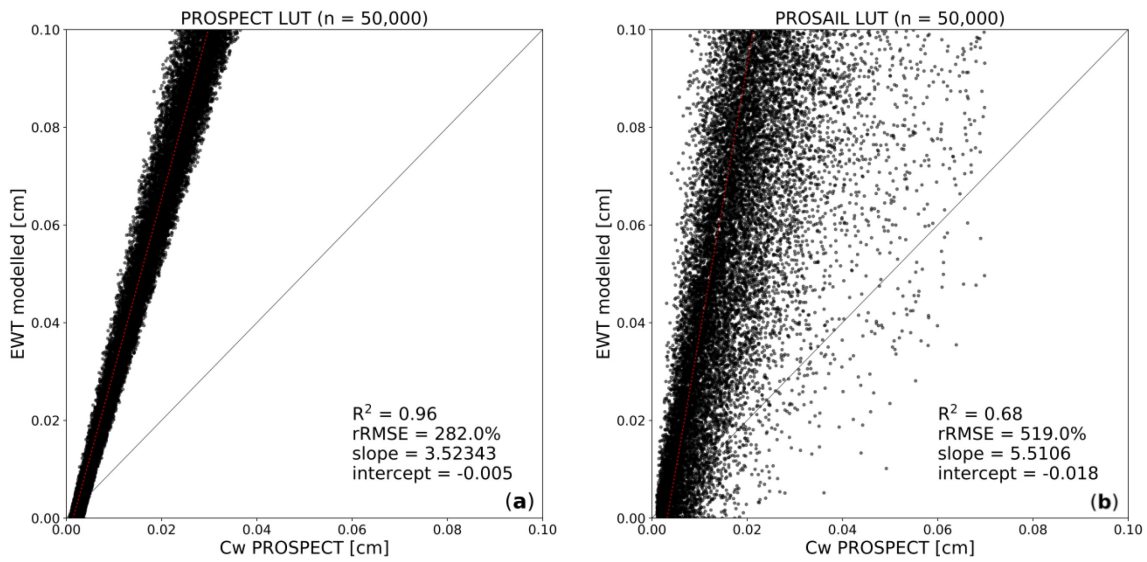

Figure 2.4. Modelled EWT results from synthetic LUT containing PROSPECT (a) and PROSAIL (b) spectra.

Applied to PROSAIL spectra (Figure 2.4b) the R^2-results (0.68) are significantly lower and although model results correspond to LUT C_w-values, both regression residuals and intercept do not show a systematic bias. However, within the created LUT, several parameter combinations can be considered unrealistic (Wang et al. 2018), masking or flattening the water signal due to model parameter related interference with the shape of the 970 nm absorption band. The resulting outliers and overall spread of modelled C_w-values render the PROSAIL LUT unsuitable for further calibration of the model.

2.3.3 Using PROSPECT for Calibration of the PWR Model

The model was further tested on the LOPEX93 (Hosgood et al. 1995) and ANGERS (Jacquemoud et al. 2003) datasets, which showed a similar systematical bias as model results from PROSPECT spectra (Figure 2.5a,c,e). Since the overestimation seemed to be solely defined by the slope of the regression line, the water absorption coefficients in Eq. (2.5) were adjusted by multiplying the slope of the PROSPECT LUT linear regression model as a constant (Eq. (2.6)):

$$R' = \frac{R_0}{e^{-\alpha(\lambda)d*3.52343}} \tag{2.6}$$

The calibration procedure accounts for unknown effects of the leaf surface and of leaf internal structure on reflectance in the 970 nm domain (Féret et al. 2008) and for potential multiple leaf internal scattering (Carter 1991; Zhang et al. 2011). Using the calibrated water absorption coefficients (Eq. (2.6)), minimization of the objective function is achieved more quickly, resulting in lower modelled values of EWT that are consistent with the measured order of magnitude. Subsequently, the altered absorption coefficients in the 930 to 1060 nm range were used for an improved water content retrieval. Applied to the PROSPECT LUT (Figure 2.5b), EWT was estimated with a much smaller error (rRMSE = 12%). Applying

the algorithm with updated coefficients to LOPEX93 data, measured EWT was estimated with $R^2 = 0.93$ and rRMSE = 22% and for ANGERS data with 0.93 and 39% respectively (Figure 2.5d,f).

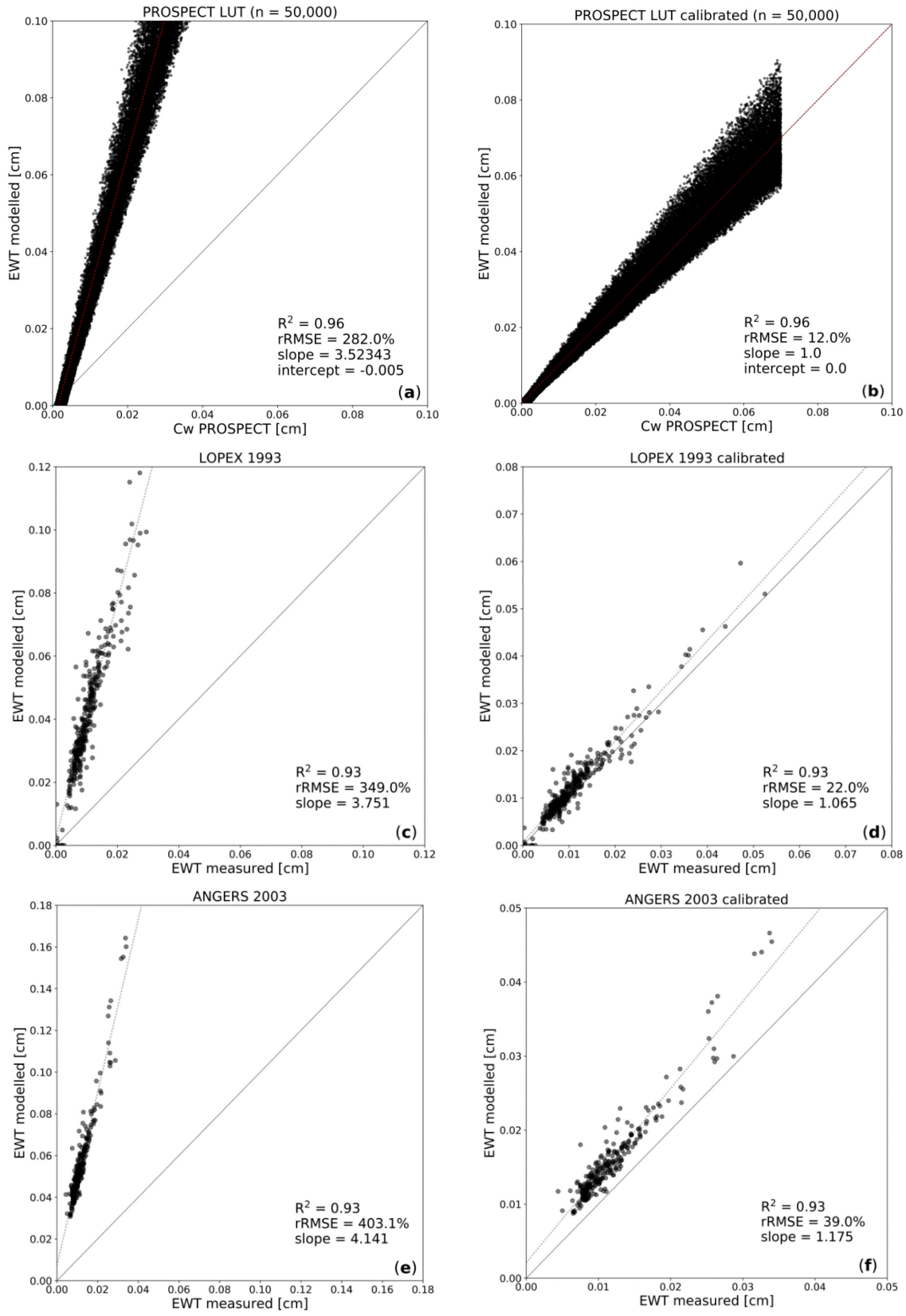

Figure 2.5. Uncalibrated PWR-results for the PROSPECT LUT (a); LOPEX93 data (c); and ANGERS data (e); compared to results after calibration: PROSPECT LUT (b) LOPEX93 (d); and ANGERS (f).

2.4 Results

The minimization process for retrieving optically active water using the PWR model with recalibrated absorption coefficients (factor 3.52342, Eq. (2.6)) was applied to both in-situ winter wheat and corn spectral data. The results were compared to combinations of destructively measured leaf, stalk, and ear or cob water contents. For further analysis, the BBCH-scale was included to relate to growth stage dependencies of the model results.

2.4.1 Winter Wheat Data

Considering only the measured water content of wheat leaves, the results showed low correlation (Figure 2.6a: $R^2 = 0.27$; rRMSE = 81%); however, annotated BBCH-values showed good results for tillering (20+) and stalk elongation stages (30+) and progressing senescence (87). On the other hand, heading (47+) and flowering stages (60+) as well as ear development and ripening stages (70+) were invariably overestimated by the model. The sum of leaf and stalk water content yielded better results (Figure 2.6b: $R^2 = 0.68$; rRMSE = 52%) in particular for early growth stages. However, as growth proceeds, strong underestimation of $EWT_{leaf} + EWT_{stalk}$ occurs due to saturation.

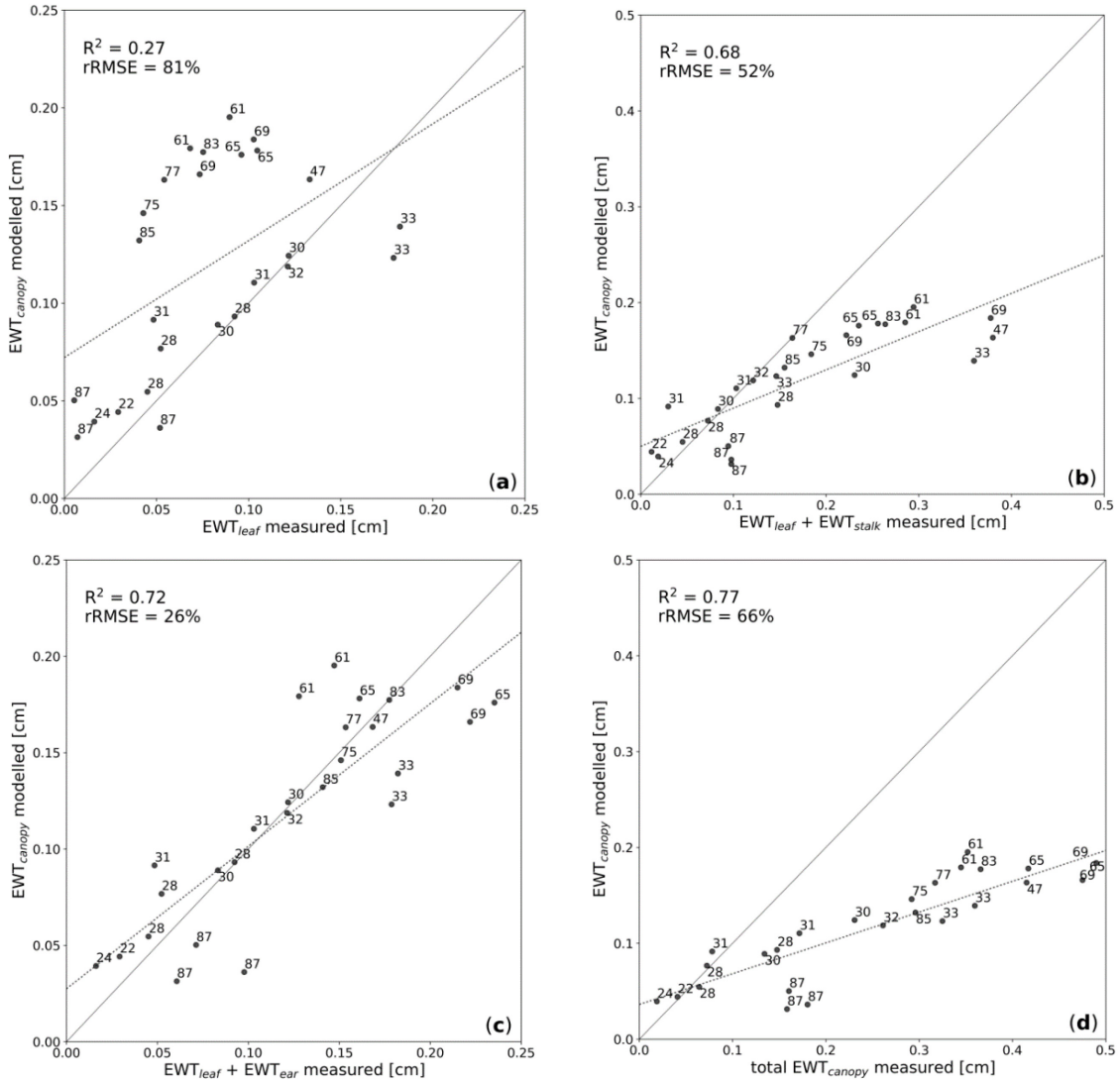

Figure 2.6. Modelled optically active water in relation to measured water contents of wheat compartments. Annotated numbers refer to secondary growth stages according to BBCH-scale. Results compared to EWT_{leaf} (a); EWT_{leaf} + EWT_{stalk} (b); EWT_{leaf} + EWT_{ear} (c); and total EWT_{canopy} (d).

The best results were obtained when combining the measured water contents of leaves and ears (Figure 2.6c: R^2 = 0.72; rRMSE = 26%). Thereby, model results adequately reflected measured EWT_{leaf} + EWT_{ear} across all phenological stages over three years. Aggregating measured EWT_{leaf}, EWT_{stalk} and EWT_{ear} (= total EWT_{canopy}) yet again largely resulted in an underestimation (Figure 2.6d: R^2 = 0.77; rRMSE = 66%); only tillering stages were modelled with reasonable accuracy.

2.4.2 Corn Data

Regarding the two-year corn dataset, best results were achieved for leaf water contents (Figure 2.7a: R^2 = 0.86; rRMSE = 23%) with a minor tendency to underestimation towards higher growth stages. Despite good correlation, the combination of leaf and stalk measured water content was largely underestimated by the model (Figure 2.7b: R^2 = 0.91; rRMSE = 95%). Aggregated EWT_{leaf} and EWT_{cob} resulted in both lower correlation and error (Figure

2.7c: $R^2 = 0.61$; rRMSE = 84%) due to underestimation when cobs were registered.

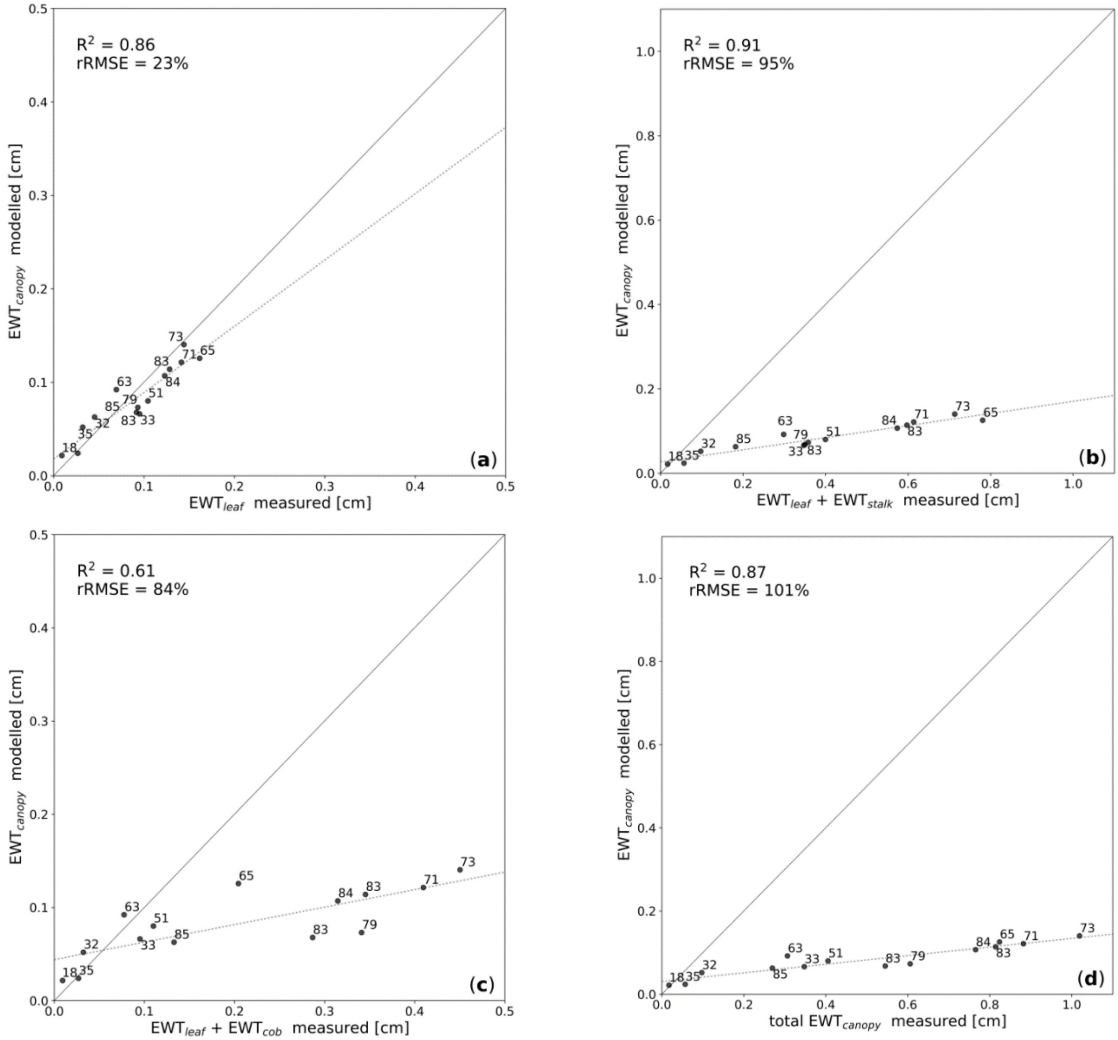

Figure 2.7. Modelled optically active water in relation to measured water contents of corn compartments. Annotated numbers refer to secondary growth stages according to BBCH-scale. Results compared to EWTleaf (a); EWTleaf + EWTstalk (b); EWTleaf + EWTcob (c); and total EWT_{canopy} (d).

In relation to total measured EWT_{canopy}, both correlation and underestimation are large (Figure 2.7d: $R^2 = 0.87$; rRMSE = 101%). In view of phenological dependencies, low water contents were consistently modelled with high accuracy during early leaf development stage (BBCH = 18) and beginning stalk elongation (30–32). Furthermore, unlike for wheat, no clear growth stage related dependencies were recognizable.

2.5 Discussion

2.5.1 Inversion of the Beer-Lambert Law for Water Content Retrieval

A simple physically-based model was developed which applies the Beer-Lambert law to inversely retrieve optically active water content on leaf and canopy scale. In view of the fact that only one parameter - the thickness of the optically active water layer d - needs to be

inverted, the algorithm allows a fast processing of large hyperspectral datasets. As shown by a GSA of the PROSPECT LUT in the 970 nm domain, interference of other parameters is marginal (Figure 2.3a) rendering C_w to be the dominant driver of leaf reflectance in this spectral region ($R^2 = 0.96$; Figure 2.4a). However, this does not apply to the PROSAIL LUT where, according to GSA, the cumulative influence of leaf and canopy structural parameters may mask the water signal (Figure 2.3b). Hereby, two issues interact: first, the 4SAIL model assumes a horizontally homogenous canopy, which may not be valid for complex canopy architectures and clumped vegetation through, e.g., formation in rows (Combal et al. 2003; Dorigo 2012; Zou et al. 2015). Second, unrealistic parameter combinations may occur in LUTs (Wang et al. 2018). Both issues may unfavorably affect modelled reflectance in the 970 nm domain, reducing the predictive power of C_w for water content information ($R^2 = 0.57$; Figure 2.4b) and rendering the PROSAIL LUT unsuitable for calibration of the presented PWR model. When applied to PROSPECT spectra the linear offset of the regression model indicates that the absorption coefficients of pure liquid water differ from those of leaves, because reflectance in interaction with the leaf surface and multiple leaf internal reflections are not accounted for (Carter 1991; Zhang et al. 2011). Using the slope of the regression from the PROSPECT LUT results as a factor to calibrate the absorption coefficients, the absolute quantification of PROSPECT C_w, LOPEX93 and ANGERS EWT significantly improved (Figure 2.5). The high correlation of $R^2 = 0.96$ between PROSPECT C_w and modelled EWT approved application of the model to in-situ measured TOC data. Nevertheless, using PROSPECT for calibration implies that potentially occurring canopy architectural effects on radiation (Kuester and Spengler 2018) are being neglected. Hence, the PWR model considers the 970 nm absorption to be caused solely by liquid water. In addition, since reflected radiance in the 930–1060 nm range is also affected by atmospheric water vapor (Gao and Goetz 1995; Datt 1999), the process of accurate atmospheric correction is a critical prerequisite when the PWR model is applied to future available hyperspectral TOC reflectance acquired from space.

2.5.2 Dependency of Canopy Water Detection on Canopy Structure

Absolute measures of EWT_{canopy} were inversely extracted from a three-year TOC winter wheat and two-year corn spectral dataset by means of the proposed PWR model. The results indicated a strong correlation between water absorption centered around 970 nm and measured EWT_{canopy}. However, the comparison of retrieved EWT_{canopy} from in-situ spectra with measured aggregations of plant compartment specific water contents raises the question, how deep radiation at 970 nm penetrates into the canopy and thus, which amounts of water actually can be observed by optical sensors (Sims and Gamon 2003). Although absorption by water and vegetation in the NIR is low and penetration depth of radiation is higher in this wavelength range (Peñuelas et al. 1993; Serrano et al. 2000), the presented results showed that not all of the contained canopy water is detected by the sensor. Our results suggest that in the case of winter wheat modelled EWT_{canopy} largely reflects the

absolute water contained in the leaves and present ears (Figure 2.6c). Taking only EWT_{leaf} as a reference, EWT_{canopy} is overestimated due to the presence of EWT_{ear}, which manifests in the spectral response but is not reflected by the in-situ data (Figure 2.6b,d). This also implies potential water content overestimation for wheat when referencing is done based on CWC records, which in the case of barley can be seen in the results of Vohland (2008). On the other hand, including measured EWT_{stalk}, the underestimation resulting with advanced growth stage indicates that radiation at 970 nm cannot penetrate increasingly hardened stalk tissue and thus cannot transport information about the water contained within. This has also been noted by Sims and Gamon (2003) and Champagne et al. (2003). This finding is further supported by the fact that residual water in ripe wheat (BBCH = 87) is consistently underestimated, rendering the PWR model unable to detect residual water in senescent wheat.

Despite good results of modelled EWT_{canopy} for EWT_{leaf} of corn, the results indicate a tendency to underestimation towards higher water contents (Figure 2.7a) due to maximum radiation transmission through stacked leaves (Lillesaeter 1982). Once stalks and cobs have developed, the underestimation of total corn EWT_{canopy} reveals the limited ability of NIR radiation to penetrate the thick stalk/cob tissues or the canopy depth or both (Figure 2.7b-d).

In summary, the retrieval results of winter wheat and corn vary because—depending on canopy structure—different plant components manifest in the 970 nm water absorption band. Several other studies also raised the fact of canopy structural influence on crop variables retrieval (Trombetti et al. 2008; Berger et al. 2012; Richter et al. 2012; Kuester and Spengler 2018; Transon et al. 2018). Cereal crops with prominent ears will not be satisfactorily modelled if the ear water content is not included in the in-situ measurements as it can be seen in the study of Champagne et al. (2003). On the contrary, when modelling corn water content, it may be sufficient to only collect leaf samples since only the water fraction of the leaves can be estimated directly from optical sensors. The specific structure of corn mostly covers the stalks and cobs, masking the water stored in these plant compartments.

In recent studies, mostly parametric regression models based on vegetation indices (Vohland 2008; Yi et al. 2014), derivative- (Clevers et al. 2008, 2010), or integration-based (Pasqualotto et al. 2018) indices have been applied to retrieve crop canopy water content information from hyperspectral data. Verrelst et al. (2016b) obtained very good CWC correlation on SPARC03 data (R^2 = 0.95) by applying Gaussian process regression with integrated sequential backward band removal. Cernicharo et al. (2013) used both an ANN and a LUT approach to estimate CWC from CHRIS/PROBA data (R^2 = 0.82 and R^2 = 0.64, respectively). Earlier studies which presented retrieval methods based on the Beer-Lambert law include Champagne et al. (2003) with good results for corn but an overestimation of wheat canopy water content, because EWT_{ear} has not been sampled

separately (index of agreement D = 0.80 and D = 0.38, respectively). The findings of this study are also confirmed by the Beer-Lambert law based study of Sims and Gamon (2003), in which best results for water content of thin tissues were obtained (R^2 = 0.66), whereas total canopy water content was underestimated (R^2 = 0.35).

The presented PWR model is considered superior to empirical regression models by its physical basis, allowing insights into the physical meaning of results, while outperforming other Beer-Lambert law-based approaches by the possibility to infer absolute measures of canopy water content from measured TOC reflectance spectra. This absolute quantifiability of canopy water content represents a novelty among available retrieval approaches. Besides, the accurate underlying data basis proved transferability of the model to different sites and crop types and, given that a sensor detects the maximal depth of the 970 nm water absorption, promises applicability also to hyperspectral data on an operational basis.

2.6 Conclusions

The proposed PWR model based on the inversion of the Beer-Lambert law effectively succeeds in the determination of wheat EWT_{leaf} and EWT_{ear} with consistent results over a three-year dataset (R^2 = 0.72; rRMSE = 26%). For corn EWT_{leaf} was estimated from two-year data with even better results (R^2 = 0.86; rRMSE = 23%). Since the detectability of canopy water content fractions seems to be largely dependent on the crop type, its canopy structure, depth, and growth stage, it is recommended to collect EWT_{leaf}, EWT_{stalk} and EWT_{fruit} data and corresponding reflectance for different crop types over all phenological stages along the growing cycle. However, an evaluation is needed to assess limits of canopy water content retrieval in terms of optical radiation penetration depth through thick canopies and tissues, also in view of a possibly improved retrieval from off-nadir spectroscopy (Danner et al. 2017). Our study could proof the transferability of the developed PWR model to other sites and crop types and represents a novelty in crop water content absolute quantifiability. The PWR model will be provided as a slim and applicable tool within the open source software EnMAP-Box (van der Linden et al. 2015) to accurately and efficiently retrieve water content information from ground-based, airborne and spaceborne hyperspectral data, as it will become available through future missions.

Acknowledgments

The study was supported by the Space Agency of the German Aerospace Center (DLR) in the frame of the project “EnMAP Scientific Advisory Group Phase III—Developing the EnMAP Managed Vegetation Scientific Processor” through funding by the German Federal Ministry of Economic Affairs and Energy (BMWi) based on enactment of the German Bundestag under the grant code number 50EE1623. The responsibility for the content of this publication lies with the authors.

3 Paper II: RTM-based Dynamic Absorption Integrals for the Retrieval of Biochemical Vegetation Traits

This study has been published in the *International Journal of Applied Earth Observation and Geoinformation*:

Wocher, M., Berger, K., Danner, M., Mauser, W., & Hank, T. (2020). RTM-based dynamic absorption integrals for the retrieval of biochemical vegetation traits. *International Journal of Applied Earth Observation and Geoinformation*, 93, 102219. https://doi.org/10.1016/j.jag.2020.102219.

Journal Impact Factor: 7.97 (2022)

Author Contributions: Conceptualization, M.W., K.B. and T.H.; Data curation, M.W.; Formal analysis, M.W. and K.B.; Funding acquisition, W.M. and T.H.; Investigation, M.W.; Methodology, M.W.; Project administration, W.M. and T.H.; Resources, M.W.; Software, M.W. and M.D.; Supervision, W.M. and T.H.; Validation, M.W. and K.B.; Visualization, M.W.; Writing—original draft, M.W.; Writing—review & editing, M.W., K.B., M.D. and T.H.

Transition to Paper II: Paper II presents a parametric hybrid approach to simultaneously derive chlorophyll and carotenoid contents, as well as water content from spectrometric imagery through an automated separation of the respective absorption feature spaces by combining peak detection, convex hulls, log-transformation, and integration methods. The study was realized within the framework of the EnSAG Phase III collaboration project 1.1.: "Development of a Canopy Reflectance Model Environment for the retrieval of biophysical variables of agriculturally managed and forested sites" between the EnMAP Team Agriculture at LMU, the EnMAP Team Forest at University of Trier and the EnMAP-Box Development Team at HU Berlin. The developed algorithm produces robust 3-band outputs, pointing at the respective biochemical traits in the form of Spectral Integral Ratios (SIR). These can then be converted into physical quantities based on a calibration using PROSPECT and PROSAIL. An important secondary result is the demonstrated necessity of implementing physiological constraints into a synthetic database. This is performed in the form of naturally occurring green peaks and chlorophyll-carotenoid dependencies. The SIR algorithm has been implemented into the EnMAP-Box Agricultural Applications as the 'Analyze Spectral Integral' (ASI) tool which allows the interactive visualization of the convex hull to graphically adjust the accurate separation of the absorption features (Appendix A.2).

Abstract

Information about pigment and water contents provides comprehensive insights for evaluating photosynthetic potential and activity of agricultural crops. In this study, we present the concept of using spectral integral ratios (SIR) to retrieve three biochemical traits, namely chlorophyll a and b (C_{ab}), carotenoids (C_{cx}), and water (C_w) content, simultaneously from hyperspectral measurements in the wavelength range 460-1100 nm. The SIR concept is based on automatic separation of respective absorption features through local peak and intercept analysis between log-transformed reflectance and convex hulls. The algorithm was tested on two synthetically established databases using a physiologically constrained look-up-table (LUT) generated by (i) the leaf optical properties model PROSPECT and (ii) the canopy radiative transfer model (RTM) PROSAIL. LUT constraints were realized based on natural C_{cx}-C_{ab} relations and green peak locations identified in the leaf optical database ANGERS. Linear regression between obtained SIRs and model parameters resulted in coefficients of determination (R^2) of 0.66 (i and ii) for C_{cx}, $R^2 = 0.85$ (i) and 0.53 (ii) for C_{ab}, and $R^2 = 0.97$ (i) and 0.67 (ii) for C_w, respectively. Using the model established from the PROSPECT LUT, leaf level validation was carried out based on ANGERS data with reasonable results both in terms of goodness of fit and root mean square error (RMSE) (C_{cx}: $R^2 = 0.86$, RMSE = 2.1 µg cm^{-2}; C_{ab}: $R^2 = 0.67$, RMSE = 12.5 µg cm^{-2}; $C_w = 0.89$, RMSE = 0.007 cm). The algorithm was applied to airborne spectrometric HyMap data acquired on 12th July 2003 in Barrax, Spain and to AVIRIS-NG data recorded on 2nd July 2018 southwest of Munich, Germany. Mapping of the SIR results as multiband images (3-segment SIR) allows for intuitive visualization of dominant absorptions with respect to the three considered biochemical variables. Barrax *in situ* validation using linear regression models derived from PROSAIL LUT showed satisfactory results regarding C_{ab} ($R^2 = 0.84$; RMSE = 9.06 µg cm^{-2}) and canopy water content (CWC, $R^2 = 0.70$; RMSE = 0.05 cm). Retrieved C_{cx} values were reasonable according to C_{ab}-C_{cx}-dependence plausibility analysis. Hence, the presented SIR algorithm allows for computationally efficient and RTM supported robust retrievals of the two most important vegetation pigments as well as of water content and is ready to be applied on satellite imaging spectroscopy data available in the near future. The algorithm is publicly available as an interface supported tool within the Agricultural applications of the EnMAP-Box 3 hyperspectral remote sensing software suite.

3.1 Introduction

Growth of global population and the concurrent requirement of reducing environmental impacts of agriculture demands that yields per area must be increased and farming management systems must be optimized (Godfray et al. 2010). To meet this challenge in a changing environment, the observational power of spectral Earth observation data, but in

particular spaceborne imaging spectrometers providing a continuous spectrum, should be exploited to provide spatiotemporally explicit quantifications of biochemical and structural vegetation variables (Verrelst et al. 2019; Berger et al. 2020b).

In this context, content measurements of the primary light harvesting pigments chlorophyll a, chlorophyll b (C_{ab}), and carotenoids (C_{cx}), which include secondary light harvesting carotenes and photoprotective xanthophylls (Demmig-Adams and Adams 1996; Blackburn 1998b), provide important information about vegetation photosynthetic potential and activity (Chappelle et al. 1992; Goetz and Prince 1996). Along with these pigments, information about water content (C_w) is important for evaluating vegetation physiological status and health (Peñuelas et al. 1993; Peñuelas et al. 1997; Blackburn 1998a) and the respective foliar contents and compositions serve as indicators for numerous stresses (Gamon et al. 1992; Carter and Knapp 2001). Due to its close connection to nitrogen content (Evans 1989), knowledge about pigment content is valuable for supporting decisions on fertilization procedures (Li et al. 2016). On the other hand, information on water content can be used for irrigation management (Ben-Gal et al. 2009) and crop ripening monitoring (Hank et al. 2019).

With the increased availability of remotely sensed data with narrowband continuous spectral coverage (hyperspectral) in the optical domain (400-2500 nm), a multitude of approaches for estimating foliar pigments or water content from absorption features in the corresponding wavelength region on leaf and canopy scale have been developed. In view of current and future hyperspectral satellite missions like PRISMA (Loizzo et al. 2018; Loizzo et al. 2019), SBG/former HyspIRI (Lee et al. 2015), SHALOM (Feingersh and Ben-Dor 2015), EnMAP (Guanter et al. 2015) and ESA's Copernicus high priority candidate CHIME (Nieke and Rast 2018a), fast, efficient, and flexible methods for the retrieval of vegetation properties from these huge data streams are required.

Most commonly, empirical relationships between *in situ* measured variables and wavelength-specific observations are derived using narrowband spectral indices. Although these simple parametric regression methods are computationally fast and thus desirable for large-scale applications, their fundamental problems are limited generality and transferability (Verrelst et al. 2015a). Accordingly, results from parametric regression models are site-, time-, and crop-specific (Baret and Guyot 1991; Houborg et al. 2007) and selection of only few discrete narrow bands may underexploit the information density of contiguous spectrometric measurements (Atzberger et al. 2011).

To address the latter, integration-based indices were proposed to more extensively exploit absorption feature spaces contained in spectroscopic data (Kokaly and Clark 1999; Verrelst et al. 2015a). Commonly, these indices are calculated by (1) creating envelopes (either by inserting straight line segments or convex hulls) covering unique absorption features as baseline for continuum removal and (2) relate the subjacent area to either a single maximum absorption depth or to the area sheathing the continuum removed

reflectance curve. Most of the integration-based indices are targeting the retrieval of C_{ab} in the 600-700 nm wavelength region (Broge and Leblanc 2001; Oppelt and Mauser 2004; Malenovský et al. 2006; Delegido et al. 2010; Schlerf et al. 2010). Some studies have tested integration-based indices to retrieve vegetation water content from the liquid water absorption features found in the near infrared (NIR) at 970 and 1100 nm (Kokaly et al. 2003; Stimson et al. 2005; Clevers et al. 2010; Pasqualotto et al. 2018). Regarding C_{cx}, estimations are more challenging, since its absorption feature is masked by C_{ab} in the 400-550 nm wavelength range (Gitelson et al. 2002; Gitelson et al. 2009). For this reason, C_{cx} is often expressed as ratio to C_{ab} or its inverse (Gamon et al. 2016). While many narrowband indices have been proposed to extract C_{cx} (Chappelle et al. 1992; Blackburn 1998a; Gitelson et al. 2002), integration-based methods have not yet been applied.

In contrast to empirical methods with parameterized regression models, physically-based approaches explore the underlying causality between inputs and outputs to quantify vegetation pigments and water contents. For example, the widely used radiative transfer model (RTM) PROSAIL (Jacquemoud et al. 2009) simulates top-of-canopy reflectance and transmittance by coupling the leaf optical properties model PROSPECT-D (Féret et al. 2017) with the canopy structure RTM 4SAIL (Verhoef 1984; Verhoef and Bach 2007). PROSAIL has been successfully applied by various studies due to its comparatively limited number of parameters (Berger et al. 2018b). A variety of strategies have been applied for the inversion of PROSAIL to infer vegetation biophysical and biochemical traits from remote sensing observations. These include numerical optimization algorithms (e.g. Bicheron and Leroy (1999); Jacquemoud et al. (1995)), look-up-table (LUT) approaches (e.g. Weiss et al. (2000); Richter et al. (2008)) and hybrid approaches using machine learning regression algorithms (for a general overview refer to Verrelst et al. (2015a); (Verrelst et al. 2019)). Although RTM-based inversion methods are physically sound, the techniques require profound knowledge, and iterative minimization of objective functions in a multi-dimensional feature space are computationally demanding and mathematically highly nonlinear (Jacquemoud et al. 2000). Further limitations of RTM-inversion include the equifinality of model inversion, i.e. different parameter configurations may be equally valid in terms of their ability to reproduce a measured reflectance spectrum (Atzberger and Richter 2012; Verrelst et al. 2019). In addition, LUT parameter entries that serve as basis for any conceivable inversion process are usually uncorrelated, which does not hold true in nature. As a result, unrealistic parameter combinations occur within unconstrained LUTs (Yebra and Chuvieco 2009; Jurdao et al. 2013; Wang et al. 2018), which unfavorably predetermine estimation results, in particular when machine learning algorithms are trained over these LUTs.

Therefore, the objective of the present study was to develop a dynamic, absorption features auto-delimiting integration-based approach to simultaneously retrieve C_{cx}, C_{ab} and C_w from reflectance spectra with a contiguous spectral coverage in the optical domain.

Within the retrieval workflow, full detection of absorption ranges with realistic LUT-related boundary conditions will be assured. The presented algorithm adopts a hybrid approach, combining the robustness and generality of a physically-based method (i.e., RTM) with a computational feasible and dynamic integration-based algorithm.

3.2 Material & Methods

3.2.1 Validation Datasets

Validation on leaf level was performed on the leaf optical dataset ANGERS (Jacquemoud et al. 2003) acquired 2003 at INRA in Angers (France). It associates transmittance and reflectance measurements in the range of 400–2500 nm with biophysical and biochemical measurements of 43 species. While woody species make up the majority of the ANGERS database, the dataset represents a large variety of leaf internal structure and spectra (Table 3.1).

Table 3.1. Statistical summary of samples in the ANGERS dataset: ranges (mean; standard deviation)

Samples	Cab [µg cm-2]	Ccx [µg cm-2]	Cw [cm]
260	4.4-106.7 (35.5; 21.1)	1.9-25.3 (8.9; 4.9)	0.005-0.034 (0.011; 0.004)

Tests on canopy level were conducted using HyMap airborne spectrometric image data with 15 nm sampling in 126 spectral bands (438-2483 nm). The data was acquired during the ESA Spectra Barrax Campaign (SPARC03) on 12th July 2003 in Barrax, La Mancha, Spain (39°3' N, 2°6' W) at 6 m ground sampling distance. The *in situ* measurements covered multiple crop types of diverse canopy structures, i.e. alfalfa (*medicago sativa*), potato (*solanum tuberosum*), sugar beet (*beta vulgaris*), garlic (*allium sativum*), onion (*allium cepa*), poppy (*papaver*) and corn (*zea mays*) at different phenological stages. EWT was estimated destructively from three top level leaf samples, while the surface area of the sampled leaves was determined via vertical photographs over grid paper, and was upscaled to canopy water content (CWC) via multiplication with LAI. Observations of effective LAI were collected using a Plant Canopy Analyzer LAI-2000 instrument (LI-COR Inc., Lincoln, NE, USA). C_{ab} content was measured using a CCM-200 Chlorophyll Content Meter (ICT International, Armidale, Australia) and calibrated through laboratory analysis (Gandia et al. 2004). Note that only field average C_{ab} values were stored in the data. Since no C_{cx} measurements were conducted during SPARC03, it is assessed via plausibility of image statistics in view of the natural C_{cx}-C_{ab} relationship.

Applicability and plausibility tests were further applied to airborne data acquired on 2nd July 2018 in the area of Oberpfaffenhofen, Germany. The data was recorded during CHIME preparatory activities using the AVIRIS-NG sensor with 425 ~5.5 nm spectral bands at 5.2 m GSD in the range 377—2500 nm (Chapman et al. 2019).

3.2.2 Radiative Transfer Models and Look-Up Table Compilation

Preliminary tests and optimization of the retrieval approach presented in this study were performed on PROSPECT-D and PROSAIL LUTs containing 5000 simulated spectra. PROSAIL (Jacquemoud et al. 2009) is coupling the *Leaf Optical Properties Spectra* model PROSPECT (Jacquemoud and Baret 1990) and the turbid medium canopy reflectance model 4SAIL: *Scattering by Arbitrarily Inclined Leaves* (Verhoef 1984; Verhoef and Bach 2007). The latest recalibrated version PROSPECT-D (Féret et al. 2017) simulates bidirectional-hemispherical reflectance and transmittance of leaves in the optical domain as a function of leaf pigments (C_{ab}, C_{cx}) and anthocyanins (C_{anth}), dry matter content (C_m), and brown pigments (C_{brown}) as well as leaf mesophyll structure (N), and equivalent water thickness (EWT/C_w). The canopy model 4SAIL calculates bidirectional reflectance factors of 1-D turbid medium plant canopies including the brightness parameter (p_{soil}) which denotes a scaling factor between two model-implemented soil spectra (wet/dark – dry/bright). With regard to leaf optical properties and reflectance of the underlying soil, 4SAIL implements canopy structure as a function of leaf area index (LAI), average leaf inclination angle (ALA) or optionally, ellipsoidal leaf inclination distribution (LIDF), and hot spot size (h_{spot}) for a given illumination and viewing geometry (observation zenith angle (OZA), relative azimuth angle (rAA) between sun and sensor, and the solar zenith angle (SZA)).

For the LUT generation, parameters with sensitivity in the VNIR region were distributed over a wide value range (Table 2.3) to incorporate a large variety of crop types, based on prior information on plausible dynamic ranges for input parameters according to previous studies (Verrelst et al. 2016b; Féret et al. 2017; Berger et al. 2018b). Since the presented algorithm relies on direct absorption expressions within the reflectance curve, the expected unfavorable masking of C_{ab} absorption by background soil reflectance is reduced by limiting minimum LAI to 0.5 m^2m^{-2}. Unfavorable influences, mainly in the NIR domain are also expected from fluctuating sun-sensor-target geometries. Therefore, nadir view (OZA = 0°) is assumed at constant SZA (= 35°) to mitigate potential hotspot effects in off-nadir observations. Although C_{anth} is distributed in the LUT, a narrow value range is assumed with regard to low contents in most agricultural crops.

Table 3.2. Parameter ranges for combined PROSPECT-D + 4SAIL (PROSAIL) LUT. Specified ranges are uniformly (range) or gauss-distributed (mean; standard deviation), single values are fixed. C_{cx} was distributed depending on C_{ab} (Figure 3.1).

PROSPECT-D Parameters	Range	Notation [Unit]	4SAIL Parameters	Range	Notation [Unit]
N	1.0-2.0 (1.5, 0.2)	[-]	LAI	0.5-7.5 (4.0; 2.0)	[m^2 m^{-2}]
C_{ab}	0-100 (50; 40)	[µg cm^{-2}]	ALA	25-65 (45; 15)	[deg]
C_w	0.005-0.07 (0.04; 0.02)	[cm]	h_{spot}	0.01	[-]
C_m	0.002-0.01	[g cm^{-2}]	OZA	0	[deg]
C_{brown}	0.0-0.8 (0.3, 0.15)	[-]	SZA	35	[deg]
C_{cx}	C_{ab}-dependent	[µg cm^{-2}]	rAA	0 (N/D)	[deg]
C_{anth}	1.0-5.0 (2.0, 0.8)	[µg cm^{-2}]	p_{soil}	0-1	[-]

3.2.3 Preparation of a Physiologically Constrained LUT

An inherent problem of LUTs consists of implausible spectra produced by unrealistic combinations of input parameters (Yebra and Chuvieco 2009). Although parameters are randomly drawn within specified ranges and distributions, the resulting individual parameters are uncorrelated, which for most vegetation parameters does not hold true in nature. To tackle this problem some studies excluded physiologically unrealistic combinations based on *in situ* measured ranges (Houborg et al. 2009; Yebra and Chuvieco 2009; Jurdao et al. 2013; Wang et al. 2018) or *a priori* knowledge (Combal et al. 2003). While determination of generally valid, cross-parameter constraints is a complex multidimensional and nonlinear challenge, some generally valid, direct dependencies are observable from measurements. In this study, two new filter criteria have been implemented in the employed LUT with the first (i) considering the carotenoid-chlorophyll relation: Figure 3.1a shows a strong linear relationship ($R^2 = 0.94$) between C_{cx} and C_{ab} as observed from measurements in the ANGERS leaf optical database. Without consideration of C_{cx}-C_{ab} dependence, values within a LUT are uncorrelated in an unrealistic way (Figure 3.1b). In this study C_{cx} therefore was simulated as a function of C_{ab} by using the linear regression obtained from ANGERS and assuming an upper and lower boundary condition. The boundaries ($B_{C_{cx}(high)}$; $B_{C_{cx}(low)}$) were determined by means of the standard deviation (= 4.684 µg cm^{-1}) of linearly derived C_{cx} values:

$$B_{C_{cx}(high)} = 0.223 * \frac{4.684}{3} * C_{ab} + 2 * 0.986 \tag{3.1}$$

$$B_{C_{cx}(low)} = \frac{0.223}{4.684} * 3 * C_{ab} \tag{3.2}$$

Using Eqs. (3.1) and (3.2) as boundary conditions, C_{cx} was Laplace distributed around the regression line with an iterative reassignment of outliers. Note that, due to the iterative reassignment, C_{cx} is no longer Laplace distributed, yet generated C_{cx} LUT entries remain close to observed conditions (Figure 3.1c).

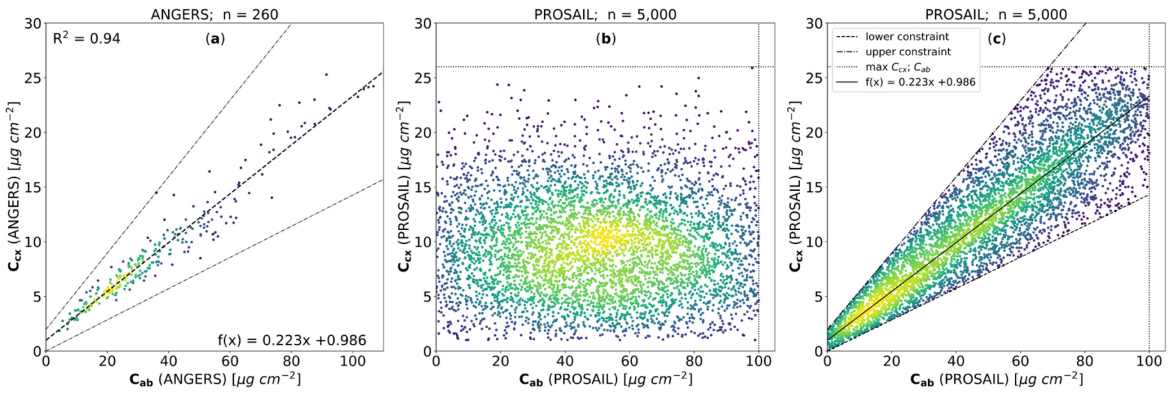

Figure 3.1. Linear dependence of C_{cx} from C_{ab} in ANGERS data (a), uncorrelated relationship in an unrestricted LUT (b), forced linear relationship in the used LUT applying constraints obtained from ANGERS (c).

As second constraint (ii), a condition about valid green peak locations was implemented: some $C_{ab} > C_{cx}$ combinations ($C_{ab} \cong 5 * C_{cx}$) within the defined boundaries (Eqs. (3.1) and (3.2)) result in an inadmissible green peak shift towards shorter wavelengths within PROSAIL simulated reflectance (Figure 3.2).

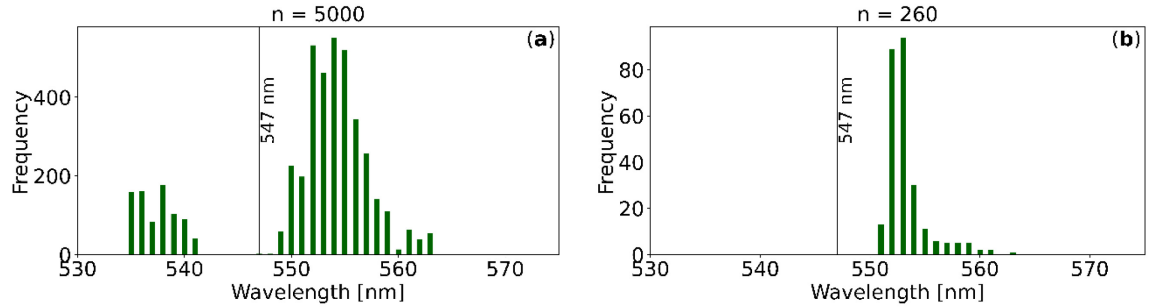

Figure 3.2. Green peaks frequency distribution from PROSAIL LUT (a) and ANGERS data (b). From 4709 detected, 1090 (23%) green peaks were considered invalid (< 547 nm).

Therefore, detected LUT entries with green peaks < 547 nm were automatically excluded from the LUT and not used for further analysis. Although this reduced the number of LUT-members by 23%, green peaks at positions < 547 nm were considered invalid based on observations of naturally occurring green peaks within the leaf optical dataset ANGERS (Figure 3.2b) (Jacquemoud et al. 2003) and reflectance measurements of three sensors, HyMap (D'Urso et al. 2004), AVIRIS-NG (Chapman et al. 2019) and field spectroradiometer (Danner et al. 2017; Wocher et al. 2018; Danner et al. 2019).

3.2.4 Dynamic Separation of Convex Hull and Absorption Features

Pigment absorption occurs in the visible wavelength range (VIS) between 400 and 700 nm. C_{ab} generates two separate absorption peaks in the 400-500 nm and 650-700 nm spectral domains, whereas absorption by C_{cx} is limited to the 400-540 nm spectral range (Figure 3.3). The absorption feature at 970 nm represents the first liquid water absorption band. Further C_w absorption bands follow at 1200, 1450, and 1930 nm. In this study, we focus exclusively on the 970 nm feature due to optimal preconditions in terms of vegetation water detectability (for a discussion of this topic refer to Wocher et al. (2018)).

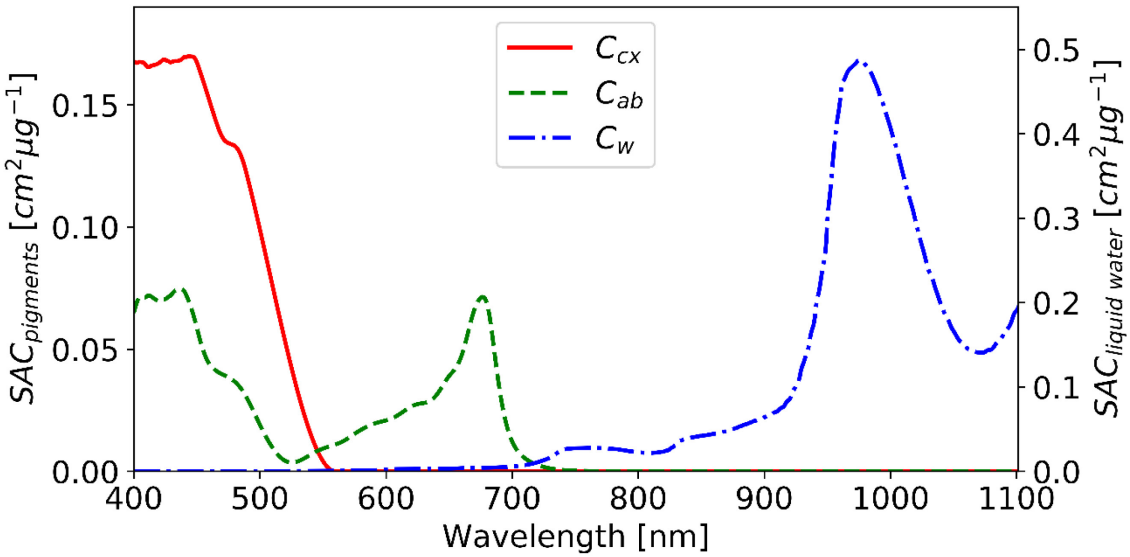

Figure 3.3. Specific absorption coefficients (SAC) for C_{cx}, C_{ab}, and C_w in the wavelength range 400-1100 nm. SACs are from Féret et al. (2008); Féret et al. (2017).

The basic concept of the approach is to dynamically delimit the specific absorption ranges of C_{cx}, C_{ab}, and C_w by determining the respective area fractions of the absorptions in each spectrum. For the calculation of the developed spectral integral ratio (SIR) each reflectance spectrum is dynamically separated into three segments (i-iii) to allow for the differentiation of the absorption features and to retrieve C_{cx}, C_{ab}, and C_w simultaneously (Figure 3.4). The segmentation is based on automated local peak and intercept detection. If implausible results are returned by the automated approach, prefixed thresholds are used. The following assumptions apply for the segmentation: the first segment (i) for the retrieval of C_{cx} uses the green peak, which is automatically detected using a local peak detection algorithm (Billauer 2012). If no green peak is found, e.g. due to low C_{ab} contents, the default value to limit the first segment was set to 554 nm, the mean value of detected green peaks in the LUT. With regard to green peaks located at ≥ 547 nm, the convex hull (red in Figure 3.4a) of the wavelength range 460-1100 nm is calculated using Andrew's monotone chain convex hull algorithm (Andrew 1979). In case that intercepts between hull and reflectance are found at smaller wavelengths than the detected green peaks, the C_{cx} segment is limited to those intercepts. The second segment (ii), enclosing C_{ab} absorption in the red wavelength region, covers the range from the detected green peaks to the intercepts between hull and spectrum at around 770 nm at the NIR shoulder.

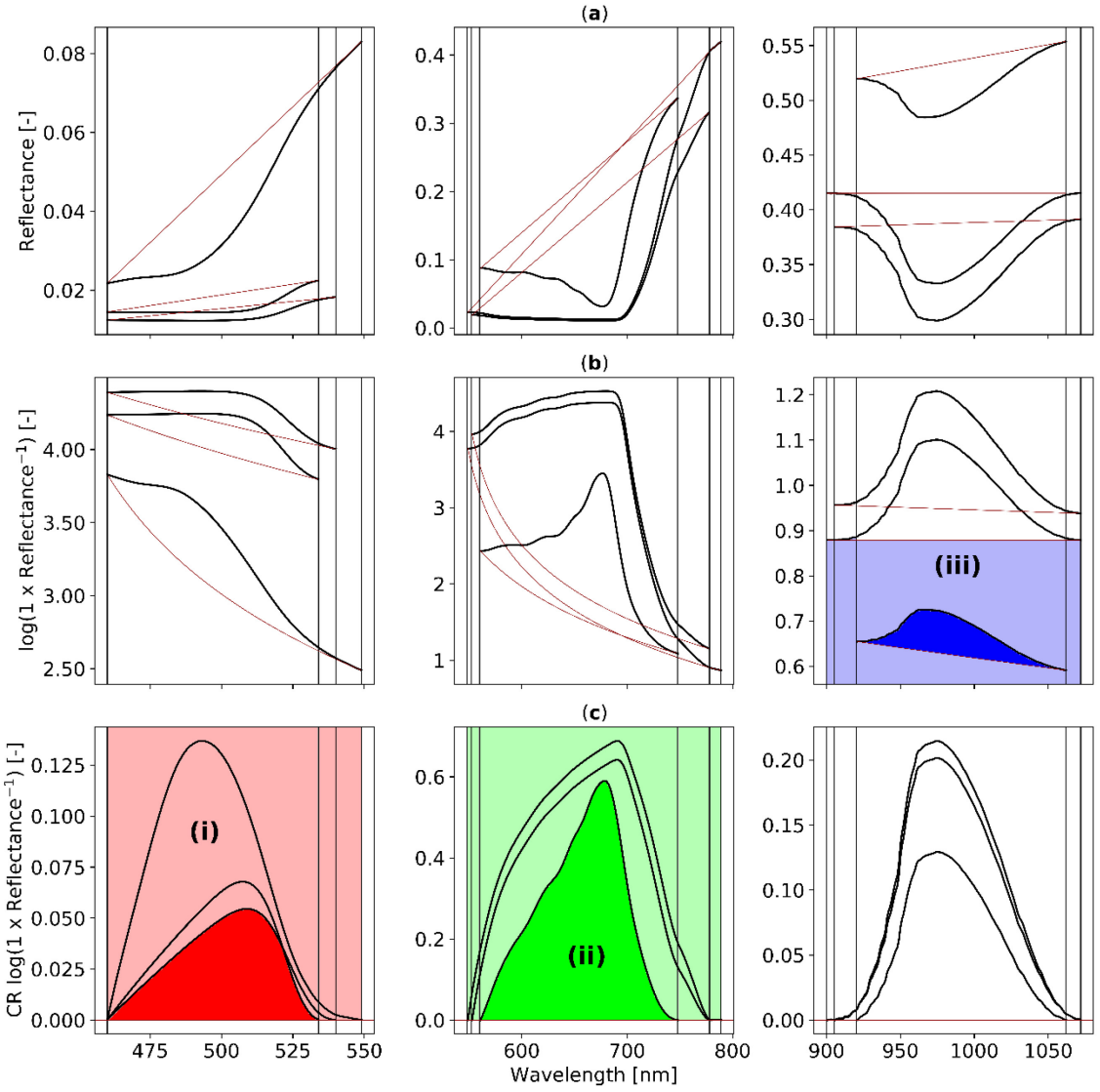

Figure 3.4. Separation of C_{cx} (i), C_{ab} (ii), and C_w (iii) absorption features in the wavelength range 460-1100 nm through local peak and intercept analysis of reflectance (black) and convex hull (red). Exemplarily shown are automatically detected absorption ranges (vertical black lines) of three synthetic PROSAIL reflectance spectra (a) together with their log-inverted (b), and continuum removed (CR) log-inverted equivalent (c). RGB-colors (full & pale) represent areas for ratio calculation (Eq. (3.3) and (3.4)) and their later corresponding 3-segment false color image (3-segment SIR) counterpart.

The third segment (iii) crosses the first liquid water absorption at 970 nm (Figure 3.4a) from either optionally locally detected NIR peaks (else 920 nm if no peaks are detected) or intercepts at 910-950 nm to the intercepts between hull and spectrum at around 1070 nm (else 1100 nm). After segmentation of the absorption features sensitive to C_{cx}, C_{ab}, and C_w both hull and reflectance are log-inverted to pseudo absorbance $A' = log(R^{-1})$ in accordance with Yoder and Pettigrew-Crosby (1995) to increase the value depth and decrease the risk of saturation for ratio calculation (Figure 3.4b). For the retrieval of C_{cx} and C_{ab} the segmented convex hull is used to remove the continuum of the spectra and to calculate the respective spectral integral ratios (SIR; Figure 3.4c) with normalization by the maximum

absorption feature width (Eq. (3.3)):

$$C_{cx},\ C_{ab}\ \mathrm{SIR}(a,b) = \left\{ \sum_{\lambda_a}^{\lambda_b} [R'(\lambda_i) - \mathrm{H}'(\lambda_i)] * \left[\sum_{\lambda_a}^{\lambda_b} R'(\lambda_i) \right]^{-1} \right\} * [\max(\lambda_b - \lambda_a)]^{-1} \qquad (3.3)$$

where λ_a and λ_b define the respective wavelength ranges of a segment, $H'(\lambda_i)$ and $R'(\lambda_i)$ are the log-inverse upper convex hull and spectral reflectance at wavelength λ, respectively.

For the retrieval of C_w, however, the continuum is taken into account because high radiation penetration in the NIR (Newton and Blackman 1970; Lillesaeter 1982; Bull 1991; Sims and Gamon 2003) leads to an increase in 970 nm water absorption with increasing LAI. This effect is reduced when the continuum is considered by using the area subjacent to the NIR reflectance plane (Figure 3.4b) as reference to the C_w absorption feature (Eq. (3.4)):

$$C_w\ \mathrm{SIR}(a,b) = \left\{ \sum_{\lambda_a}^{\lambda_b} [R'(\lambda_i) - \mathrm{H}'(\lambda_i)] \right\} * \left\{ \max \left[\sum_{\lambda_a}^{\lambda_b} H'(\lambda_i) \right] \right\}^{-1} \qquad (3.4)$$

In contrast to fixed threshold wavelengths, dynamic detection assures full consideration of the particular absorption feature dimensions. SIR results for C_{cx}, C_{ab}, and C_w are stored as 3-band raster images (3-segment SIR) to allow for a comprehensive interpretation of pigments and water within false color RGB imagery.

3.3 Results

3.3.1 Calibration on Synthetic Database

The 3-segment SIR algorithm was applied to the two previously created LUTs, first at leaf level to the PROSPECT-LUT and then at canopy level to the PROSAIL-LUT (Figure 3.5). The algorithm was implemented in Python 3, where calculation for 5000 spectra at 1 nm resolution was completed in 56 s on an Intel Core i5-3570K @ 3.40 GHz.

C_{cx} SIR (Eq. (3.3)) cannot be used to estimate C_{cx} directly due to masking by C_{ab} at 400-550 nm (Gamon et al. 2016). However, the ratio between C_{cx} SIR and C_{ab} SIR (C_{cx}/C_{ab} SIR) shows an exponential relationship (coefficients of determination (R^2) = 0.66; 0.66) to corresponding PROSPECT and PROSAIL C_{cx} (Figure 3.5a, d). Owing to saturation of absorption at 550-800 nm by C_{ab}, increasing SIR values reflect an exponential increase (R^2 = 0.85; 0.53) of PROSPECT and PROSAIL C_{ab} (Figure 3.5b, e). Thereby, higher SIR results are retrieved from PROSAIL spectra due to increase of NIR-reflectance at high LAI and/or low leaf inclination angles. When comparing C_w SIR (Eq. (3.4)) results in the region of the liquid water absorption band at 970 nm with PROSPECT / PROSAIL C_w (Figure 3.5c, f), linear relationships are revealed (R^2 = 0.97; 0.67). Difference in regression slopes indicate higher absorption depths at canopy than at leaf level. Although dispersion of the three retrieved parameters from PROSAIL spectra is large, Gaussian kernel-density (based on Scott (2015)) peaks of the retrievals (colored in Figure 3.5) tend to be stable in location over LUTs where fewer parameters were varied (not shown). Outliers with low probability

density values result from unrealistic parameter combinations in the LUT, for instance in association with the PROSAIL parameters C_m, LAI, and ALA.

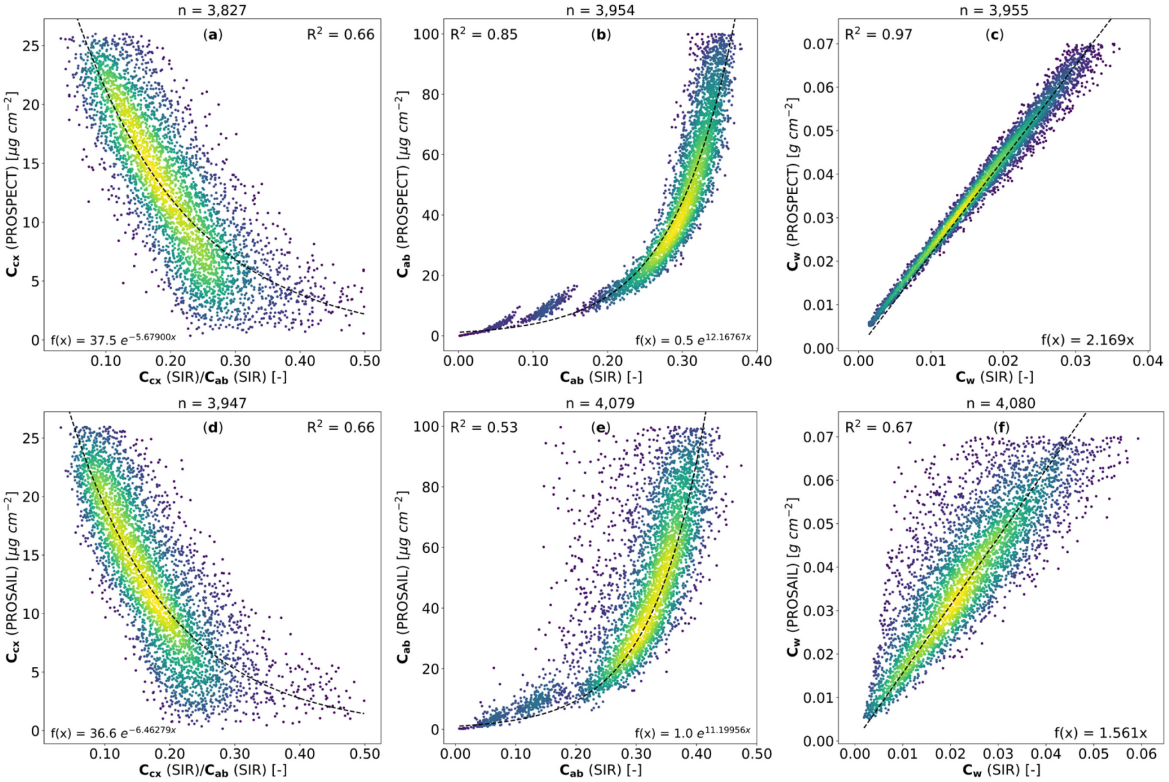

Figure 3.5. Modelled SIR results from synthetic PROSPECT (a-c) and PROSAIL LUT (d-f) for C_{cx}/C_{ab} SIR, chlorophyll C_{ab} and water content C_w. The color gradient from purple to yellow represents kernel-density estimates from low to high using Gaussian kernels. The reduced sample counts (by $5000 - n$) indicate excluded spectra with green peaks < 547 nm or zero division at non-existent absorption.

As obtained from the linear regression models, equations to map leaf and canopy C_{cx}, C_{ab}, and C_w from PROSPECT SIR and PROSAIL SIR were derived as follows (Eqs. (3.5)-(3.10)):

$$C_{cx}(leaf) = 37.5 * \exp\left[-5.67900 \ * \ \left(\frac{C_{cx}(SIR)}{C_{ab}(SIR)}\right)\right] \ with \ C_{ab}(SIR) \neq 0 \tag{3.5}$$

$$C_{cx}(canopy) = 36.6 * \exp\left[-6.46279 * \ \left(\frac{C_{cx}(SIR)}{C_{ab}(SIR)}\right)\right] \ with \ C_{ab}(SIR) \neq 0 \tag{3.6}$$

$$C_{ab}(leaf) = 0.5 * \exp[12.16767 \ * \ C_{ab}(SIR)] \tag{3.7}$$

$$C_{ab}(canopy) = 1.0 * \exp[11.19956 \ * \ C_{ab}(SIR)] \tag{3.8}$$

$$C_w(leaf) = 2.169 * C_w(SIR) \tag{3.9}$$

$$C_w(canopy) = 1.561 * C_w(SIR) \tag{3.10}$$

3.3.2 Validation on ANGERS Leaf Optical Data

The presented approach of calculating three combined SIRs was applied to 260 leaf spectra of the ANGERS leaf optical database. SIR results were converted to physical measures using the regression models obtained from the PROSPECT LUT (Eqs. (3.5), (3.7), (3.9)). As for measured C_{cx}, the C_{cx}/C_{ab} SIR model yielded good correlation ($R^2 = 0.86$, RMSE = 2.085 µg cm^{-2}) at slight overestimation (Figure 3.6a). Measured C_{ab} was modelled less robustly ($R^2 = 0.67$, RMSE = 12.5 µg cm^{-2}) and particularly showed high dispersion at moderate C_{ab} contents between 30 and 70 µg cm^{-2} with underestimation at values > 70 µg cm^{-2} (Figure 3.6b). ANGERS C_w was traced by C_w SIR with $R^2 = 0.89$ and RMSE = 0.007 cm showing increasing overestimation at higher water contents. (Figure 3.6c).

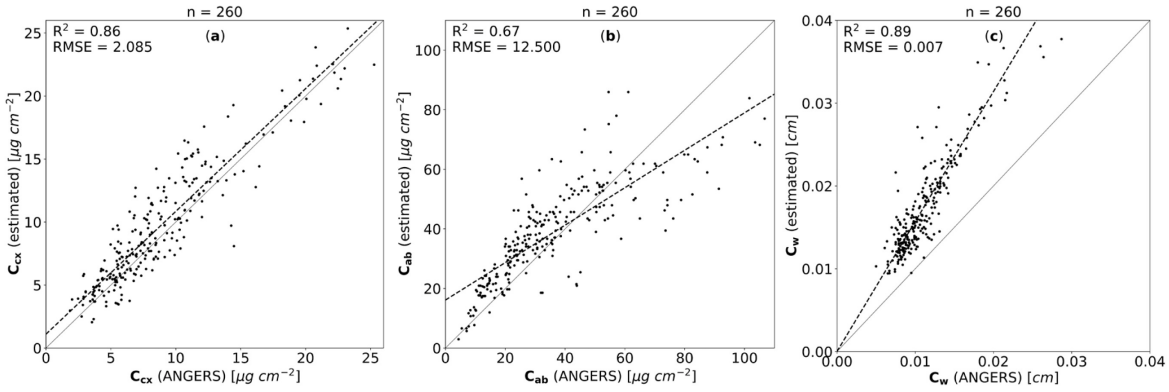

Figure 3.6: Validation for C_{cx}, C_{ab}, and C_w using leaf level Eqs. (3.4), (3.6), and (3.8) on ANGERS leaf *in situ* measurements.

3.3.3 Validation on SPARC03 Campaign Data

Figure 3.7a shows the results of the three SIRs combined to a 3-band false color representation of absorptions by C_{cx} (Red), C_{ab} (Green) and C_w (Blue), allowing for intuitive interpretation of the prevailing absorption conditions between the three constituents of different crops. Surfaces exhibiting no absorption features in the respective wavelength segments turn dark (e.g. bare soil). While generally bright colors indicate more pronounced C_{cx}, C_{ab} or C_w absorptions, cyan colors for instance suggest predominance of C_{ab} and C_w over C_{cx} (e.g. corn fields). Yellowish colors in Figure 3.7a point at low C_w though high C_{cx} and C_{ab} content (e.g. upper alfalfa field) and magenta implies low C_{ab} at high levels of C_{cx} and C_w. Beyond the mere visual interpretation, quantitative content information was retrieved from the image data using the previously defined canopy related Eqs. (3.6), (3.8), and (3.10) as obtained from PROSAIL regression models (Figure 3.7b, c, d).

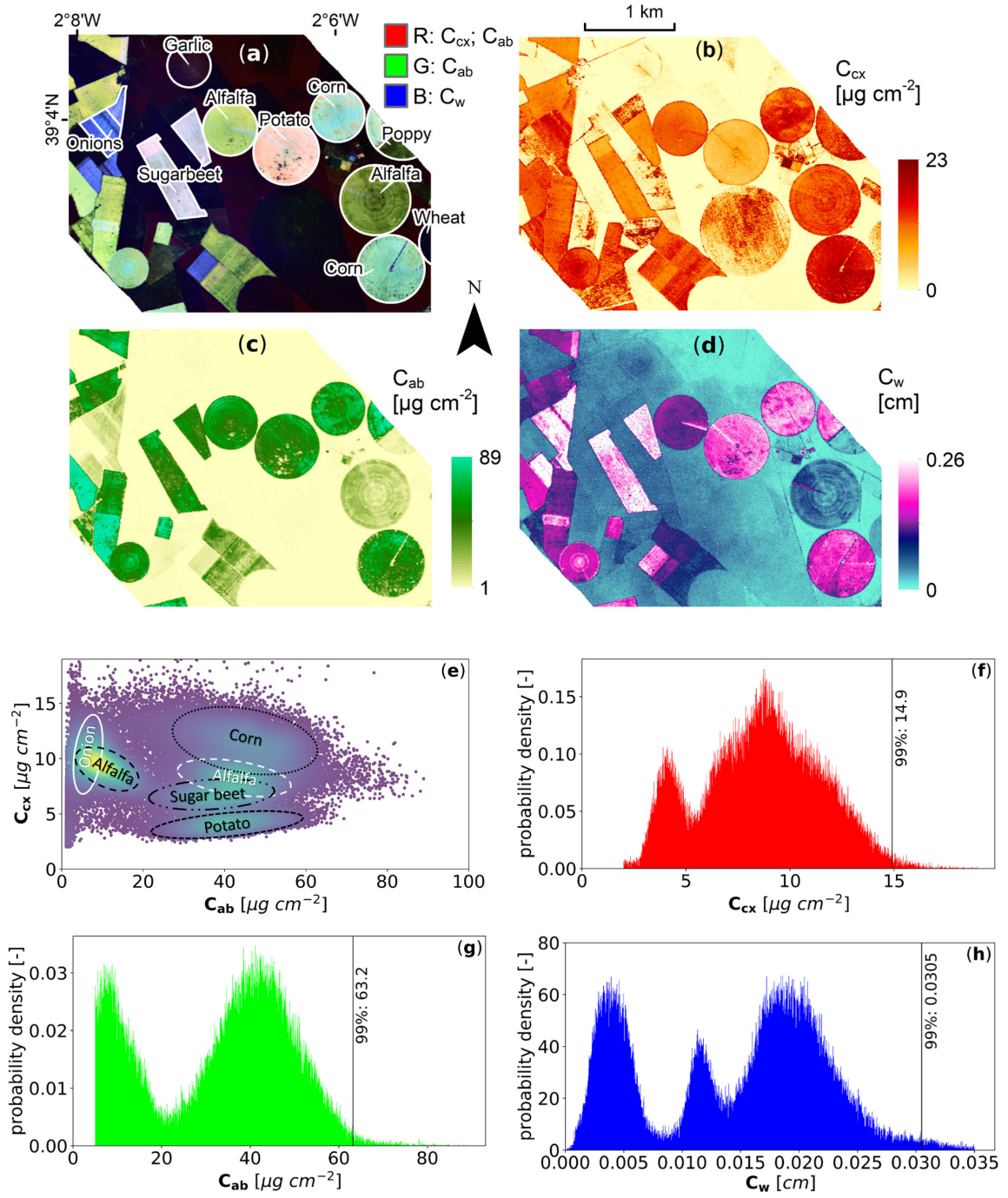

Figure 3.7. Sectional 3-band false color image of SIR results from spectrometric image data (12th July 2003, Barrax, La Mancha, Spain, HyMap airborne sensor) and annotated crops (a). Spatial results for C_{cx} (b), C_{ab} (c), and C_w (d) as derived from SIR using Eqs. (3.6), (3.8), and (3.10). C_{ab}-C_{cx}-relation as colored Gaussian kernel densities for plausibility analysis with principal crop feature spaces (e). Extracted probability density plots for retrieved C_{cx} (f), C_{ab} (g), and C_w (h). For C_{cx}, values < 2 µg cm^{-2}, for C_{ab} values < 5 µg cm^{-2}, and for C_w values > 0.035 were omitted for better visibility.

Compared to retrieved C_{ab} content, it becomes apparent that C_{cx} persists in fields where decomposition of C_{ab} has already taken place – for instance in the largest center-pivot irrigated field (wheat). Inter-field variations of C_{cx} and C_{ab} reveal crop type specific content differences (Figure 3.7e). In-field heterogeneities of both C_{cx} and C_{ab} are continuously mapped (Figure 3.7b, c). With regard to the crop specific C_{ab}-C_{cx}-relations (Figure 3.7e),

green vegetation modelled values are within the defined boundaries (Eqs. (3.1) and (3.2)). Retrieved contents above the upper boundary are considered appropriate for advanced senescent stands with remnants of C_{cx} and already degraded C_{ab} (e.g. onion and alfalfa). Within the respective probability density plots calculated over the whole image section (Figure 3.7f and g) this aspect manifests in bimodal distributions of C_{cx} and C_{ab}. Within retrieved C_{cx} values, the area of the 0.99 quantile is found within a plausible value range of 0-16 µg cm^{-2} in the displayed image section (Figure 3.7f). C_{ab} was modelled within a realistic range (1-84 µg cm^{-2}) with 60.6 µg cm^{-2} delimiting the 0.99 quantile (Figure 3.7g). As defined in Eq. (3.5), the lowest value that possibly will be returned is 1 µg cm^{-2}, leaving some room for uncertainty at very low C_{ab} contents. Results for C_w tend to be appropriate with regard to its leaf level representation in PROSPECT.

Canopy C_w (assumed as CWC (estimated) = C_w (estimated) $*$ LAI (measured)) falls into a range between 0 and 0.15 cm with 0.0162 cm delimiting the 99% quantile. Values above the 99% quantile indicate pixels with strong liquid water signals, where center-pivot irrigation systems were currently active at the time of image acquisition (e.g. alfalfa & corn fields). Probability density of C_w (Figure 3.7h) shows multiple peaks, which reflect prevailing water content conditions in the different crops with different growth stages.

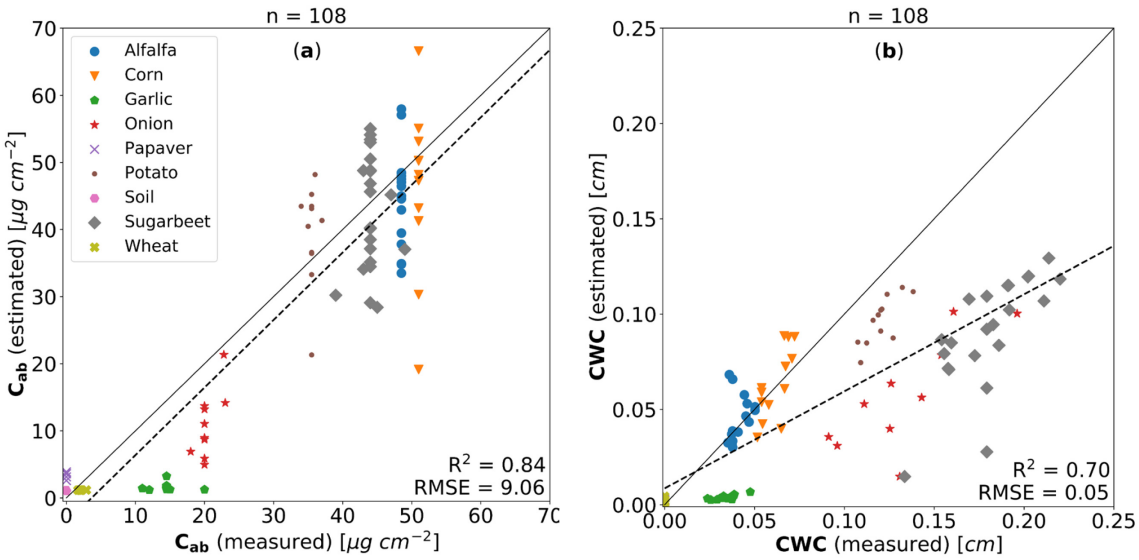

Figure 3.8. Measured C_{ab} (a) and CWC (b) per crop type compared to SIR-based model results of C_{ab} and CWC. Note that regarding C_{ab} measurements, only average values per field were available.

With regard to quantitative validation, C_{ab} measurements in the SPARC03 Campaign dataset are only available as multiple equal average values per field. Although in-field differing spectral signatures are therefore not reflected by single *in situ* data points, Figure 3.8a reveals good agreement between estimated C_{ab} and average C_{ab} per field (R^2 = 0.84, RMSE = 9.06 µg cm^{-2}). Obtained results are also more accurate than those received from ANGERS. CWC (Figure 3.8b) was estimated adequately for alfalfa and corn fields but underestimated for others depending on crop type and canopy structure (RMSE = 0.07 cm). Nevertheless, increasing crop specific water contents are reflected by higher CWC values in

the SIR results ($R^2 = 0.70$). Crop specific underestimations indicate discrepancies between the analyzed 970 nm signature and the scaling of measured leaf EWT to canopy level via the LAI.

3.3.4 AVIRIS-NG Data Application Example

Since the SIR Algorithm is designed to operate channel based, the bands closest to boundary wavelengths (460-1100 nm) and bands closest to dynamic segment limits are automatically detected. Based on this principle, the algorithm is applicable on hyperspectral data with different band and spectral specifications. Figure 3.9 shows 3-segment SIR and modelled C_{cx}, C_{ab}, and C_w results from AVIRIS-NG data acquired on 2nd July 2018 near Oberpfaffenhofen, Germany. Since no *in situ* data was obtained during overflights, the displayed imagery only exemplifies the applicability of the SIR approach on datasets of different sensory origin. Nevertheless, subsequent to AVIRIS-NG measurements, crop types were determined in the area of image acquisition. Similar to the 3-segment SIR RGB false color representation in SPARC03 Hymap data, crop types are optically distinguishable in terms of their individual C_{cx}, C_{ab}, and C_w relationships and RGB-manifestations (Figure 3.9a).

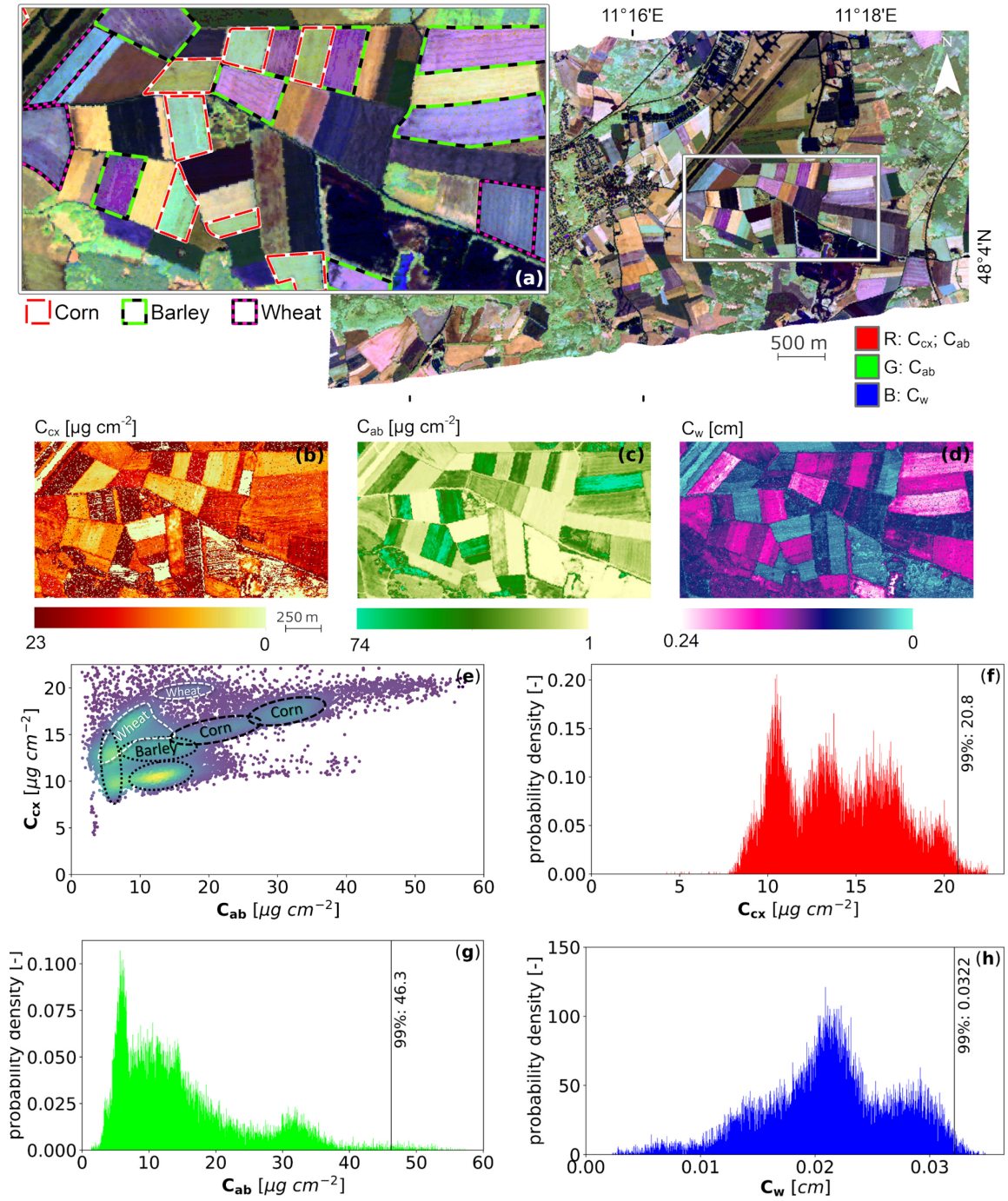

Figure 3.9. Sectional 3-band false color image of SIR results from AVIRIS-NG data (2nd July 2018, Oberpfaffenhofen, Germany) with cultivated crops in sectional zoom (a). Spatial results for $C_{cx} \leq 23$ µg cm^{-2} (b), C_{ab} (b), and C_w (c) as derived from SIR using Eqs. (3.6), (3.8), and (3.10). Extracted crop C_{ab}-C_{cx}-relation as colored Gaussian kernel densities for plausibility analysis with annotated crops (e). Probability density plots for retrieved C_{cx} (f), C_{ab} (g), and C_w (h). Values of $C_w > 0.035$ were omitted for better visibility.

While in corn, C_{ab} is dominant over C_{cx}, barley exhibits higher shares of C_{cx}. Wheat on the other hand is characterized by high C_w contents. Quantitative estimations of the three constituents from Eqs. (3.6), (3.8), and (3.10) lie within reasonable ranges (Figure 3.9b, c, d). Regarding C_{cx}, confidence in the results decreases with higher estimated contents due to the ambiguity of the present C_{cx}-C_{ab} fraction in Eq. (3.6). The C_{cx}-C_{ab}-relationship indicates

predominantly low C_{ab} conditions (Figure 3.9e) due to emerging senescence of cereals and early growth stage of corn. The low C_{ab} conditions are visible in the probability density of Figure 3.9g. Generally lower C_{ab} SIR values result in higher modelled C_{cx} (Figure 3.9f) compared to those retrieved from SPARC03 HyMap data (Figure 3.7f). Retrieved C_w results are consistent with results from SPARC03 HyMap data. The multimodal probability density of C_w is attributed to water content conditions of different crop types with e.g. wheat containing more water than barley and corn at the particular point of time and growth stage (Figure 3.9h).

3.4 Discussion

In this study, we propose the calculation of auto-delimited absorption integrals for the estimation of essential biochemical variables, such as carotenoid, chlorophyll and water content on both leaf and canopy level. Prior to evaluating the SIR approach, preliminary considerations influenced functioning and calibration of the algorithm, which finally resulted in Eqs. (3.5)-(3.10) that allow for quantitative estimation of C_{cx}, C_{ab}, and C_w from hyperspectral data.

3.4.1 LUT parameterization and physiological constraints

A pre-processing step of the study was the predefinition of ranges and distributions of PROSAIL parameters during the LUT-compilation process. Although selected ranges and distributions were in accordance with other studies (Borel 2009; Atzberger and Richter 2012; Locherer et al. 2015) and *in situ* observations of wheat and corn (Danner et al. 2017; Wocher et al. 2018; Danner et al. 2019), using such general LUTs might lead to biased estimations due to averaging over a wide range of possible leaf and canopy states. This constitutes a main problem when using LUTs: improbable spectra can be simulated based on unrealistic parameter combinations due to random drawing from broad range distributions. This issue has been addressed in our study by implementing physiological constraints, for instance in view of the natural dependence between C_{ab} and C_{cx} as manifested in the ANGERS leaf optical data (Féret et al. 2008). A similar relationship was discovered in the LOPEX dataset (Hosgood et al. 1995) and by other authors (e.g. Lichtenthaler and Buschmann 2001; Sims and Gamon 2002; Danson and Bowyer 2004; Hallik et al. 2017). The iterative redistribution of C_{cx} as a function of C_{ab} including upper (Eq. (3.1)) and lower (Eq. (3.2)) boundaries resulted in a more realistic distribution of C_{cx} within the LUT. Moreover, the strong correlation between C_{ab} and C_{cx} decreases with progressing senescence, since C_{ab} tends to decline more rapidly than C_{cx} (Merzlyak et al. 1999). Although residual C_{cx} was detected by SIR C_{cx}/C_{ab} in SPARC03 HyMap (Figure 3.7) and AVIRIS-NG imagery (Figure 3.9), a high degree of uncertainty must be expected when modelled C_{cx} is greater than modelled C_{ab}. Due to the linearity assumption between C_{cx} and C_{ab} and the applied C_{cx}-C_{ab} ratio, the model is not able to depict possibly higher C_{cx} contents than C_{ab} contents. Also, at non-vegetated

pixels, C_{cx} results might become noisy due to division of small value pairs.

Besides narrowing down the LUT to realistic green vegetation C_{cx}-C_{ab} ratios, one additional constraint was implemented with regards to the green peak wavelength position. Analysis of SPARC03 HyMap imagery (D'Urso et al. 2004), AVIRIS-NG imagery (Chapman et al. 2019) and field spectrometer data (Wocher et al. 2018) revealed that green peaks were never observed at wavelengths < 547 nm but nonetheless may occur within PROSAIL simulated reflectance at certain $C_{ab} > C_{cx}$ combinations ($C_{ab} \cong 5 * C_{cx}$). Hence, PROSAIL simulated spectra with green peaks < 547 nm were excluded from analysis. Physiological constraints were introduced by Yebra and Chuvieco (2009) (there referred to as ecological constraints) to achieve a more realistic representation of dependencies between fuel moisture content (FMC), C_{ab} and C_m in a LUT. Similar criteria were applied by Jurdao et al. (2013) regarding FMC and LAI.

3.4.2 Confounding Factors and other Sources of Uncertainties

Certain conditions negatively affect integration-based methods. For instance, at plants with high variability of C_{anth} (Gitelson et al. 2001), application of SIR is problematic due to a shift of the VIS reflectance peak towards the red wavelength region (Gitelson et al. 2009), which impacts retrieved quantities of C_{cx} and C_{ab}. The same applies for the brown pigments parameter C_{brown}, which alters both the shape of the green peak and the red edge (Danner et al. 2019). Also, external confounding factors on the canopy spectral signal such as soil background affect integration-based retrievals, particularly in C_{ab} sensitive wavelengths in the VNIR with a strong impact on parameter scaling from leaf to canopy level (Vuolo et al. 2008; Wang et al. 2017b). In canopies with low LAI, absorption by leaf C_{ab} is hampered through spectral mixing with underlying soil reflectance and thus leaf level C_{ab} is underestimated using absorption area ratios. For this reason, minimum LAI was assumed at 0.5 $m^2 m^{-2}$ to prevent occurrence of high C_{ab} at very low LAI in the PROSAIL LUT. Preliminary tests showed that consideration of LAI values < 0.5 m^2m^{-2} results in outliers with low C_{ab} SIR at moderate to high PROSAIL C_{ab} (Figure 3.5e). These outliers cause faster saturation of C_{ab} SIR values and thus a higher exponential regression slope constant in Eq. (3.6), leading to overestimation of measured C_{ab} at high LAI-C_{ab} combinations. Estimation of C_w is also affected by increasing LAIs which intensify the expression of the 970 nm water absorption band. The extent of this effect was reduced by referencing the absorption area to the continuum-maintained log-transformed reflectance in Eq. (3.4). Another external influence factor relates to surface moisture. Moist surface/canopy conditions, e.g. from dew or other intercepted water, increase the dimension of the 970 nm absorption leading to overestimation of C_w because cell internal liquid water cannot be separated from external moisture. This effect can be observed in the C_w spatial retrieval results at pixels close to currently running pivot irrigation systems (Figure 3.7d). Further, spectral signatures can change depending on sun-sensor-target geometries (Danner et al. 2017). Calibration of the SIR algorithm presumes nadir observations. At nadir, influence of

SZA on reflectance is relatively low at moderate angles (30-90°) but increases considerably at SZAs < 30° (Danner et al. 2017). Also, at tilted OZAs and co-dependent rAAs, possible hotspot effects may alter the reflectance signature. Therefore, the SIR algorithm requires reassessment for spectral measurements at oblique observation angles. It must also be noted that the quality of integration-based retrievals essentially depends on an accurate atmospheric correction of recorded reflected radiance at airborne or spaceborne remote sensors, particularly in the water vapor affected region between 900-1000 nm (Gao and Goetz 1990). Besides, to obtain consistent 3-segment SIR results, reflectance data preprocessing may also be subjected to spikes removal using smoothing filters (e.g. Savitzky-Golay filter).

3.4.3 Performance of Spectral Integral Ratios

Functionally, transforming reflectance by $log(R^{-1})$ for continuum removal and SIR calculation, increases the available data depth and amplifies small changes within the considered absorption features. This leads to sharpened absorption-related patterns in 3-segment SIR imagery. Yoder and Pettigrew-Crosby (1995) also found this effect with regard to increased R^2-values for narrowband spectral indices which was also confirmed by Gitelson et al. (2003). As reference for ratio formation, some studies promoted the maximum absorption depth obtained through continuum removal (Mutanga et al. 2005; Malenovský et al. 2006). However, during our analysis concerns were raised that a single defined maximum value may be prone to potential noise in measured reflectance data.

The presented SIR approach extends other integration-based approaches in two domains: the algorithm is (i) able to automatically separate the absorption features of C_{cx}, C_{ab}, and C_w. In this way, absorption feature spaces are completely captured despite shifting green peak and red edge positions. Simple integration-based indices with predetermined fixed ranges (as e.g. in Broge and Leblanc 2001; Delegido et al. 2010; Malenovský et al. 2006; Oppelt and Mauser 2004; Schlerf et al. 2010) are not able to take the shifting nature of absorptions into account. (ii) C_{cx} and C_{ab} related two-time referencing of the continuum removed absorption area to first, its envelope area, and second, the maximum absorption wavelength range, assures consistent scaling of the resulting index with increasing absorption (Eq. (3.3)). In contrast, continuum removal to retrieve C_w from 970 nm absorption is not recommended. Here, considering changes in LAI, the area subjacent to log-transformed reflectance was used as reference which reduced deviation of retrieved C_w (Eq. (3.4)). Further, log-transformed absorption features showed a lower tendency to saturation compared to using unchanged bidirectional reflectance.

The leaf-related Eqs. (3.5), (3.7), and (3.9) derived to retrieve C_{cx}, C_{ab}, and C_w from three dedicated SIR segments were validated on ANGERS leaf spectra with good results for C_{cx} ($R^2 = 0.86$; RMSE = 2.085 µg cm^{-2}) and C_w ($R^2 = 0.87$; RMSE = 0.007 cm), though less robust results for C_{ab} ($R^2 = 0.67$; RMSE = 12.5 µg cm^{-2}). One reason for the general overestimation of C_{ab} is that mainly woody species with high values of mesophyll structure

parameter N and dry matter content make up the samples in the ANGERS database (Jacquemoud et al. 2003; Féret et al. 2008). These high values were not adequately taken into account during LUT-compilation for reasons of the targeted general validity for agricultural applications. The same applies for potentially high C_{anth} contents in woody leaf species present within the ANGERS database like e.g. dogwood (*cornus alba*) or sycamore maple (*acer pseudoplatanus*) (Gitelson et al. 2009). In addition, the high diversity of sampled species also contributed to the high dispersion within estimated C_{ab} values. Retrievals of C_{cx} were more satisfactory than those of C_{ab} on leaf level: integration-based retrievals depend largely on the shape of reflectance, whose variability is less pronounced in the green peak region than in the NIR (Danner et al. 2019). Therefore, SIR based retrievals of C_{cx} are expected to be more stable in transition from leaf to canopy level which is observable in similar constants in Eqs. (3.5) and (3.6) and was also shown by Blackburn (1999) through stacking of leaves under a laboratory spectroradiometer.

Applied to HyMap and AVIRIS-NG spectrometric imagery, SIR results are encouraging in terms of plausible physical ranges of retrieved C_{cx}, C_{ab}, and C_w. Displaying 3-segment SIR as RGB imagery allows for intuitive interpretation of interactions between different biochemicals within fields or across different crops. Although only field averages of *in situ* measured C_{ab} were available for validation, SIR based estimations from SPARC03 HyMap data derived field internal variabilities and reflected the average field conditions ($R^2 = 0.84$; RMSE = 9.06 µg cm^{-2}) as observed in Figure 3.8a.

Regarding C_w (Figure 3.8b: $R^2 = 0.7$; RMSE = 0.05 cm), due to an increase of vegetation reflectance in the NIR, radiation can penetrate more deeply into the canopy (Newton and Blackman 1970; Lillesaeter 1982; Bull 1991; Sims and Gamon 2003). Although this comes along with advantages for canopy C_w retrievals at 970 nm (Wocher et al. 2018), the respective absorption feature is less pronounced in single leaf reflectance spectra due to high transmittance. This is indicated by the different regression slopes in C_w retrievals from PROSPECT (Eq. (3.9)) and PROSAIL (Eq. (3.10)). Wocher et al. (2018) also indicated, that estimations of canopy C_w largely depend on 970 nm radiation penetration through thick tissues and canopies. In case of densely growing sugar beet and potato, absorption at 970 nm might not be able to detect all the water contained in the canopy. On the other hand, underestimation of onion C_w can be attributed to high spectral influence of the underlying soil due to large leaf inclination angles. The shape of the 970 nm absorption can also be unfavorably altered by surface moisture, e.g. following irrigation.

Potentially, 3-segment SIR provides more information about vegetation vitality compared to individually considering single variables. In the sense of crop type specific interdependencies between C_{cx}, C_{ab}, and C_w, the suitability of 3-segment SIR to serve as endmember for crop type discrimination by machine learning should be tested. Results shown in our study were limited to specific acquisition dates. In the future, time series information mapped from actual or future imaging spectrometers (e.g. PRISMA, EnMAP,

SBG) may support 3-segment SIR based crop discrimination through incorporation of crop type and growth stage specific C_{cx}, C_{ab}, and C_w developments. In spite of the presented promising results, SIR based retrievals of C_{cx} need to be verified on canopy level against *in situ* measurements of airborne as well as spaceborne hyperspectral imagery.

Note that in our study we only focused on the performance of spectral integral ratios. The selection of this modelling approach was mainly based on the three advantages of (1) simplicity, (2) computational efficiency, (3) exploitation of full spectral bands. Hence, we aimed to demonstrate the applicability of HyMap (and AVIRIS data) to estimate biochemical traits in an efficient and reliable way for the first time using this specific approach. Comparing our method with different existing ones was beyond the scope of this study.

Finally, to deal with the high diversity of the LUT, smart sampling strategies also known as active learning (AL) could be implemented within a future study (Pasolli et al. 2012; Verrelst et al. 2020). To our knowledge, no study has applied AL heuristics to optimize LUTs for the purpose to optimize diversity of integration approaches. This could provide an efficient solution in view of developing cost-effective regression models within operational biochemical retrieval workflows.

3.5 Conclusion

A dynamic integral based model for the simultaneous retrieval of C_{cx}, C_{ab}, and C_w was developed that combines the computational advantage of parametric regression models with the robustness of RTM-based calibration and generality of multi-species leaf spectra validation. It was shown that multi-segment-SIR produced plausible results from RTM, leaf *in situ*, and airborne spectrometric data for all three biochemical variables that were investigated in this study. Nevertheless, a conclusive evaluation is needed based on spectrometric data and *in situ* measurements of C_{ab} and C_w, and particularly C_{cx} to address the uncertainties associated with C_{cx} SIR/C_{ab} SIR ratio. In the near future several imaging spectroscopy missions will finally generate continuous streams of hyperspectral spatio-temporal data. Thereupon, quantitative biochemical traits retrieval algorithms are needed that:

(1) are calibrated on realistic RTM-based LUTs to allow for transfers to diverse environmental conditions;
(2) derive robust estimations in a computationally efficient way from large datasets;
(3) have a transparent and accessible algorithmic design to be able to discuss both the underlying assumptions and quality of retrieval results;
(4) provide quick 'one-click' insights into the biochemical conditions of agricultural crops.

The SIR algorithm including optional RGB display of 3-segment SIR has been implemented into the 'Agricultural Applications' suite of the open source software EnMAP-Box 3 (van der Linden et al. 2015) as a slim and applicable tool supported by an intuitive graphical user interface. The tool 'Analyze Spectral Integral (ASI)' visualizes the convex hull from hyperspectral imagery and graphically assists with the adjustment of options for both the manual segmentation of absorption features and peak detection for SIR calculation. 3-segment SIR is applicable for any sensor with contiguous spectral coverage in the optical spectral domain between 460-1100 nm and thus enables quick and effective biochemical vegetation product retrieval from atmospherically corrected hyperspectral imagery.

Acknowledgments

The study was supported by the Space Agency of the German Aerospace Center (DLR) in the frame of the project "EnMAP Scientific Advisory Group Phase III—Developing the EnMAP Managed Vegetation Scientific Processor" through funding by the German Federal Ministry of Economic Affairs and Energy (BMWi) based on enactment of the German Bundestag under the grant code number 50EE1623. The responsibility for the content of this publication lies with the authors.

4 Paper III: Retrieval of Carbon Content and Biomass from Hyperspectral Imagery over Cultivated Areas

This study has been published in the *ISPRS Journal of Photogrammetry and Remote Sensing*:

Wocher, M., Berger, K., Verrelst, J., & Hank, T. (2022). Retrieval of carbon content and biomass from hyperspectral imagery over cultivated areas. *ISPRS Journal of Photogrammetry and Remote Sensing*, 193, 104-114. https://doi.org/10.1016/j.isprsjprs.2022.09.003.

Journal Impact Factor: 11.91 (2022)

Author Contributions: Conceptualization, M.W., K.B., and T.H.; Data curation, M.W.; Formal analysis, M.W.; Funding acquisition, T.H.; Investigation, M.W.; Methodology, M.W., K.B., and J.V.; Project administration, T.H.; Resources, M.W.; Software, J.V.; Supervision, T.H.; Validation, M.W.; Visualization, M.W.; Writing—original draft, M.W., K.B.; Writing—review & editing, M.W., K.B., J.V., and T.H.

Transition to Paper III: Paper III focuses on the retrieval of the three crucial variables dry and fresh biomass, as well as carbon content through application of dimensionality reduction, active learning, and the ML algorithm GPR. The study was performed in the framework of the project "EnVAL: supporting the hyperspectral satellite mission EnMAP through validation of algorithms for the retrieval of agriculturally relevant biochemical and biophysical information products" in collaboration with the Image Processing Lab (IPL) of the University of Valencia, Spain, contributing with the powerful MATLAB-based machine learning software suite Automated Radiative Transfer Model Operator (ARTMO). The presented method comprises three GPR models, trained over an optimized RTM-simulated database using PCA and AL approaches and tuned over the 4-years spanning *in situ* dataset acquired during the Munich-North-Isar (MNI) campaigns. The models achieved excellent performances for all three variables on an independent flight campaign dataset after adding bare soil spectra to the training database. Once established, these models can be easily applied to any spectrometric image data at high mapping speeds. The analysis of the results largely benefited from the uncertainty intervals that were provided by GPR. Alongside, a factor is presented that allows the conversion of the PROSPECT parameter CBC into area-based carbon content based on leaf-, stalk-, and fruit-separated carbon content measurements from the MNI campaigns. Additionally, previously gained experience regarding the establishment of PROSAIL databases led to the implementation of a physiological constraint regarding CBC content > protein content (C_p) as a knowledge-based addition to AL.

Abstract

Spaceborne imaging spectroscopy is a highly promising data source for all agricultural management and research disciplines that require spatio-temporal information on crop properties. Recently launched science-driven missions, such as the Environmental Mapping and Analysis Program (EnMAP), deliver unprecedented data from the Earth's surface. This new kind of data should be explored to develop robust retrieval schemes for deriving crucial variables from future routine missions. Therefore, we present a workflow for inferring crop carbon content (C_{area}), and aboveground dry and wet biomass (AGB_{dry}, AGB_{fresh}) from EnMAP data. To achieve this, a hybrid workflow was generated, combining radiative transfer modeling (RTM) with machine learning regression algorithms. The key concept involves: (1) coupling the RTMs PROSPECT-PRO and 4SAIL for simulation of a wide range of vegetation states, (2) using dimensionality reduction to deal with collinearity, (3) applying a semi-supervised active learning technique against a 4-years campaign dataset, followed by (4) training of a Gaussian process regression (GPR) machine learning algorithm and (5) validation with an independent *in situ* dataset acquired during the ESA Hypersense experiment campaign at a German test site. Internal validation of the GPR-C_{area} and GPR-AGB models achieved coefficients of determination (R^2) of 0.80 for C_{area} and 0.80, 0.71 for AGB_{dry} and AGB_{fresh}, respectively. The Mapping capability of these models was successfully demonstrated using airborne AVIRIS-NG hyperspectral imagery, which was spectrally resampled to EnMAP spectral properties. Plausible estimates were achieved over both bare and green fields after adding bare soil spectra to the training data. Validation over green winter wheat fields generated reliable estimates as suggested by low associated model uncertainties ($< 40\%$). These results suggest a high degree of model reliability for cultivated areas during active growth phases at canopy closure. Overall, our proposed carbon and biomass models based on EnMAP spectral sampling demonstrate a promising path toward the inference of these crucial variables over cultivated areas from future spaceborne operational hyperspectral missions.

4.1 Introduction

Quantification and knowledge of carbon-based plant constituents are crucial for all terrestrial ecosystems. Since the terrestrial biosphere is a significant sink for atmospheric CO_2, the carbon (C) stored in vegetation plays an important role for a balanced radiative budget and thus influences the global climate system (Denman et al. 2007; Kaminski et al. 2012; Paustian et al. 2019). Agricultural areas globally cover almost 40% of the terrestrial land surface, with one-third used as cropland, and two-thirds consisting of grasslands and pastures for grazing livestock (FAO 2022). Hence, there is a significant contribution of cultivated areas to the global CO_2 storage in form of soil organic carbon, influencing the soil C budget (Paustian et al. 2019). Atmospheric CO_2 is transferred into biotic and pedologic

C pools of the plant ecosystem, whereas C among others enters the soil via decomposition of roots or aboveground biomass (Jansson et al. 2021). Storing a vast amount of carbon, aboveground biomass thus presents a crucial ecological variable for evaluating potential changes of the climate system (Lu 2006; Fang et al. 2021). For this reason, it has been defined as one of the Essential Climate Variables (ECV) by the Global Climate Observing System (GCOS 2022). In the last decades, an unprecedented amount of Earth observation (EO) data with increasing spatial, temporal, and spectral resolution capabilities became available providing unique opportunities for deriving biomass and carbon contents. A particular focus was on operational multispectral systems, such as the Copernicus Sentinel-2 sensors of the European Space Agency (ESA) or their predecessors. However, multispectral data are limited in their ability to provide substantial information about plant carbon contents, mostly because the relevant absorption features in the shortwave infrared (SWIR) cannot be resolved by these sensors. At present we are approaching a new era of spaceborne imaging spectrometers, being already launched, under design or planned (Ustin and Middleton 2021). By means of these upcoming data streams, we will be able to timely monitor the state and dynamics of cultivated land in higher spectral detail, essential among others, for agricultural management systems (Hank et al. 2019). As opposed to multispectral data sources, hyperspectral sensors are capable of resolving subtle absorption features, such as those caused by specific pigments, proteins or carbon. Important scientific precursor missions include the PRecursore IperSpettrale della Missione Applicativa (PRISMA) (Loizzo et al. 2019), launched on 22nd March 2019, and the Environmental Mapping and Analysis Program (EnMAP) (Guanter et al. 2015), which entered into orbit on 1st April 2022. PRISMA and EnMAP will be followed by the operational NASA Surface Biology and Geology observing system (SBG) (National Academies of Sciences 2018) and the Copernicus Hyperspectral Imaging Mission for the Environment (CHIME) (Nieke and Rast 2019). Thus, new opportunities arise for the development of retrieval models for higher-level vegetation products from hyperspectral data.

In the last three decades, significant progress was achieved with improving leaf optical properties models, such as the PROSPECT family (Jacquemoud and Baret 1990; Féret et al. 2008; Féret et al. 2017). Féret et al. (2017) recently introduced carbon-based constituents (CBC) in the PROSPECT-PRO model version, differentiating the spectral contribution of dry matter content into the signals caused by proteins and CBC. The authors demonstrated that CBC can be successfully estimated from the optical properties of both fresh and dry leaves. To obtain such agriculturally relevant traits from satellite data, upscaling of simulated leaf optical properties to the canopy level is required, which is typically done by combining leaf and canopy radiative transfer models (RTMs). For instance, the PROSPECT-PRO model was coupled with the Scattering by Arbitrarily Inclined Leaves model (4SAIL) (Verhoef and Bach 2007) to PROSAIL-PRO by Berger et al. (2020a) and by Verrelst et al. (2021b) to simulate canopy nitrogen content (CNC). Inversion of the

model simulations is then required to estimate the crop properties of interest from received satellite signals. Traditional physically-based inversion, such as numerical optimization or look-up-table methods (Kimes et al. 2000; Vohland et al. 2010), relied on direct comparison of simulated against observed spectra through diverse cost functions (e.g., Verrelst et al. (2013a). However, the major drawback of these techniques is the high computational demand that makes them unsuitable for the real-time processing of large scenes, as they are now beginning to become available from hyperspectral satellites. Currently, efficient hybrid methods have become popular (Verrelst et al. 2015b; Verrelst et al. 2019), where machine learning (ML) regression algorithms are trained over simulated databases generated by means of these RTMs (e.g., Berger et al. 2020a; Brede et al. 2020; De Grave et al. 2020; Berger et al. 2021a; Danner et al. 2021; Verrelst et al. 2021b). Combining physical awareness with the inductive capabilities of data-driven ML approaches, these methods blend previous efforts and may soon be considered state-of-the-art for agricultural mapping activities and beyond (Baker et al. 2018; Verrelst et al. 2019; Svendsen et al. 2020; Machwitz et al. 2021). Straightforward parametric regressions making use of empirical relationships between spectral observations (or vegetation indices) and *in situ* measured variables (Glenn et al. 2008; Verrelst et al. 2015b) may be easily implemented and are computationally fast. However, these models depend on a mathematically continuous relationship between the variable of interest and its corresponding absorptive signal. Once established, parametric regressions clearly under-exploit the available spectral information of hyperspectral data and in addition lack transferability to other instruments and sites both temporally and spatially (Atzberger et al. 2011; Verrelst et al. 2019; Wocher et al. 2020). In respect to ML algorithms, in particular the Bayesian approaches of Gaussian process regression (GPR) (Rasmussen and Williams 2006) demonstrated high performances in the context of Earth observation regression problems (e.g., Verrelst et al. 2011; Zhou et al. 2018; Verrelst et al. 2020; Camacho et al. 2021; de Sá et al. 2021; Mateo-Sanchis et al. 2021). The high performance of GPR can be traced to theoretical and practical advantages specific to these algorithms, for instance, the design of appropriate covariance functions, enabling the inclusion of prior knowledge about the signal characteristics (Rasmussen and Williams 2006; Camps-Valls et al. 2016). GPR algorithms and established models further provide a particular advantage over other ML strategies: they deliver predictive variance or uncertainty intervals. In this way, the models provide quality information about their prediction capabilities, which is in particular interesting when transferring the models to other sites, sensors and vegetation types (Verrelst et al. 2013b). However, a drawback of GPR algorithms within hybrid retrieval schemes is that they come with a computational cost, especially when large training datasets are processed in the training phase (Rivera-Caicedo et al. 2017; Danner et al. 2021). This can be alleviated, for instance, by applying spectral dimensionality reduction, such as principal component analysis (PCA) (Jolliffe and Cadima 2016). Nonetheless, reduction in the spectral domain alone may not suffice in view

of the huge number of potentially redundant samples generated by RTMs. Therefore, optimization in the sampling domain is required as well. A solution to the sampling problem is given by semi-supervised approaches, also known as active learning (AL). Using diversity and uncertainty strategies, AL aims to optimize training datasets through intelligent sampling by means of an iterative procedure (Settles 2009; Berger et al. 2021c). Several studies successfully implemented AL techniques within hybrid retrieval workflows, for instance to estimate leaf biochemical variables and upscaled canopy-traits from Sentinel-2 top-of-canopy (Salinero-Delgado et al. 2021) and top-of-atmosphere data (Estévez et al. 2022), crop nitrogen content (Verrelst et al. 2020; Verrelst et al. 2021b), nonphotosynthetic crop biomass (Berger et al. 2021b) or multiple crop traits from the PRISMA (Tagliabue et al. 2022) or CHIME-simulated missions (Candiani et al. 2022). However, the majority of these studies incorporated the fully sampled ground datasets in the AL-tuning procedures, or found only a limited transferability of established models to independent datasets of other sites (Estévez et al. 2022). In view of the prioritization of specific variables by near-term operational missions, it remains to be investigated if hybrid models including AL heuristics can obtain sufficiently high and transferable retrieval performances.
Therefore, the objective of the current study was to evaluate the quantification and mapping of crop carbon content as well as wet and dry biomass from future EnMAP hyperspectral mission data. To achieve this, we employed *in situ* sampled field datasets from two different campaigns for model training, optimization, and independent testing, particularly focusing on the spectral configuration of the EnMAP sensor in preparation for future routine observations.

4.2 Materials and methods

4.2.1 Model Building Workflow

For the retrieval of crop carbon content (C_{area}), dry biomass (AGB_{dry}) and wet biomass (AGB_{fresh}) a hybrid approach was applied. Figure 4.1 schematically shows the workflow, which is itemized into seven main steps:

1. preparing a training dataset with PROSAIL-PRO;
2. reducing the dimensionality of full range spectral information using PCA;
3. applying active learning methods to condense and optimize the training sample pool;
4. training of GPR models and testing of internal model performance based on field campaign datasets;
5. improving mapping capability by adding bare soil spectra to the training database and retraining GPR models;
6. processing of airborne AVIRIS-NG spectrometric imagery;
7. validating retrieved carbon and biomass contents based on independent *in situ* data.

In the next sub-sections, these steps will be described in detail.

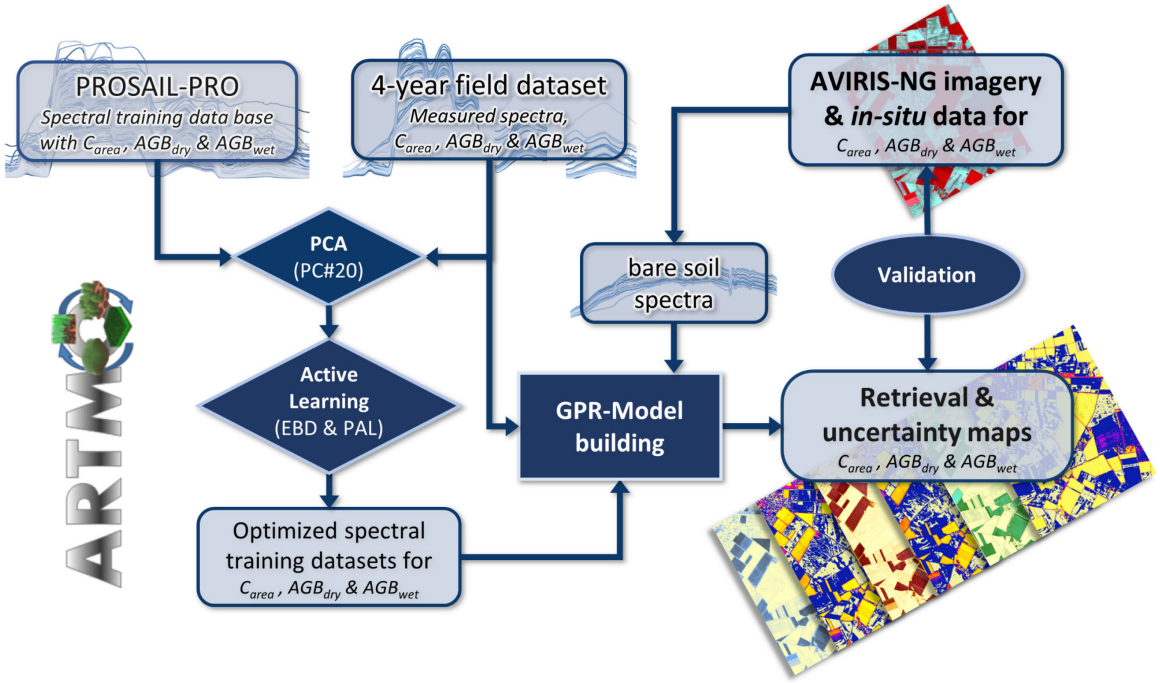

Figure 4.1: Schematic workflow for carbon and biomass mapping.

4.2.2 Field Campaign Dataset for Model Training and Validation

During the Munich-North-Isar (MNI) (Wocher et al. 2018) field campaigns in the years 2017, 2018, 2020, and 2021, hyperspectral signatures and plant traits from corn, winter wheat, and winter barley were collected weekly over the whole growing season on communal farmland 15 km north of Munich, Southern Germany. Spectral reflectance was measured from 350 to 2500 nm using an ASD FieldSpec 3 Jr at a height of one meter above the canopy. Field spectrometer data available at 1 nm spectral sampling interval was resampled to EnMAP band configuration according to pre-launch expected 242 spectral bands (423–2439 nm) (Guanter et al. 2015) with the further exclusion of nine bands in the visible to near-infrared (VNIR)-SWIR sensor overlap region (bands 89–98: 905–996 nm). This finally resulted in 233 bands at average full-width-half-maxima (FWHM) of 7.8 nm in the VNIR and 12.0 nm in the SWIR. Plant biomass samples were collected destructively, cutting an area of 0.25 m^2 at soil level. AGB_{fresh} and AGB_{dry} weights were determined separately for leaves, stalks, and fruits. Total AGB_{fresh} was weighed in the field and separately right after arrival in the laboratory. The samples then were oven-dried until constant weight for 24 h at 105°C before AGB_{dry} was determined. Furthermore, after milling of the samples, a CHNS-Analyzer (Elementar vario EL cube) was used to determine the carbon concentration (C_{mass}) of the samples in [%]. Afterwards, C_{area} in [g m^{-2}] of leaves, stalks and fruits were calculated by multiplying AGB_{dry} with C_{mass}. Based on preliminary tests and prior studies, model training and validation were focused on the sum of measured leaf + stalk contents as radiation is limited in penetrating thick tissues of plant fruit organs (refer to discussions

in Wocher et al. (2018); Berger et al. (2020a)). Leaf area index (LAI) in [$m^2\ m^{-2}$] was determined using a LI-COR LAI-2200C Plant Canopy Analyzer. A statistical summary of available *in situ* data is shown in Table 4.1.

Table 4.1: MNI site measured ranges (mean; standard deviation) and number of measurements (#N) for in situ leaf + stalk sums of C_{area}, AGB_{dry}, AGB_{fresh}, as well as LAI and BBCH growth stages determined according to Meier (2018). Values correspond to measurements with available spectral reflectance data.

Year	Crop Type	BBCH [-]	LAI [$m^2\ m^{-2}$]	C_{area} [$g\ m^{-2}$]	AGB_{dry} [$g\ m^{-2}$]	AGB_{fresh} [$g\ m^{-2}$]
2017	Winter wheat (#11)	25–87	1.6–6.2 (4.8; 1.6)	71–450 (338; 117)	70–988 (659; 316)	437–4059 (2993; 1332)
	Corn (#8)	30–85	0.2–3.9 (2.3; 1.4)	13–392 (150; 204)	26–872 (460; 334)	165–4361 (2712; 1605)
2018	Winter wheat (#7)	28–87	1.5–6.2 (4.8; 1.6)	56–534 (289; 203)	127–1205 (456; 651)	560–3632 (2046; 1134)
	Corn (#6)	32–83	1.8–3.6 (3.2; 0.7)	95–631 (425; 181)	236–1454 (964; 413)	2841–6720 (5496; 1376)
2020	Winter wheat (#13)	26–92	0.6–6.2 (3.9; 2.1)	28–579 (286; 176)	66–1313 (671; 388)	226–5706 (3211; 2042)
	Corn (#9)	11–80	0.1–3.1 (1.4; 1.4)	1–507 (191; 222)	3–1170 (439; 512)	25–6950 (2740; 3162)
2021	Winter wheat (#7)	26–85	0.4–4.6 (2.0; 1.7)	18–533 (190; 204)	41–1268 (440; 480)	168–5689 (1705; 2098)
	Winter barley (#5)	26–30	0.5–3.2 (1.5; 1.1)	29–169 (83; 54)	69–412 (132; 199)	319–2030 (943; 661)

4.2.3 Hypersense Experiment Campaign

In the context of the ESA CHIME mission preparations, Next Generation Airborne Visible Infrared Imaging Spectrometer (AVIRIS-NG) airborne hyperspectral images were acquired over the Irlbach site (48°49' N, 12°44' E), southeast Germany on 30th May 2021 in an area of intensive agriculture (Figure 4.2). The AVIRIS-NG instrument provides similar spectral properties as CHIME will have once in orbit. The campaign was managed by the University of Zurich, bringing the aircraft with the instrument from the USA to the Dübendorf airbase near Zurich in Switzerland. From there, measurement flights were performed with AVIRIS-NG over more than 20 test sites in Europe, among those the Irlbach site.

The AVIRIS-NG sensor recorded reflectance in the range from 377–2501 nm in 425 bands (FWHM ≈ 5.5 nm) at 5.3 m ground sampling distance (GSD) (Chapman et al. 2019). To comply with established retrieval models, spectrometric imagery likewise was resampled to 233 EnMAP spectral bands. Parallel to the overflight *in situ* measurements of C_{area}, AGB_{dry}, AGB_{fresh}, as well as LAI-sampling were carried out in the same manner as for MNI site (see chapter 4.2.2). Note that access was only possible to winter wheat fields at similar growth stages (stem elongation phase, no ears), limiting measured cross-field data variability. Nevertheless, the campaign generated a dataset to validate the GPR models independently of the model building process combining spectrometric imagery and 20 *in situ* data points (Table 4.2) of six fields.

Table 4.2: Irlbach site ranges (mean; sd) for 20 winter wheat measurements collected on 30th May 2021 of LAI and total C_{area}, AGB_{dry}, and AGB_{fresh}.

BBCH [-]	LAI [$m^2\ m^{-2}$]	C_{area} [$g\ m^{-2}$]	AGB_{dry} [$g\ m^{-2}$]	AGB_{fresh} [$g\ m^{-2}$]
32	2.5–4.8 (3.5; 0.7)	230–522 (334; 70)	543–1220 (796; 160)	1882–4020 (2968; 512)

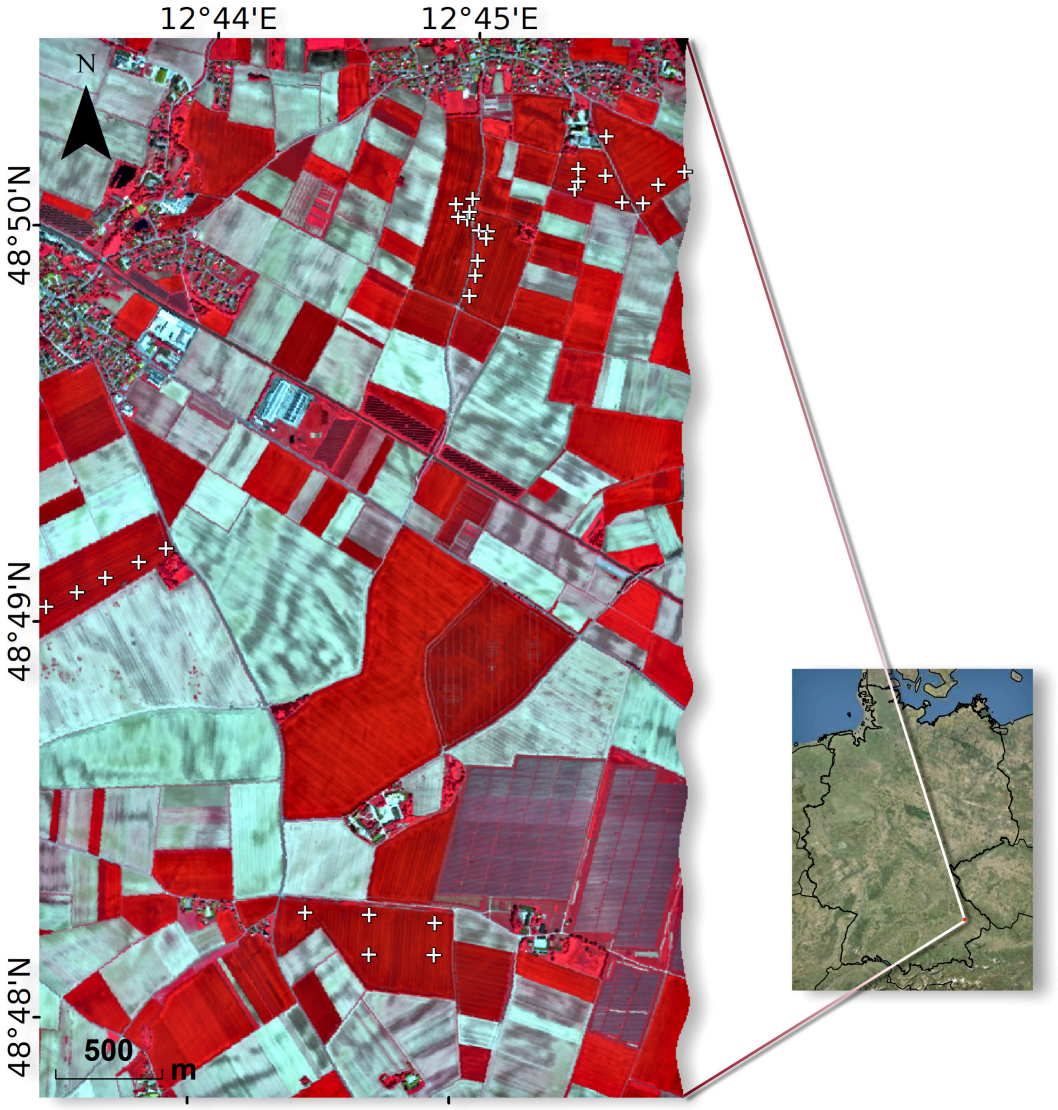

Figure 4.2: Location of the ESA CHIME site Irlbach in Southeastern Germany (Hypersense experiment campaign): false-color infrared section of AVIRIS-NG imagery covering winter wheat sampling points (crosses) on 30th May 2021.

4.2.4 Radiative Transfer Modeling and Synthetic Training Database

For the hybrid model building process, first, a PROSAIL-PRO training database was generated. PROSAIL (Jacquemoud et al. 2009) combines the *Leaf Optical Properties Spectra* model PROSPECT (Jacquemoud and Baret 1990) and the turbid medium canopy reflectance model 4SAIL: *Scattering by Arbitrarily Inclined Leaves* (Verhoef and Bach 2007). The leaf RTM version PROSPECT-D (Féret et al. 2017) simulates reflectance and transmittance of leaves in the optical domain as a function of leaf pigments, i.e. chlorophyll a and b (C_{ab}), carotenoids (C_{cx}), and anthocyanins (C_{anth}), a leaf mesophyll structure parameter (N), brown pigments (C_{brown}) and equivalent water thickness (C_w) as well as leaf dry matter content (C_m). In the latest recalibrated version PROSPECT-PRO (Féret et al. 2021), C_m was separated into nitrogen-containing proteins (C_p) and carbon-based

constituents (CBC), which include both non-structural carbohydrates (sugars and starch) as well as lignin, cellulose, and hemicellulose, each having a specific carbon content (Ma et al. 2018). Therefore, in order to retrieve carbon content from spectral observations, a conversion factor needs to be implemented. Based on measurements of C_{mass} during the MNI-campaigns and in accordance with similar findings of Ma et al. (2018), this factor is set to 2.31 (see Eq. (4.1), representing mean C_{mass} (43.3%) of leaves (43.8%), stalks (42.1%), and fruits (43.9%).

To upscale optical properties from leaf to canopy-level and to account for structural effects, the 4SAIL model was employed. 4SAIL simulates the bi-directional reflectance factor of a plant turbid medium (Jacquemoud et al. 2009) as a function of LAI, brightness of the underlying soil (p_{soil}), average leaf inclination angle (ALA) or optionally, ellipsoidal leaf inclination distribution (LIDF), and hot spot size (h_{spot}) for a given illumination and viewing geometry (observation zenith angle (OZA), relative azimuth angle (rAA) between sun and sensor, and the solar zenith angle (SZA)).

Table 4.3: Parameter ranges for generating the PROSPECT-PRO + 4SAIL (PROSAIL-PRO) training database. Specified ranges are uniformly (range) or Gauss-distributed (mean; sd), and single values are fixed.

PROSPECT-PRO parameters	Range	Notation [Unit]	4SAIL parameters	Range	Notation [Unit]
N	1.0–3.0	[-]	LAI	0.01–6.5 (4.0; 2.0)	[m^2 m^{-2}]
C_{ab}	0–60	[µg cm^{-2}]	ALA	30–70	[deg]
C_w	0.001–0.06	[g cm^{-2}]	h_{spot}	0.01–0.5	[-]
C_p	0.0–0.0025	[g cm^{-2}]	SZA	40	[deg]
CBC	0.0–0.03 (0.01; 0.02)	[g cm^{-2}]	OZA	0	[deg]
C_{brown}	0.0–0.8	[-]	rAA	0	[deg]
C_{cx}	C_{ab}-dependent[a]	[µg cm^{-2}]	p_{soil}	0.0–1.0	[-]
C_{anth}	0.0–2.0	[µg cm^{-2}]			

[a] according to Wocher et al. (2020)

For the simulation and correct representation of diverse crop states, parameters were varied over a wide value range (Table 4.3). Ranges were set based on prior knowledge of the authors and previous studies (Wocher et al. 2020; Berger et al. 2021b; Berger et al. 2021c; Danner et al. 2021; Verrelst et al. 2021b). The key parameters CBC and LAI were sampled according to a Gaussian distribution to realistically reflect measured patterns during the growth cycle. This sampling strategy is common practice in retrieval studies and leads to valid and generic models, as e.g., demonstrated by (Berger et al. 2018c). For the acquisition angles, fixed values in nadir view at 40° SZA were assumed to prevent the occurrence of hot spot effects in simulated spectra. To allow the global applicability of the models, all other parameters were sampled uniformly. Since both LAI and CBC show an impact on reflectance over the entire optical domain, the full spectral range is considered for model training. In terms of practical applicability, data homogeneity, as well as reduction of computational effort, PROSAIL 1 nm reflectance output was resampled to EnMAP

spectral resolution @233 bands. Due to a large number of parameter variations, the training database size was set to 3000 members. To further reduce inherent unrealistic combinations of input parameters within the training database (Yebra and Chuvieco 2009), entries with $C_p > CBC$ were considered implausible and were deleted, resulting in a model training database of 2868 members.

Thus, to derive canopy carbon and biomass from imaging spectroscopy data the corresponding PROSPECT-PRO parameters were upscaled according to Eqs. (4.1), (4.2), and (4.3):

$$C_{area} = \frac{CBC * LAI * 10{,}000}{2.31} \ [g\ m^{-2}] \tag{4.1}$$

$$AGB_{dry} = (C_p + CBC) * LAI * 10{,}000 \ [g\ m^{-2}] \tag{4.2}$$

$$AGB_{fresh} = (C_p + CBC + C_w) * LAI * 10{,}000 \ [g\ m^{-2}] \tag{4.3}$$

As a last step, simulated C_{area}, AGB_{dry} and AGB_{fresh} distributions were compared and verified against *in situ* leaf + stalk sums to ensure broad coverage of simulated against measured value ranges. PROSAIL-PRO training database generation was performed using the 'Create Look-up-Table' tool provided within the open source software EnMAP Box 3 (van der Linden et al. 2015) 'Agricultural Applications' (Hank et al. 2021).

4.2.5 Spectral and Sampling Optimization

To boost processing speed, PCA was applied. PCA is a useful technique to reduce the dimensionality of datasets which the in case of hyperspectral reflectance data manifests in radiometric collinearity issues (Kumar 1975; Verrelst et al. 2019) between multiple close adjacent spectral bands. With PCA, measured and simulated reflectance spectra are converted into a lower-dimensional feature space, maximizing algorithmic interpretability and minimizing information loss (Jolliffe and Cadima 2016; Verrelst et al. 2016a; Rivera-Caicedo et al. 2017). In accordance with previous studies that used PCA to retrieve vegetation traits from hyperspectral data (De Grave et al. 2020; Morata et al. 2021; Verrelst et al. 2021a; Pascual-Venteo et al. 2022), the number of principal components (PCs) was set to #20. Pascual-Venteo et al. (2022) demonstrated that the first components may provide significant relevance, but the most important features are located in higher components, depending on the targeted variable. Hence, this number is considered as an acceptable trade-off between a sufficient representation of full optical range spectral variability and calculation effort during model training (Morata et al. 2021). Prior internal tests also showed that the inclusion of more than 20 PCs did not contribute to further error reduction.

Training databases created by random sampling of model input parameters result in redundancies of both the contained spectral representations and within the parameter set itself. Furthermore, large training databases drastically decrease the processing speed of the

training process and inherently imply an aggravation of parameter ill-posedness, i.e. the probability of multiple different parameter sets defining similar spectral responses. To counteract these issues, AL techniques (Verrelst et al. 2020; Berger et al. 2021c) were deployed. Specifically, two algorithms were tested. First, the Euclidian distance-based diversity (EBD) strategy proved suitable both in terms of processing speed and accuracy (Douak et al. 2013), whereas sampling candidates are selected based on the squared Euclidean distance to a sample already contained in the training set. Second, the variance-based pool of regressors (PAL) strategy was applied. PAL predicts the target value by means of a respective ML regression algorithm based on multiple training subsets, computes the variance of the predictions by the resulting regressors, and finally adds the samples with the greater disagreements. Although PAL proved to require more computing time then other AL methods, it often performed superior in terms of retrieval accuracy (Douak et al. 2013; Verrelst et al. 2016a). Both EBD and PAL were initialized based on 2% (N = 58) randomly selected members of the training database and with a maximum selection of 300 spectra as a stopping criterion. These thresholds were chosen according to internal tests, experience of the authors and recommendations of prior studies (Verrelst et al. 2020; Berger et al. 2021c; Verrelst et al. 2021b). With each sample added, overall accuracy against *in situ* data was evaluated by the root mean square error (RMSE). By this crosscheck, only samples that contribute to an improved RMSE are included in the reduced database. The iteration continued until all samples of the training database were evaluated.

Adequate and accurate mapping of C_{area}, AGB_{dry}, and AGB_{fresh} using full scenes of future satellite imagery is the primary focus of this study. Hence, subsequent to the initial internal model performance evaluation, 24 bare soil spectra with defined respective variable contents of zero were selected from the AVIRIS-NG image and were added to the training database. The number of 24 spectra was chosen in accordance with the study by Verrelst et al. (2021b). In this way, mapping uncertainties due to unknown soil signatures can be reduced by augmenting the models' ability to distinguish between bare soil and sparsely vegetated pixels.

4.2.6 Machine Learning Regression Algorithm

The regression algorithm used within this study was based on GPR as formulated by Rasmussen and Williams (2006). Along with proven solid performances, as demonstrated in various previous studies (Verrelst et al. 2011; Verrelst et al. 2015b; Camps-Valls et al. 2019; Berger et al. 2021b; Pipia et al. 2021), GPR provides analytical estimates of predictive uncertainties together with the variable estimates. Due to their probabilistic handling of regression tasks in a Bayesian framework, the provision of relative uncertainties as prediction intervals renders GPR particularly attractive for solving highly nonlinear regression problems within remote sensing data analysis (Verrelst et al. 2019). Analyzing these prediction intervals enables useful insights into uncertainties of model parameterization and input data. Moreover, information about uncertainties can be used to

assess the transferability of the models to other locations and times (Verrelst et al. 2013b). A downside of GPR is its limited ability to process large samples of several thousand within reasonable running time due to its time complexity of $\mathcal{O}(n^3)$ by inversion of a $n \times n$ matrix (Rasmussen and Williams 2006). Although previous studies suggested training datasets of only 1000 samples (Lázaro-Gredilla et al. 2013; Berger et al. 2021b), in preliminary tests, this number turned out to be too small to cover the possible spectral variability produced by the here considered PROSAIL-PRO parameter range definitions. Since one training database as a single generally valid baseline for all three target variables (and potentially others) is aimed, the decision was made to increase the size of the training database to 3000. This size still led to tolerable processing times of ~12 min on an intel i7-10700 @2.9 GHz when using a standard configuration of a squared exponential covariance (kernel) function Gaussian process. The implementation of GPR models, as well as PCA dimensionality reduction, AL strategies, and mapping, were provided within the Automated Radiative Transfer Models Operator (ARTMO) machine learning regression algorithms (MLRA) toolbox (Verrelst et al. 2012).

4.3 Results

4.3.1 AL-tuning and Validation over MNI Site

First of all, the selected PROSAIL-PRO spectra were compressed into 20 PCs to efficiently reduce the processing speed for GPR models. In the second step, AL was applied to optimize the training datasets in the sampling domain for the GPR algorithm and model-building process. The predictive power of the models is assessed using absolute RMSE and normalized RMSE (nRMSE [%] = RMSE/measured value range $*$ 100) for model intercomparison, as well as the coefficient of determination (R^2) to evaluate goodness-of-fit. Figure 4.3 illustrates the RMSE convergence results of PAL and EBD methods regarding retrieval of MNI *in situ* data during GPR training. For all three variables of interest, PAL performed better than EBD with highest discrepancy for AGB_{fresh}, where PAL reached a RMSE of 1153 g m^{-2} compared to 1236 g m^{-2} with EBD (Figure 4.3c) after iterative selection of 300 samples. For C_{area} (Figure 4.3a) and AGB_{dry} (Figure 4.3b), PAL reduced RMSE from initially 190 and 423 g m^{-2} to 85 (EBD: 88) and 190 g m^{-2} (EBD: 198), respectively. Although the PAL sequence needed ~10 times longer than EBD to select the most suitable spectral samples from the training database, it was chosen as the optimal AL method due to its consistent best performance. Overall, AL reduced the size of the training database from 2868 samples by 88% to 358 samples.

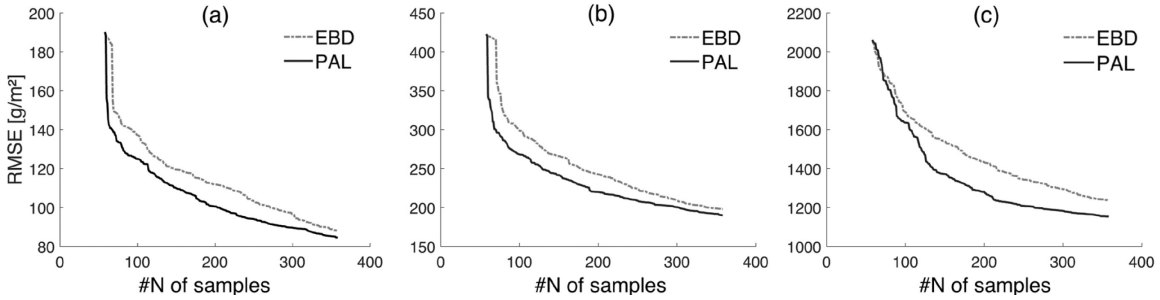

Figure 4.3: RMSE convergence for C_{area} (a), AGB_{dry} (b) and AGB_{fresh} (c) applying EBD and PAL methods on a full PROSAIL-PRO training database (i.e., 2868 samples) against MNI in situ data.

The performance of the models against MNI *in situ* data after reduction of the training database using PAL are shown in Figure 4.4. For C_{area} and AGB_{dry} good results were obtained ($R^2 = 0.80$; nRMSE = 13% for both; Figure 4.4a and b). For AGB_{fresh} (Figure 4.4c) retrieval performance is lower but still acceptable ($R^2 = 0.71$; nRMSE = 16%). Generally, the GPR models succeeded in estimating all three variables, but with a slight tendency to underestimate higher contents. Particularly for AGB_{fresh}, this underestimation may be connected to saturation effects of high specific concentrations in the respective measured spectral signals. Regarding GPR uncertainty intervals, for most data points, predicted value ranges are relatively stable with a coefficient of variation (CV) below 35%. Note that naturally, high CV values mostly correspond to low absolute values. However, some points with a high relative uncertainty in the higher value range may indicate that *in situ* measured quantities poorly correspond to the spectral acquisition on that particular day and spot. Despite these predictive uncertainties, GPR is able to successfully incorporate these data points into the regression scheme. Besides, the models' performances were clearly affected by the abundant availability of *in situ* data covering four full seasons (N = 66). The attempt of using only two years (2017 and 2018; N = 32) for training and keeping the years 2020 and 2021 (N = 34) for validation, yielded lower performing GPR models for C_{area} ($R^2 = 0.71$) and AGB_{dry} ($R^2 = 0.65$), and even failed for AGB_{fresh} ($R^2 = 0.01$).

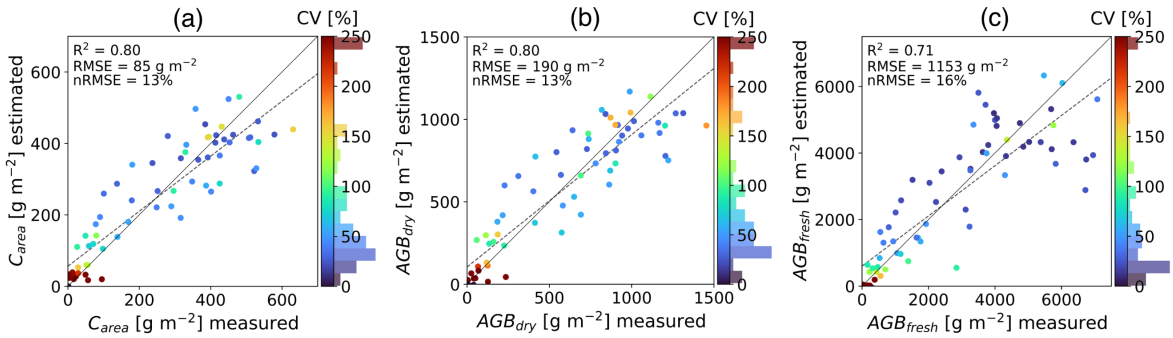

Figure 4.4: GPR validation results against MNI in situ data for C_{area} (a), AGB_{dry} (b), and AGB_{fresh} (c) using GPR retrieval models built on optimized PCA and PAL training databases. Relative uncertainty is expressed as coefficient of variation (CV), i.e. standard deviation/mean $*$ 100 [%]. CV frequency distributions are indicated as colored bars.

4.3.2 Optimizing GPR-C_{area} and GPR-Biomass Models for Mapping Activities

The GPR retrieval models were prepared for mapping by including 24 bare soil spectra in each PAL-reduced training database. The GPR algorithms were then retrained based on the optimized training datasets composed of 382 samples (random 58 initial 2% + 300 PAL-selected + 24 bare soils) for each of the three variables. Results are shown in Figure 4.5. In spite of increased nRMSE and point spread for C_{area} ($R^2 = 0.76$; nRMSE = 17%; Figure 4.5a) and AGB_{dry} ($R^2 = 0.72$; nRMSE = 18%; Figure 4.5b), underestimation of high contents does no longer occur. Additionally, mean relative uncertainties decreased by 40% for C_{area} and 38% for AGB_{dry}, being indicative of the models' improved ability to differentiate between soil spectral influence, the crop signal, and particularly the signal of crop senescence. However, this does not apply for AGB_{fresh} (Figure 4.5c), where prediction performance with added bare soil spectra changed only marginally and the tendency to underestimation is not resolved. Here, mean relative uncertainty decreased by 12%.

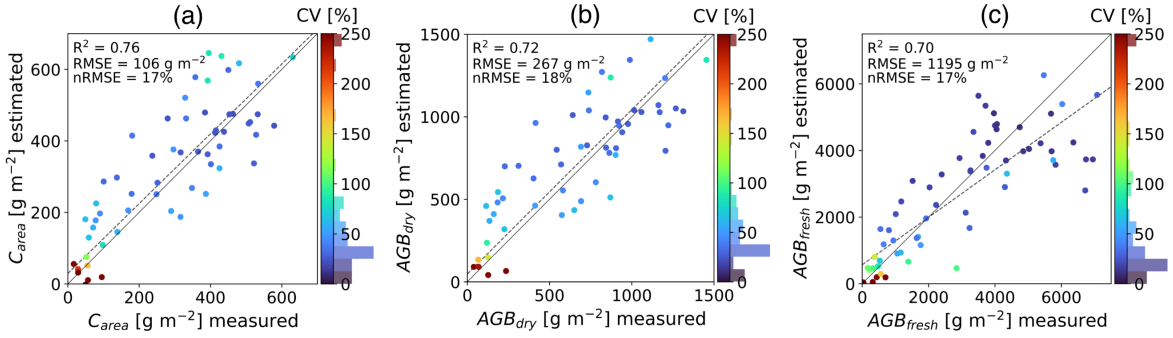

Figure 4.5: Performance of final GPR-C_{area} (a), GPR-AGB_{dry} (b), and GPR-AGB_{fresh} (c) models against MNI in situ data and predictive relative uncertainties. CV frequency distributions are indicated as colored bars.

4.3.3 Validation over Irlbach Site

Subsequent to retraining with added bare soil spectra, the GPR-C_{area}, GPR-AGB_{dry}, and GPR-AGB_{fresh} models were applied to AVIRIS-NG imagery (spectrally resampled to

EnMAP). The resulting maps show that all three variables were derived with appropriate plausibility (Figure 4.6a, b, c (left)). Due to the small GSD of 5.3 m, which was maintained from the airborne campaign and was not converted to EnMAP 30 m spatial resolution, the results adequately reflect within-field heterogeneities attributable to expositional and/or soil related site factors as well as to row sowing structure of the fields. Furthermore, fine cross-field variations of the mapped contents can be identified. As it can also be recognized in the probability density histograms, high contents indicate lush green cereal crops (mostly winter wheat and winter barley), as typically present in this region at the end of May. Also, many fields are still barely vegetated (corn and sugar beet). Yet, the retrieval models succeeded in discerning bare soil from recently sprouted crops, notable as fine lines of low particular contents in these fields.

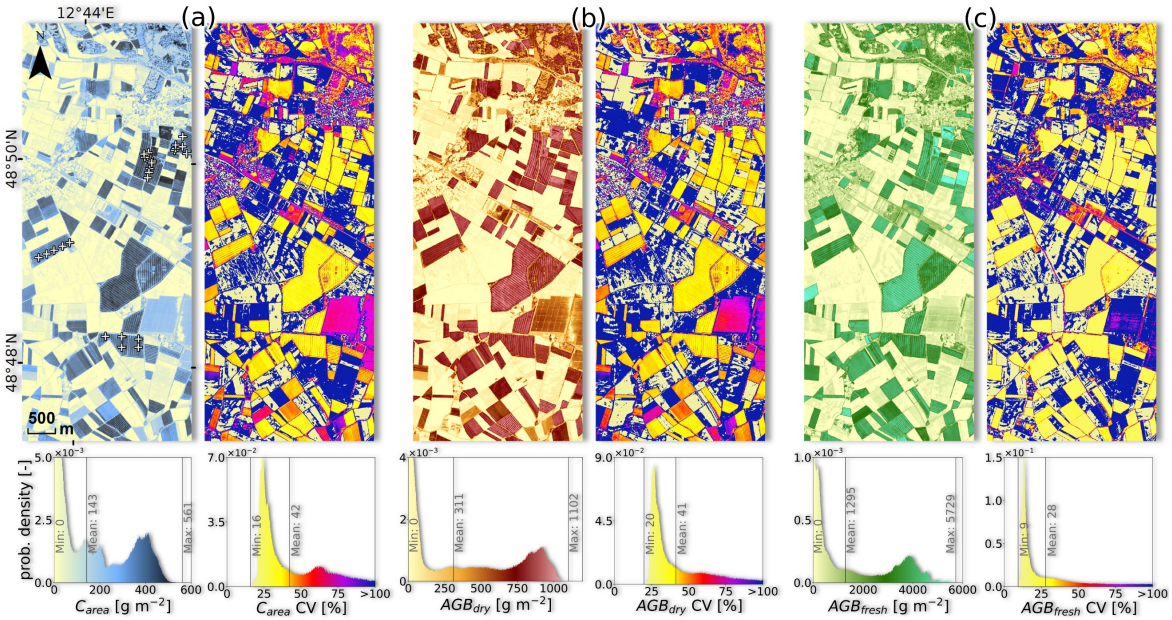

Figure 4.6: Mapping results and relative uncertainties (CV) for C_{area} (a), AGB_{dry} (b), and AGB_{fresh} (c) with spatial probability density distributions applying established GPR-C_{area} and GPR-Biomass models on EnMAP resampled AVIRIS-NG imagery of Irlbach site from 30th May 2021.

Relative uncertainties are presented in Figure 4.6a, b, c (right). Uncertainties for green fields were consistently low ($< 40\%$, yellow colored), and low uncertainties of unambiguously identified bare soil pixels illustrate the importance of adding bare soil spectra to the training database. High degrees of relative uncertainty ($> 50\%$, red to $> 100\%$, blue colored) mostly occurred in scarcely vegetated areas where, nonetheless, absolute contents were correctly recognized as low. However, high uncertainties prevailed in areas which spectrally were not considered by the training database, such as anthropogenic structures and forests.

Comparison of pixel-based estimates and *in situ* measured quantities (Figure 4.7) shows that regarding the mean estimates, all three variables tended to be overestimated with nRMSEs for $C_{area} = 29\%$, $AGB_{dry} = 25\%$, and $AGB_{fresh} = 36\%$. However, considering that biomass measurements of winter wheat at similar growth stages feature such large variations

themselves, these variations are well reflected by the range of the estimates. Only for AGB_{dry} maximum estimated values appear limited resulting in underestimation of high *in situ* measured contents (Figure 4.7b). With respect to absolute RMSEs, these were even lower by 20% for C_{area} (85 g m^{-2}), 36% for AGB_{dry} (170 g m^{-2}), and 35% for AGB_{fresh} (770 g m^{-2}) than compared to the final training results (Figure 4.5).

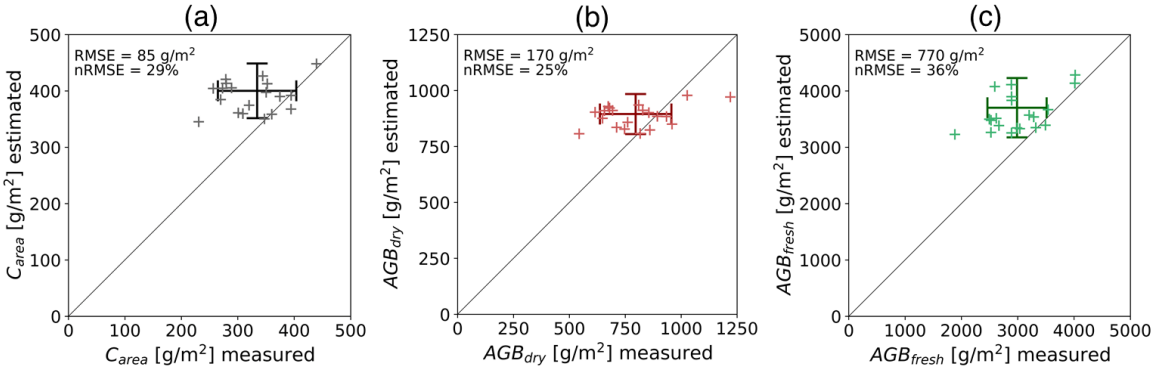

Figure 4.7: Validation of the carbon and biomass maps obtained for the Irlbach area against winter wheat in situ data for C_{area} (a), AGB_{dry} (b), and AGB_{fresh} (c). Single measurements are displayed as small crosses, measurement and estimation means and standard deviations are shown as large crosses.

4.4 Discussion

In this study, we adapted a hybrid workflow for the retrieval of plant carbon content as well as dry and wet biomass from simulated EnMAP data. In the following, the key findings are discussed, involving: (1) active learning and spectral dimensionality reduction, (2) carbon and biomass mapping, and (3) opportunities and challenges for the EnMAP mission.

4.4.1 Active Learning and Spectral Dimensionality Reduction

A key result of our study is that all three retrieval models could be better optimized by applying the AL method PAL than EBD. This is contrasting to previous studies identifying the EBD method as most the accurate and fastest (e.g., Upreti et al. 2019; Verrelst et al. 2020), see also review by Berger et al. (2021c). Comparing both methods, we showed that EBD outperformed PAL with respect to computation time for the learning process but not in terms of optimization accuracy as was also demonstrated by Douak et al. (2013). This aspect should be considered when using kernel-based methods, such as GPR, for establishing operational retrieval models. Nonetheless, both approaches provided significant improvements over using full data sets and consequently, we can recommend the implementation of both, regressor uncertainty (e.g. PAL) or diversity AL methods (e.g. EBD), into hybrid workflows. The consideration of AL in the processing chain leads to small but representative training data sets (here 88% training database size reduction; 358 members instead of 2868) and thus to efficient and lightweight models to estimate the

variables of interest. It must be noted that involving *in situ* data for tuning retrieval models may bring the drawback of decreasing the models' transferability. However, obtained results revealed that our AL optimized models performed relatively well when transferring them to another location and sensor, as done here from handheld spectrometer measurements at the MNI site (data used for AL tuning) to EnMAP-resampled airborne AVIRIS-NG imagery at the Irlbach site (independent validation). Similar findings are reported by Tagliabue et al. (2022), who provided fairly robust and exportable AL-tuned models for multiple leaf and canopy level traits. Still, a more versatile validation *in situ* dataset covering diverse crop types sampled during different growth stages at different geographical sites would be required to ensure the generation of overall robust retrieval models. This so far has been limited by the monotemporal character of airborne campaigns and is likely to be resolved now as hyperspectral satellites will provide regular observations.

Multiple studies focused on hybrid retrieval algorithms in combination with PCA for the retrieval of various vegetation variables (e.g., Rivera-Caicedo et al. 2017; De Grave et al. 2020; Verrelst et al. 2020; Berger et al. 2021b; Danner et al. 2021; Candiani et al. 2022; Pascual-Venteo et al. 2022; Tagliabue et al. 2022). The feature transformation approach PCA provides the attractive property of converting full range spectral information from the imaging spectrometer into a defined number of unique components while disregarding the target variables. This leads to a richer dataset for the training of machine learning algorithms compared to selecting a few bands, based on feature extraction approaches (Rivera-Caicedo et al. 2017; Berger et al. 2020a). However, the question of the optimal number of components to resolve a prediction problem remained to be clarified. In a recent study, this number was investigated, leading to the result that 18 components covered 99.95% of the variance (Pascual-Venteo et al. 2022). This confirmed prior studies demonstrating that 20 PCs represent an optimal compromise to ensure high retrieval performance for targeting diverse variables and at the same time avoiding the risks of exploring noisy data (Danner et al. 2021; Morata et al. 2021; Verrelst et al. 2021b).

In this study, we successfully applied GPR as a core retrieval algorithm, which shows potential to be implemented into the EnMAP-Box software to solve agriculturally relevant retrieval problems. GPR has provided outstanding performances in multiple studies (Verrelst et al. 2013b; Camps-Valls et al. 2016; Camps-Valls et al. 2018; Camps-Valls et al. 2019; Estévez et al. 2021; Estévez et al. 2022) and also provides the particular capability of providing uncertainty estimates along with the estimations (Verrelst et al. 2013a). Nonetheless, other machine learning regression algorithms could be tested in a future setup, such as random forest regression or powerful designs of artificial neural networks, provided that uncertainty measures can be made available along with the model results.

4.4.2 Carbon and Biomass Mapping

Apart from a physical evaluation of our models, we also investigated the spatial portability of our approach through mapping of C_{area}, AGB_{dry}, and AGB_{fresh} over an

agricultural area using airborne hyperspectral imagery.

Provided relative uncertainties add information about GPR model internal stability and confidence, as demonstrated in Figure 4.6a, b, c (right). The consistent low uncertainties for green fields indicate a high degree of model reliability for cultivated areas during phases of active growth at canopy closure. Also, the obtained plausible low contents and low uncertainties for bare soil pixels that were returned by the models illustrate the importance of adding bare soil spectra to the training database. Note that adding bare soil spectra directly from the considered imagery may reduce transferability to other observations. However, preliminary mapping tests without consideration of bare soil spectra led to overestimated quantities with high uncertainties at bare soil locations. Anthropogenically influenced and forested areas provided lower confidence, i.e. higher uncertainty estimates, since these areas were not included by the training database, which was generated using PROSAIL-PRO assuming uniform turbid medium plant canopies (Berger et al. 2018d).

Given the high confidence of these maps, in principle they can be further used within prognostic models for the simulation of terrestrial carbon fluxes. These models may strongly be supported by assimilating observational information, such as plant carbon content, resulting in reduced uncertainty of carbon balance simulations. Ingesting the spatial and temporal dynamics, which are contained in Earth Observation data into prognostic models, can provide a better understanding of the terrestrial carbon sinks. Results of these models then may contribute to efficient management strategies, such as in agriculture, to mitigate climate change and related severe effects to the environment (Kaminski et al. 2012). Future operational retrieval schemes can build upon the proposed workflow to monitor plant carbon content relevant for multiple topics in cropping systems. These include for instance improved knowledge about the potential of carbon farming, i.e. soil carbon sequestration methods as a negative emission strategy (Paustian et al. 2019; Jansson et al. 2021).
Dry biomass, also known as lignocellulosic biomass, further provides opportunities for production of renewable liquid fuels (Welker et al. 2015). Hereby, thermochemical conversion can be used as an efficient method to convert biomass into biofuels (Zhang and Zhang 2019). Since lignocellulosic material for biofuel and biochemical production may reduce CO_2 emissions (Stigka et al. 2014), the spatio-temporal mapping over vast agricultural regions supports activities towards climate change mitigation.

4.4.3 Opportunities and Challenges for the EnMAP mission

This work was carried out within the activities of the hyperspectral EnMAP mission preparation for agricultural applications (Hank et al. 2019; Danner et al. 2021). The German hyperspectral mission has been prepared for many years until final launch on 1st April 2022. From experience with prior hyperspectral sensors, such as Hyperion installed on NASA's EarthObserver-1 satellite, the signal-to-noise ratio (SNR) is of overriding importance for the usability of hyperspectral data. The development time of the EnMAP instrument therefore was repeatedly extended to ensure that EnMAP will be able to provide high-quality

measurements from space, for instance due to excellent SNR. In addition, for many environmental scientific and commercial applications, repeated observations of the same point on the Earth's surface are crucial, requiring a mobile platform and stable geometry, which is also provided by the mission. Since the AVIRIS-NG imagery was spectrally resampled to EnMAP, we essentially present the first canopy carbon content and aboveground biomass maps as they can also be realized with the hyperspectral precursor. EnMAP also provides great opportunities due to its similarity with the PRISMA sensor. The joint observation capabilities of both instruments can increase the density of time series, which are dearly needed for agriculturally relevant products (Salinero-Delgado et al. 2021). The combined use of PRISMA and EnMAP data will be particularly advantageous for agricultural studies preparing future operational missions, such as CHIME (Verrelst et al. 2021a; Verrelst et al. 2021b; Candiani et al. 2022), which may provide further validation of the proposed workflow.

4.5 Conclusions

Hybrid modeling approaches have become a cornerstone for solving inference problems from Earth observation data due to their synergistic use of physical, expert and domain knowledge of mechanistic models, combined with the high flexibility, accuracy and consistency from machine learning algorithms. In our study, we explored such a hybrid design for deriving carbon and biomass content of croplands, succeeding in high transferability of the established models. For this, we trained GPR algorithms over simulated datasets generated by the PROSAIL-PRO model, employing PCA and active learning heuristics tuned on *in situ* data of the German MNI test site. The established models were transferred to an EnMAP resampled AVIRIS-NG scene of a similar agricultural area, achieving high mapping accuracy but moderate validation performance over a limited field data set with nRMSE ranging from 25% to 36%. These results point towards the need of further model adaptations and optimizations exploring field data sets of a larger variety of crop types and growth stages. Monitoring carbon temporarily stored in vegetation by means of hyperspectral Earth Observation data will support carbon farming, aiming to enhance the removal of CO_2 from the atmosphere through conversion of plant material and soil organic matter to soil organic carbon.

We conclude that the suggested workflow presents an appealing path towards reliable mapping of plant carbon and cropland biomass by spaceborne imaging spectroscopy missions. We also anticipate that EnMAP data, along with complementary hyperspectral missions, will constitute a valuable and crucial source for the preparation of future operational missions providing high priority crop products for multiple research fields and applications.

Acknowledgements

K.B. was mainly funded within the EnMAP scientific preparation program under the DLR Space Administration with resources from the German Federal Ministry of Economic Affairs and Energy, grant number 50EE1923. J.V. and K.B. were funded by the European Research Council (ERC) under the ERC-2017-STG SENTIFLEX project (grant agreement 755617) and Ramón y Cajal Contract (Spanish Ministry of Science, Innovation and Universities). This publication is also the result of the project implementation: "Scientific support of climate change adaptation in agriculture and mitigation of soil degradation" (ITMS2014+313011W580) supported by the Integrated Infrastructure Operational Programme funded by the ERDF. Further, the research was supported by the Action CA17134 SENSECO (Optical synergies for spatiotemporal sensing of scalable ecophysiological traits) funded by COST (European Cooperation in Science and Technology, www.cost.eu).

5 Conclusions and Outlook

This thesis demonstrates three different novel methods to derive agricultural relevant biophysical and biochemical variables from imaging spectroscopy data. These encompass canopy water content, chlorophyll and carotenoid content, as well as dry and fresh biomass and carbon content. All approaches follow a hybrid retrieval scheme as defined in chapter 1.2.4. All are based on the PROSPECT or PROSAIL RTMs for calibration or training and *in situ* data and/or airborne spectrometric imagery for validation. In the following, the in chapter 1.3.1 formulated research questions will be answered based on the theoretical background, the obtained results and discussions in the three presented papers, and the experience of the author.

***Q1**: Are PROSAIL-simulated databases suitable for both training and calibration of retrieval methods and what are the main sources of uncertainty?*

PROSAIL has become by far the most widely applied RTM for the estimation of biophysical and biochemical crop traits. Although this seems to be justified in view of satisfactory estimation results obtained, assumptions and simplifications made for the purpose of invertibility should always be considered as a source of uncertainty. Due to a continuous development and steady recalibration efforts, the number of considered leaf biochemical parameters in the leaf RTM PROSPECT increased from n = 3 in 1990 to n = 9 in 2021 which largely promoted the model's ability to reproduce radiative transfer in leaves and enabled, e.g., the first-time quantitative retrieval of crop carbon content (paper III). Using PROSAIL for the development of methods, a high degree of uncertainty is introduced in the transition from leaf to canopy level using 4SAIL, assuming a horizontally homogeneous canopy, which may not be valid for complex canopy architectures. Nonetheless, this simple 1-D turbid medium assumption may be difficult to improve prior to the claim of model invertibility. One possible improvement may be a more elaborated handling of soil background by either including a specific soil model or by including soil spectra observed in the study area into the calibration or training database.

Another fundamental issue are unrealistic parameter combinations that may occur in databases created with PROSAIL. Proposed strategies comprise physiological constraints, as realized in this thesis, for instance by applying plausibility checks by means of the C_{cx}-C_{ab}-relationship and green peak verification (paper II), or the $CBC > C_p$ condition (paper III). A generally valid approach to allow only realistic combinations to be simulated would be highly desirable but seems to be almost impossible to realize in view of highly nonlinear parameter interrelationships and edge cases (e.g., senescence). Another promising strategy is the application of AL heuristics, as demonstrated in paper III with an effective reduction of redundancy in the training samples. While these techniques, so far have only been applied in combination with ML approaches, implementing AL methods to reduce the number of potentially unrealistic spectra may also be beneficial as a preprocessing step

before calibration of parametric approaches.

***Q2**: Can RTM-calibrated parametric methods compete with nonparametric nonlinear ML approaches in terms of retrieval performance, and in view of general applicability and transferability?*

State-of-the-art hybrid ML approaches, such as the one presented in paper III of this thesis, are anticipated as a highly promising approach for solving inference problems from hyperspectral Earth observation data due to their synergistic use of physically-based models and the high flexibility, accuracy and consistency of nonlinear nonparametric methods. For this reason, optimized ML approaches will be indispensable toward reliable mapping of crop traits from spectrometric imagery of the EnMAP mission and other upcoming spaceborne hyperspectral sensors. However, although uncertainty intervals, as provided by GPR, support the interpretation of results, complete insight into detailed mechanisms of the methodology cannot be obtained. In contrast, this is very much the case for the methods presented in paper I and II whose mechanisms are well describable and interpretable. This transparency led to important findings, such as, the limited detectability of water due to the limited radiation penetration depth in conjunction with the canopy architecture (paper I) or possible inadmissible green peaks as simulated by PROSAIL that were only detected due to unrealistic results that occurred during the development of the SIR algorithm (paper II). Also, transferability and general applicability have been demonstrated for the parametric methods, but final validation is needed based on consistent spaceborne observations as will be available with EnMAP data. Incidentally, advanced indices that make full use of the available hyperspectral information such as 3-segment SIR may also be used in future studies as physics-aware dimensionality reduced input for ML algorithms to either improve estimations or to serve as endmember for crop type discrimination when additional time series information is available. Available detailed crop type information may then also add to improved crop type specific water content estimations by specifically setting the calibration factor in the Beer-Lambert law inversion scheme.

***Q3**: How meaningful is the validation of retrieval methods based on limited in situ measurements with varying levels of differentiation?*

All presented methods in this thesis were validated and checked for plausibility on various *in situ* datasets. These comprise the MNI dataset, spanning four full seasons of spectrometer and variable measurements of diverse crops and various airborne spectrometric imagery of the HyMAP, AVIRIS, and AVIRIS-NG sensors. For some flight campaigns also crop traits ground measurements were available, such as from the 2003 ESA SPARC campaign and from the 2021 ESA Hypersense Campaign. The validation of quantitative model-based estimations is crucial to evaluate and improve their performance in terms of the underlying assumptions, model parameterizations, and input data. When validation of retrieval methods is performed, the level of measured variable differentiation is of outmost

importance. For instance, destructive separate leaf, stalk, and fruit aboveground biomass-based water content and carbon measurements as obtained in the MNI and Hypersense campaigns provided accurate information about water and carbon detectability in grain and/or corn canopies. This kind of measurements are very labor intensive and thus measured crop variability is limited. On the other hand, as was rarely so successfully achieved like in the SPARC 2003 campaign, a field team can manage measuring biochemical variables on leaf level for many crop types during one day of fieldwork. These leaf measurements can then be upscaled to canopy level using LAI data. Hence, captured variability is high but crop type specific information content is low due to erroneous LAI upscaling as discussed in paper I. Nevertheless, a high captured crop variability supports the evaluation of model performance which is commonly performed using regression analysis. When collecting more accurate destructive measurements, this necessary data variability can only be obtained by laborious repeated temporal samplings over the whole growth cycle at study sites with short access routes such as the LMU MNI site. Although many field spectrometer measurements were performed, scaling issues (e.g., BRDF-effects) between proximal sensing and remote sensing by airborne or spaceborne measurements could not be addressed. Provided that campaigns such as the MNI campaign are continued when EnMAP data is available, datasets comprising both temporal and species variability may form an essential basis for a final validation of the methods presented in this thesis. It should be noted that PRISMA data could not be used for an effective validation of the methods due to severe artefacts in the VNIR region of the atmospherically corrected reflectance product.

***Q4**: What are the opportunities that arise for agricultural monitoring from the soon-to-be-available EnMAP data streams and which developments are to be expected regarding future imaging spectroscopy missions?*

Once the EnMAP mission will leave commissioning phase, acquisitions can be scheduled and *in situ* data collection can be aligned with EnMAP overflights. Provided that the reflectance product is of high quality regarding atmospheric correction and geolocalization, the presented models are ready to be applied and can be subjected to validation under consistent spaceborne acquisition conditions. With these models, fast mapping of canopy chlorophyll, carotenoid, and water content, as well as biomass and carbon content will be possible for cultivated areas from 30 × 30 km EnMAP scenes at 30 m spatial resolution. Nonetheless, EnMAP as a scientific precursor mission will only be the beginning of spaceborne imaging spectroscopy. Further missions are planned and eventually the field of hyperspectral Earth observation will evolve toward *Global Spectroscopy* as proposed by Schaepman (2019; personal communication with Rast, M., August 8, 2022). To be useful for future practical farming, the derived high-level products may be incorporated into decision support systems for fertilization or irrigation planning, yield estimation, or estimation of the soil carbon sequestration potential.

Furthermore, synergies between hyperspectral and other systems may be explored. Insights gained from EnMAP data may contribute to the incorporation of important spectral regions for agricultural monitoring into next generation multispectral sensors with higher spatial resolutions or provide information about a best trade-off setup between contiguous spectral coverage and high spatial resolution of future sensors.

In this spirit I will conclude with the words,

"The methods are prepared and now we wait for data to be available."

6 References

Abdel-Rahman, E.M., Ahmed, F.B., and Ismail, R. (2013). Random forest regression and spectral band selection for estimating sugarcane leaf nitrogen concentration using EO-1 Hyperion hyperspectral data. *International Journal of Remote Sensing, 34*, 712-728.

Abdelbaki, A. and Udelhoven, T. (2022). A Review of Hybrid Approaches for Quantitative Assessment of Crop Traits Using Optical Remote Sensing: Research Trends and Future Directions. *Remote Sensing, 14*, 3515.

Andrew, A.M. (1979). Another efficient algorithm for convex hulls in two dimensions. *Information Processing Letters, 9*, 216-219.

Angel, Y. and McCabe, M.F. (2022). Machine Learning Strategies for the Retrieval of Leaf-Chlorophyll Dynamics: Model Choice, Sequential Versus Retraining Learning, and Hyperspectral Predictors. *Front Plant Sci, 13*, 722442.

Atzberger, C., Guérif, M., Baret, F., and Werner, W. (2010). Comparative analysis of three chemometric techniques for the spectroradiometric assessment of canopy chlorophyll content in winter wheat. *Computers and Electronics in Agriculture, 73*, 165-173.

Atzberger, C. and Richter, K. (2012). Spatially constrained inversion of radiative transfer models for improved LAI mapping from future Sentinel-2 imagery. *Remote Sensing of Environment, 120*, 208-218.

Atzberger, C., Richter, K., Vuolo, F., Darvishzadeh, R., and Schlerf, M. (2011). Why confining to vegetation indices? Exploiting the potential of improved spectral observations using radiative transfer models. SPIE.

Bach, H. (1995). Die Bestimmung hydrologischer und landwirtschaftlicher Oberflächenparameter aus hyperspektralen Fernerkundungsdaten. Geobuch-Verlag.

Baker, R.E., Peña, J.-M., Jayamohan, J., and Jérusalem, A. (2018). Mechanistic models versus machine learning, a fight worth fighting for the biological community? *Biology Letters, 14*, 20170660.

Balafoutis, A., Beck, B., Fountas, S., Vangeyte, J., Wal, T.V.d., Soto, I., Gómez-Barbero, M., Barnes, A., and Eory, V. (2017). Precision Agriculture Technologies Positively Contributing to GHG Emissions Mitigation, Farm Productivity and Economics. *Sustainability, 9*, 1339.

Baret, F., Clevers, J.G.P.W., and Steven, M.D. (1995). The robustness of canopy gap fraction estimates from red and near-infrared reflectances: A comparison of approaches. *Remote Sensing of Environment, 54*, 141-151.

Baret, F. and Guyot, G. (1991). Potentials and limits of vegetation indices for LAI and APAR assessment. *Remote Sensing of Environment, 35*, 161-173.

Ben-Gal, A., Agam, N., Alchanatis, V., Cohen, Y., Yermiyahu, U., Zipori, I., Presnov, E., Sprintsin, M., and Dag, A. (2009). Evaluating water stress in irrigated olives: correlation of soil water status, tree water status, and thermal imagery. *Irrigation Science, 27*, 367-376.

Berger, K., Atzberger, C., Danner, M., D'Urso, G., Mauser, W., Vuolo, F., and Hank, T. (2018a). Evaluation of the PROSAIL Model Capabilities for Future Hyperspectral Model Environments: A Review Study. *Remote Sensing, 10*, 85.

Berger, K., Atzberger, C., Danner, M., D'Urso, G., Mauser, W., Vuolo, F., and Hank, T. (2018b). Evaluation of the PROSAIL Model Capabilities for Future Hyperspectral Model Environments: A Review Study. *Remote Sensing, 10*, 85.

Berger, K., Atzberger, C., Danner, M., Wocher, M., Mauser, W., and Hank, T. (2018c). Model-Based Optimization of Spectral Sampling for the Retrieval of Crop Variables with the PROSAIL Model. *Remote Sensing, 10*, 2063.

Berger, K., Halabuk, A., Verrelst, J., Mojses, M., Gerhatova, K., Tagliabue, G., Wocher, M., and Hank, T. (2021a). Towards quantifying non-photosynthetic vegetation for agriculture using spaceborne imaging spectroscopy. *IEEE International Geoscience and Remote Sensing Symposium, IGARSS*. Brussels.

Berger, K., Hank, T., Halabuk, A., Rivera-Caicedo, J.P., Wocher, M., Mojses, M., Gerhátová, K., Tagliabue, G., Dolz, M.M., Venteo, A.B.P., and Verrelst, J. (2021b). Assessing Non-Photosynthetic Cropland Biomass from Spaceborne Hyperspectral Imagery. *Remote Sensing, 13*, 4711.

Berger, K., Hank, T., Vuolo, F., Mauser, W., and D'Urso, G. (2012). Optimal Exploitation of the Sentinel-2 Spectral Capabilities for Crop Leaf Area Index Mapping. *Remote Sensing, 4*, 561-582.

Berger, K., Machwitz, M., Kycko, M., Kefauver, S.C., Van Wittenberghe, S., Gerhards, M., Verrelst, J., Atzberger, C., van der Tol, C., Damm, A., Rascher, U., Herrmann, I., Paz, V.S., Fahrner, S., Pieruschka, R., Prikaziuk, E., Buchaillot, M.L., Halabuk, A., Celesti, M., Koren, G., Gormus, E.T., Rossini, M., Foerster, M., Siegmann, B., Abdelbaki, A., Tagliabue, G., Hank, T., Darvishzadeh, R., Aasen, H., Garcia, M., Pôças, I., Bandopadhyay, S., Sulis, M., Tomelleri, E., Rozenstein, O., Filchev, L., Stancile, G., and Schlerf, M. (2022). Multi-sensor spectral synergies for crop stress detection and monitoring in the optical domain: A review. *Remote Sensing of Environment, 280*, 113198.

Berger, K., Rivera Caicedo, J.P., Martino, L., Wocher, M., Hank, T., and Verrelst, J. (2021c). A Survey of Active Learning for Quantifying Vegetation Traits from Terrestrial Earth Observation Data. *Remote Sensing, 13*, 287.

Berger, K., Verrelst, J., Féret, J.-B., Hank, T., Wocher, M., Mauser, W., and Camps-Valls, G. (2020a). Retrieval of aboveground crop nitrogen content with a hybrid machine learning method. *International Journal of Applied Earth Observation and Geoinformation, 92*, 102174.

Berger, K., Verrelst, J., Féret, J.-B., Wang, Z., Wocher, M., Strathmann, M., Danner, M., Mauser, W., and Hank, T. (2020b). Crop nitrogen monitoring: Recent progress and principal developments in the context of imaging spectroscopy missions. *Remote Sensing of Environment, 242*, 111758.

Berger, K., Wang, Z., Danner, M., Wocher, M., Hank, T., and Mauser, W. (2018d). Simulation of Spaceborne Hyperspectral Remote Sensing to Assist Crop Nitrogen Content Monitoring in Agricultural Crops. *IGARSS 2018 - 2018 IEEE International Geoscience and Remote Sensing Symposium*, pp. 3809-3812. Valencia.

Bicheron, P. and Leroy, M. (1999). A Method of Biophysical Parameter Retrieval at Global Scale by Inversion of a Vegetation Reflectance Model. *Remote Sensing of Environment, 67*, 251-266.

Billauer, E. (2012). peakdet: Peak detection using MATLAB. http://billauer.co.il/peakdet.html. Online: Accessed 20 February 2020.

Blackburn, G.A. (1998a). Quantifying Chlorophylls and Caroteniods at Leaf and Canopy Scales: An Evaluation of Some Hyperspectral Approaches. *Remote Sensing of Environment, 66*, 273-285.

Blackburn, G.A. (1998b). Spectral indices for estimating photosynthetic pigment concentrations: A test using senescent tree leaves. *International Journal of Remote Sensing, 19*, 657-675.

Blackburn, G.A. (1999). Relationships between Spectral Reflectance and Pigment Concentrations in Stacks of Deciduous Broadleaves. *Remote Sensing of Environment, 70*, 224-237.

Blackmore, S. (1994). Precision Farming: An Introduction. *Outlook on Agriculture, 23*, 275-280.

Bohn, N., Guanter, L., Kuester, T., Preusker, R., and Segl, K. (2020). Coupled retrieval of the three phases of water from spaceborne imaging spectroscopy measurements. *Remote Sensing of Environment, 242*, 111708.

Borel, C. (2009). Algorithm for retrieving vegetative canopy and leaf parameters from multi- and hyperspectral imagery. *Proc SPIE, 7334*.

Brede, B., Verrelst, J., Gastellu-Etchegorry, J.-P., Clevers, J.G.P.W., Goudzwaard, L., Den Ouden, J., Verbesselt, J., and Herold, M. (2020). Assessment of Workflow Feature Selection on Forest LAI Prediction with Sentinel-2A MSI, Landsat 7 ETM+ and Landsat 8 OLI. *Remote Sensing, 12*, 915.

Breiman, L. (2001). Random Forests. *Machine Learning, 45*, 5-32.

Broge, N.H. and Leblanc, E. (2001). Comparing prediction power and stability of broadband and hyperspectral vegetation indices for estimation of green leaf area index and canopy chlorophyll density. *Remote Sensing of Environment, 76*, 156-172.

Bull, C.R. (1991). Wavelength selection for near-infrared reflectance moisture meters. *Journal of Agricultural Engineering Research, 49*, 113-125.

Burney, J.A., Davis, S.J., and Lobell, D.B. (2010). Greenhouse gas mitigation by agricultural intensification. *Proceedings of the National Academy of Sciences, 107*, 12052-12057.

Caicedo, J.P.R., Verrelst, J., Muñoz-Marí, J., Moreno, J., and Camps-Valls, G. (2014). Toward a Semiautomatic Machine Learning Retrieval of Biophysical Parameters. *IEEE Journal of Selected Topics in Applied Earth Observations and Remote Sensing, 7*, 1249-1259.

Camacho, F., Fuster, B., Li, W., Weiss, M., Ganguly, S., Lacaze, R., and Baret, F. (2021). Crop specific algorithms trained over ground measurements provide the best performance for GAI and fAPAR estimates from Landsat-8 observations. *Remote Sensing of Environment, 260*, 112453.

Camps-Valls, G., Martino, L., Svendsen, D.H., Campos-Taberner, M., Muñoz-Marí, J., Laparra, V., Luengo, D., and García-Haro, F.J. (2018). Physics-aware Gaussian processes in remote sensing. *Applied Soft Computing, 68*, 69 - 82.

Camps-Valls, G., Sejdinovic, D., Runge, J., and Reichstein, M. (2019). A perspective on Gaussian processes for Earth observation. *National Science Review, 6*, 616-618.

Camps-Valls, G., Verrelst, J., Munoz-Mari, J., Laparra, V., Mateo-Jimenez, F., and Gomez-Dans, J. (2016). A Survey on Gaussian Processes for Earth-Observation Data Analysis: A Comprehensive Investigation. *IEEE Geoscience and Remote Sensing Magazine, 4*, 58-78.

Candiani, G., Tagliabue, G., Panigada, C., Verrelst, J., Picchi, V., Rivera Caicedo, J.P., and Boschetti, M. (2022). Evaluation of Hybrid Models to Estimate Chlorophyll and Nitrogen Content of Maize Crops in the Framework of the Future CHIME Mission. *Remote Sensing, 14*, 1792.

Cannavó, F. (2012). Sensitivity analysis for volcanic source modeling quality assessment and model selection. *Computers & Geosciences, 44*, 52-59.

Carlson, K.M., Gerber, J.S., Mueller, N.D., Herrero, M., MacDonald, G.K., Brauman, K.A., Havlik, P., O'Connell, C.S., Johnson, J.A., Saatchi, S., and West, P.C. (2017). Greenhouse gas emissions intensity of global croplands. *Nature Climate Change, 7*, 63-68.

Carter, G.A. (1991). Primary and Secondary Effects of Water Content on the Spectral Reflectance of Leaves. *American Journal of Botany, 78*, 916-924.

Carter, G.A. and Knapp, A.K. (2001). Leaf optical properties in higher plants: linking spectral characteristics to stress and chlorophyll concentration. *American Journal of Botany, 88*, 677-684.

Ceccato, P., Flasse, S., Tarantola, S., Jacquemoud, S., and Grégoire, J.-M. (2001). Detecting vegetation leaf water content using reflectance in the optical domain. *Remote Sensing of Environment, 77*, 22-33.

Cernicharo, J., Verger, A., and Camacho, F. (2013). Empirical and Physical Estimation of Canopy Water Content from CHRIS/PROBA Data. *Remote Sensing, 5*, 5265.

Champagne, C.M., Staenz, K., Bannari, A., McNairn, H., and Deguise, J.-C. (2003). Validation of a hyperspectral curve-fitting model for the estimation of plant water content of agricultural canopies. *Remote Sensing of Environment, 87*, 148-160.

Chapman, J.W., Thompson, D.R., Helmlinger, M.C., Bue, B.D., Green, R.O., Eastwood, M.L., Geier, S., Olson-Duvall, W., and Lundeen, S.R. (2019). Spectral and Radiometric Calibration of the Next Generation Airborne Visible Infrared Spectrometer (AVIRIS-NG). *Remote Sensing, 11*, 2129.

Chappelle, E.W., Kim, M.S., and McMurtrey, J.E. (1992). Ratio analysis of reflectance spectra (RARS): An algorithm for the remote estimation of the concentrations of chlorophyll A, chlorophyll B, and carotenoids in soybean leaves. *Remote Sensing of Environment, 39*, 239-247.

Clark, R.N. and Roush, T.L. (1984). Reflectance spectroscopy: Quantitative analysis techniques for remote sensing applications. *Journal of Geophysical Research: Solid Earth, 89*, 6329-6340.

Clevers, J.G.P.W., Kooistra, L., and Schaepman, M.E. (2008). Using spectral information from the NIR water absorption features for the retrieval of canopy water content. *International Journal of Applied Earth Observation and Geoinformation, 10*, 388-397.

Clevers, J.G.P.W., Kooistra, L., and Schaepman, M.E. (2010). Estimating canopy water content using hyperspectral remote sensing data. *International Journal of Applied Earth Observation and Geoinformation, 12*, 119-125.

Cogliati, S., Sarti, F., Chiarantini, L., Cosi, M., Lorusso, R., Lopinto, E., Miglietta, F., Genesio, L., Guanter, L., Damm, A., Pérez-López, S., Scheffler, D., Tagliabue, G., Panigada, C., Rascher, U., Dowling, T.P.F., Giardino, C., and Colombo, R. (2021). The PRISMA imaging spectroscopy mission: overview and first performance analysis. *Remote Sens. Environ., 262*, 112499.

Cohen, Y. and Alchanatis, V. (2018). Spectral and Spatial Methods for Hyperspectral and Thermal Image-Analysis to Estimate Biophysical and Biochemical Properties of Agricultural Crops. In Biophysical and Biochemical Characterization and Plant Species Studies. CRC Press. Boca Raton, FL, USA.

Combal, B., Baret, F., Weiss, M., Trubuil, A., Macé, D., Pragnère, A., Myneni, R., Knyazikhin, Y., and Wang, L. (2003). Retrieval of canopy biophysical variables from bidirectional reflectance: Using prior information to solve the ill-posed inverse problem. *Remote Sensing of Environment, 84*, 1-15.

D'Urso, G., Dini, L., Vuolo, F., Alonso, L., and Guanter, L. (2004). Retrieval of leaf area index by inverting hyper-spectral, multi-angular CHRIS/Proba data from sparc 2003. *European Space Agency, (Special Publication) ESA SP*, 58-63.

Danner, M., Berger, K., Wocher, M., Mauser, W., and Hank, T. (2017). Retrieval of Biophysical Crop Variables from Multi-Angular Canopy Spectroscopy. *Remote Sensing, 9*, 726.

Danner, M., Berger, K., Wocher, M., Mauser, W., and Hank, T. (2019). Fitted PROSAIL Parameterization of Leaf Inclinations, Water Content and Brown Pigment Content for Winter Wheat and Maize Canopies. *Remote Sensing, 11*, 1150.

Danner, M., Berger, K., Wocher, M., Mauser, W., and Hank, T. (2021). Efficient RTM-based training of machine learning regression algorithms to quantify biophysical & biochemical traits of agricultural crops. *ISPRS Journal of Photogrammetry and Remote Sensing, 173*, 278-296.

Danson, F.M. and Bowyer, P. (2004). Estimating live fuel moisture content from remotely sensed reflectance. *Remote Sensing of Environment, 92*, 309-321.

Danson, F.M., Steven, M.D., Malthus, T.J., and Clark, J.A. (1992). High-spectral resolution data for determining leaf water content. *International Journal of Remote Sensing, 13*, 461-470.

Datt, B. (1999). Remote Sensing of Water Content in Eucalyptus Leaves. *Australian Journal of Botany, 47*, 909-923.

De Grave, C., Verrelst, J., Morcillo-Pallarés, P., Pipia, L., Rivera-Caicedo, J.P., Amin, E., Belda, S., and Moreno, J. (2020). Quantifying vegetation biophysical variables from the Sentinel-3/FLEX tandem mission: Evaluation of the synergy of OLCI and FLORIS data sources. *Remote Sensing of Environment, 251*, 112101.

de Sá, N.C., Baratchi, M., Hauser, L.T., and van Bodegom, P. (2021). Exploring the Impact of Noise on Hybrid Inversion of PROSAIL RTM on Sentinel-2 Data. *Remote Sensing, 13*, 648.

Delegido, J., Alonso, L., González, G., and Moreno, J. (2010). Estimating chlorophyll content of crops from hyperspectral data using a normalized area over reflectance curve (NAOC). *International Journal of Applied Earth Observation and Geoinformation, 12*, 165-174.

Demmig-Adams, B. and Adams, W.W. (1996). The role of xanthophyll cycle carotenoids in the protection of photosynthesis. *Trends in Plant Science, 1*, 21-26.

Denman, K.L., Brasseur, G., Chidthaisong, A., Ciais, P., Cox, P.M., Dickinson, R.E., Hauglustaine, D., Heinze, C., Holland, E., Jacob, D., Lohmann, U., Ramachandran, S., da Silva Dias, P.L., Wofsy, S.C., and Zhang, X. (2007). Couplings between changes in the climate system and biogeochemistry. In Solomon, S., D. Qin, M. Manning, Z. Chen, M. Marquis, K.B. Averyt, M.Tignor, and H.L. Miller (Eds.), Climate Change 2007: The Physical Science Basis. Contribution of Working Group I to the Fourth Assessment Report of the Intergovernmental Panel on Climate Change Cambridge University Press. New York, NY, USA.

Doktor, D., Lausch, A., Spengler, D., and Thurner, M. (2014). Extraction of Plant Physiological Status from Hyperspectral Signatures Using Machine Learning Methods. *Remote Sensing, 6*, 12247-12274.

Dorigo, W.A. (2012). Improving the Robustness of Cotton Status Characterisation by Radiative Transfer Model Inversion of Multi-Angular CHRIS/PROBA Data. *IEEE Journal of Selected Topics in Applied Earth Observations and Remote Sensing, 5*, 18-29.

Douak, F., Melgani, F., and Benoudjit, N. (2013). Kernel ridge regression with active learning for wind speed prediction. *Applied Energy, 103*, 328-340.

Durbha, S.S., King, R.L., and Younan, N.H. (2007). Support vector machines regression for retrieval of leaf area index from multiangle imaging spectroradiometer. *Remote Sensing of Environment, 107*, 348-361.

Emmerson, M., Morales, M.B., Oñate, J.J., Batáry, P., Berendse, F., Liira, J., Aavik, T., Guerrero, I., Bommarco, R., Eggers, S., Pärt, T., Tscharntke, T., Weisser, W., Clement, L., and Bengtsson, J. (2016). Chapter Two - How Agricultural Intensification Affects Biodiversity and Ecosystem Services. In A.J. Dumbrell, R.L. Kordas, & G. Woodward(Eds.), Advances in Ecological Research, pp. 43-97. Academic Press. Cambridge, MA, USA.

Erickson, B. and Lowenberg-DeBoer, J. (2021). Precision Agriculture Dealership Survey. Purdue University. West Lafayette, IN, USA.

Estévez, J., Berger, K., Vicent, J., Rivera-Caicedo, J.P., Wocher, M., and Verrelst, J. (2021). Top-of-Atmosphere Retrieval of Multiple Crop Traits Using Variational Heteroscedastic Gaussian Processes within a Hybrid Workflow. *Remote Sensing, 13*, 1589.

Estévez, J., Salinero-Delgado, M., Berger, K., Pipia, L., Rivera-Caicedo, J.P., Wocher, M., Reyes-Muñoz, P., Tagliabue, G., Boschetti, M., and Verrelst, J. (2022). Gaussian processes retrieval of crop traits in Google Earth Engine based on Sentinel-2 top-of-atmosphere data. *Remote Sensing of Environment, 273*, 112958.

Evans, J.R. (1989). Photosynthesis and nitrogen relationships in leaves of C3 plants. *Oecologia, 78*, 9-19.

Fang, P., Yan, N., Wei, P., Zhao, Y., and Zhang, X. (2021). Aboveground Biomass Mapping of Crops Supported by Improved CASA Model and Sentinel-2 Multispectral Imagery. *Remote Sensing, 13*, 2755.

FAO (2019). The State of the World's Biodiversity for Food and Agriculture. J. Bélanger, D. Pilling, & (Eds.). FAO Commission on Genetic Resources for Food and Agriculture Assessments. Rome, Italy.

FAO (2021). The State of Food and Agriculture 2016 - Making Agrifood Systems more Resilient to Shocks and Stresses. Food and Agriculture Organization of the United Nations. Rome, Italy.

FAO (2022). Land use in agriculture by the numbers. https://www.fao.org/sustainability/news/detail/en/c/1274219. Online: Accessed 4 July 2022.

Fei, Y., Jiulin, S., Hongliang, F., Zuofang, Y., Jiahua, Z., Yunqiang, Z., Kaishan, S., Zongming, W., and Maogui, H. (2012). Comparison of different methods for corn LAI estimation over northeastern China. *International Journal of Applied Earth Observation and Geoinformation, 18*, 462-471.

Feilhauer, H., Asner, G.P., and Martin, R.E. (2015). Multi-method ensemble selection of spectral bands related to leaf biochemistry. *Remote Sensing of Environment, 164*, 57-65.

Feingersh, T. and Ben-Dor, E. (2015). SHALOM – A Commercial Hyperspectral Space Mission. In Q. Shen-En°(Ed.) Optical Payloads for Space Missions. John Wiley & Sons, Ltd. Chichester, England, UK.

Féret, J.-B., Berger, K., de Boissieu, F., and Malenovský, Z. (2021). PROSPECT-PRO for estimating content of nitrogen-containing leaf proteins and other carbon-based constituents. *Remote Sensing of Environment, 252*, 112173.

Féret, J.-B., François, C., Asner, G.P., Gitelson, A.A., Martin, R.E., Bidel, L.P.R., Ustin, S.L., le Maire, G., and Jacquemoud, S. (2008). PROSPECT-4 and 5: Advances in the leaf optical properties model separating photosynthetic pigments. *Remote Sensing of Environment, 112*, 3030-3043.

Féret, J.-B., Gitelson, A.A., Noble, S.D., and Jacquemoud, S. (2017). PROSPECT-D: Towards modeling leaf optical properties through a complete lifecycle. *Remote Sensing of Environment, 193*, 204-215.

Gamon, J.A., Huemmrich, K.F., Wong, C.Y.S., Ensminger, I., Garrity, S., Hollinger, D.Y., Noormets, A., and Peñuelas, J. (2016). A remotely sensed pigment index reveals photosynthetic phenology in evergreen conifers. *Proceedings of the National Academy of Sciences, 113*, 13087-13092.

Gamon, J.A., Peñuelas, J., and Field, C.B. (1992). A narrow-waveband spectral index that tracks diurnal changes in photosynthetic efficiency. *Remote Sensing of Environment, 41*, 35-44.

Gandia, S., Fernández, G., García, J., and Moreno, J. (2004). Retrieval of vegetation biophysical variables from CHRIS/PROBA data in the SPARC campaign. *ESA SP, 578*, 40-48.

Gao, B.-C. (1996). NDWI—A normalized difference water index for remote sensing of vegetation liquid water from space. *Remote Sensing of Environment, 58*, 257-266.

Gao, B.-C. and Goetz, A.F.H. (1990). Column atmospheric water vapor and vegetation liquid water retrievals from Airborne Imaging Spectrometer data. *Journal of Geophysical Research: Atmospheres, 95*, 3549-3564.

Gao, B.-C. and Goetz, A.F.H. (1995). Retrieval of equivalent water thickness and information related to biochemical components of vegetation canopies from AVIRIS data. *Remote Sensing of Environment, 52*, 155-162.

Gao, B.-C., Montes, M.J., Davis, C.O., and Goetz, A.F.H. (2009). Atmospheric correction algorithms for hyperspectral remote sensing data of land and ocean. *Remote Sensing of Environment, 113*, S17-S24.

Garnett, T., Appleby, M.C., Balmford, A., Bateman, I.J., Benton, T.G., Bloomer, P., Burlingame, B., Dawkins, M., Dolan, L., Fraser, D., Herrero, M., Hoffmann, I., Smith, P., Thornton, P.K., Toulmin, C., Vermeulen, S.J., and Godfray, H.C.J. (2013). Sustainable Intensification in Agriculture: Premises and Policies. *Science, 341*, 33-34.

GCOS (2022). Above-ground Biomass - Essential Climate Variable (ECV) Factsheet. https://gcos.wmo.int/en/essential-climate-variables/biomass. Online: Accessed 13 April 2022.

Geladi, P. and Kowalski, B.R. (1986). Partial least-squares regression: a tutorial. *Analytica Chimica Acta, 185*, 1-17.

Ghulam, A., Li, Z.-L., Qin, Q., Yimit, H., and Wang, J. (2008). Estimating crop water stress with ETM+ NIR and SWIR data. *Agricultural and Forest Meteorology, 148*, 1679-1695.

Gitelson, A., Zur, Y., Chivkunova, O., and Merzlyak, M. (2002). Assessing Carotenoid Content in Plant Leaves with Reflectance Spectroscopy. *Photochemistry and Photobiology, 75*, 272-281.

Gitelson, A.A., Chivkunova, O.B., and Merzlyak, M.N. (2009). Nondestructive estimation of anthocyanins and chlorophylls in anthocyanic leaves. *American Journal of Botany, 96*, 1861-1868.

Gitelson, A.A., Gritz †, Y., and Merzlyak, M.N. (2003). Relationships between leaf chlorophyll content and spectral reflectance and algorithms for non-destructive chlorophyll assessment in higher plant leaves. *Journal of Plant Physiology, 160*, 271-282.

Gitelson, A.A., Merzlyak, M.N., and Chivkunova, O.B. (2001). Optical Properties and Nondestructive Estimation of Anthocyanin Content in Plant Leaves. *Photochemistry and Photobiology, 74*, 38-45.

Glenn, E.P., Huete, A.R., Nagler, P.L., and Nelson, S.G. (2008). Relationship Between Remotely-sensed Vegetation Indices, Canopy Attributes and Plant Physiological Processes: What Vegetation Indices Can and Cannot Tell Us About the Landscape. *Sensors (Basel), 8*, 2136-2160.

Godfray, H.C.J., Beddington, J.R., Crute, I.R., Haddad, L., Lawrence, D., Muir, J.F., Pretty, J., Robinson, S., Thomas, S.M., and Toulmin, C. (2010). Food Security: The Challenge of Feeding 9 Billion People. *Science, 327*, 812-818.

Goetz, S.J. and Prince, S.D. (1996). Remote sensing of net primary production in boreal forest stands. *Agricultural and Forest Meteorology, 78*, 149-179.

Green, R.O., Conel, J.E., Margolis, J., Bruegge J., C., and Hoover L., G. (1991). An Inversion Algorithm for Retrieval of Atmospheric and leaf Water Absorption From AVIRIS Radiance With Compensation for Atmospheric Scattering. R. Green O.°(Ed.), *3rd Airborne Visible/Infrared Imaging Spectrometer (AVIRIS) Workshop* pp. 51-61. Pasadena, CA.

Green, R.O., Conel, J.E., and Roberts, D.A. (1993). Estimation of aerosol optical depth, pressure elevation, water vapor, and calculation of apparent surface reflectance from radiance measured by the airborne visible/infrared imaging spectrometer (AVIRIS).

Summaries of the 4th Annual JPL Airborne Geoscience Workshop pp. 73-76. AVJRIS Workshop, Washington D.C..

Green, R.O., Painter, T.H., Roberts, D.A., and Dozier, J. (2006). Measuring the expressed abundance of the three phases of water with an imaging spectrometer over melting snow. *Water Resources Research, 42*.

Guanter, L., Kaufmann, H., Segl, K., Foerster, S., Rogass, C., Chabrillat, S., Kuester, T., Hollstein, A., Rossner, G., Chlebek, C., Straif, C., Fischer, S., Schrader, S., Storch, T., Heiden, U., Mueller, A., Bachmann, M., Muhle, H., Muller, R., Habermeyer, M., Ohndorf, A., Hill, J., Buddenbaum, H., Hostert, P., van der Linden, S., Leitao, P.J., Rabe, A., Doerffer, R., Krasemann, H., Xi, H., Mauser, W., Hank, T., Locherer, M., Rast, M., Staenz, K., and Sang, B. (2015). The EnMAP Spaceborne Imaging Spectroscopy Mission for Earth Observation. *Remote Sensing, 7*, 8830.

Haaland, D.M. and Thomas, E.V. (1988). Partial least-squares methods for spectral analyses. 1. Relation to other quantitative calibration methods and the extraction of qualitative information. *Analytical Chemistry, 60*, 1193-1202.

Hallik, L., Kazantsev, T., Kuusk, A., Galmés, J., Tomás, M., and Niinemets, Ü. (2017). Generality of relationships between leaf pigment contents and spectral vegetation indices in Mallorca (Spain). *Regional Environmental Change, 17*, 2097-2109.

Hank, T., Bach, H., and Mauser, W. (2015). Using a Remote Sensing-Supported Hydro-Agroecological Model for Field-Scale Simulation of Heterogeneous Crop Growth and Yield: Application for Wheat in Central Europe. *Remote Sensing, 7*, 3934-3965.

Hank, T., Berger, K., Wocher, M., Danner, M., and Mauser, W. (2021). Introducing the Potential of the EnMAP-Box for Agricultural Applications Using Desis and Prisma Data. *IEEE International Geoscience and Remote Sensing Symposium, IGARSS*, pp. 467-470. Brussels.

Hank, T.B., Berger, K., Bach, H., Clevers, J.G.P.W., Gitelson, A., Zarco-Tejada, P., and Mauser, W. (2019). Spaceborne Imaging Spectroscopy for Sustainable Agriculture: Contributions and Challenges. *Surveys in Geophysics, 40*, 515-551.

Hardisky, M., Klemas, V., and Smart, R.M. (1983). The Influence of Soil Salinity, Growth Form, and Leaf Moisture on the Spectral Radiance of Spartina Alterniflora Canopies. *Photogrammetric Engineering and Remote Sensing, 49*, 77-83.

Haykin, S. (1998). Neural Networks: A Comprehensive Foundation. Prentice Hall PTR.

Hosgood, B., Jacquemoud, S., Andreoli, J., Verdebout, A., Pedrini, A., and Schmuck, G. (1995). Leaf Optical Properties Experiment 93 (LOPEX93). European Commission.

Houborg, R., Anderson, M., and Daughtry, C. (2009). Utility of an image-based canopy reflectance modeling tool for remote estimation of LAI and leaf chlorophyll content at the field scale. *Remote Sensing of Environment, 113*, 259-274.

Houborg, R., Soegaard, H., and Boegh, E. (2007). Combining vegetation index and model inversion methods for the extraction of key vegetation biophysical parameters using Terra and Aqua MODIS reflectance data. *Remote Sensing of Environment, 106*, 39-58.

Hughes, G. (1968). On the mean accuracy of statistical pattern recognizers. *IEEE Transactions on Information Theory, 14*, 55-63.

Hunt, E.R. and Rock, B.N. (1989). Detection of changes in leaf water content using Near- and Middle-Infrared reflectances. *Remote Sensing of Environment, 30*, 43-54.

Hunt, E.R., Rock, B.N., and Nobel, P.S. (1987). Measurement of Leaf Relative Water Content by Infrared Reflectance. *Remote Sensing of Environment, 22*, 429-435.

Hunt, E.R., Ustin, S.L., and Riaño, D. (2013). Remote Sensing of Leaf, Canopy, and Vegetation Water Contents for Satellite Environmental Data Records. In J. Qu, A. Powell, & M.V.K. Sivakumar(Eds.), Satellite-based Applications on Climate Change, pp. 335-357. Springer Netherlands. Dordrecht.

Jacquemoud, S., Bacour, C., Poilvé, H., and Frangi, J.P. (2000). Comparison of Four Radiative Transfer Models to Simulate Plant Canopies Reflectance: Direct and Inverse Mode. *Remote Sensing of Environment, 74*, 471-481.

Jacquemoud, S. and Baret, F. (1990). PROSPECT: A model of leaf optical properties spectra. *Remote Sensing of Environment, 34*, 75-91.

Jacquemoud, S., Baret, F., Andrieu, B., Danson, F.M., and Jaggard, K. (1995). Extraction of vegetation biophysical parameters by inversion of the PROSPECT + SAIL models on sugar beet canopy reflectance data. Application to TM and AVIRIS sensors. *Remote Sensing of Environment, 52*, 163-172.

Jacquemoud, S., Bidel, C., and Pavan., F.G. (2003). ANGERS Leaf Optical Properties Database (2003). Data set. Available online [http://ecosis.org] from the Ecological Spectral Information System (EcoSIS). Online: Accessed 14 November 2017.

Jacquemoud, S., Verhoef, W., Baret, F., Bacour, C., Zarco-Tejada, P.J., Asner, G.P., François, C., and Ustin, S.L. (2009). PROSPECT+SAIL models: A review of use for vegetation characterization. *Remote Sensing of Environment, 113*, S56-S66.

Jansson, C., Faiola, C., Wingler, A., Zhu, X.-G., Kravchenko, A., de Graaff, M.-A., Ogden, A.J., Handakumbura, P.P., Werner, C., and Beckles, D.M. (2021). Crops for Carbon Farming. *Frontiers in Plant Science, 0*.

Jolliffe, I.T. and Cadima, J. (2016). Principal component analysis: a review and recent developments. *Philosophical Transactions of the Royal Society A, 374*, 20150202.

Jurdao, S., Yebra, M., Guerschman, J.P., and Chuvieco, E. (2013). Regional estimation of woodland moisture content by inverting Radiative Transfer Models. *Remote Sensing of Environment, 132*, 59-70.

Kaminski, T., Knorr, W., Scholze, M., Gobron, N., Pinty, B., Giering, R., and Mathieu, P.-P. (2012). Consistent assimilation of MERIS FAPAR and atmospheric CO2 into a terrestrial vegetation model and interactive mission benefit analysis. *Biogeosciences, 9*, 3173-3184.

Kimes, D.S., Knyazikhin, Y., Privette, J.L., Abuelgasim, A.A., and Gao, F. (2000). Inversion methods for physically-based models. *Remote Sensing Reviews, 18*, 381-439.

Knipling, E.B. (1970). Physical and physiological basis for the reflectance of visible and near-infrared radiation from vegetation. *Remote Sensing of Environment, 1*, 155-159.

Kokaly, R.F. and Clark, R.N. (1999). Spectroscopic Determination of Leaf Biochemistry Using Band-Depth Analysis of Absorption Features and Stepwise Multiple Linear Regression. *Remote Sensing of Environment, 67*, 267-287.

Kokaly, R.F., Despain, D.G., Clark, R.N., and Livo, K.E. (2003). Mapping vegetation in Yellowstone National Park using spectral feature analysis of AVIRIS data. *Remote Sensing of Environment, 84*, 437-456.

Kou, L., Labrie, D., and Chylek, P. (1993). Refractive indices of water and ice in the 0.65- to 2.5- μ m spectral range. *Applied Optics, 32*, 3531-3540.

Krutz, D., Sebastian, I., Eckardt, A., Venus, H., Walter, I., Günther, B., Säuberlich, T., Neidhardt, M., Zender, B., Lieder, M., Müller, R., Peschel, T., Müller, S., Arloth, S., Grote, U., Wojtkowiak, A., Schrandt, F., Fischer, C., Soszyńska, A., Carmona, E., and Reulke, R. (2018). DESIS - DLR earth sensing imaging spectrometer for the International Space Station ISS. SPIE.

Kuester, T. and Spengler, D. (2018). Structural and Spectral Analysis of Cereal Canopy Reflectance and Reflectance Anisotropy. *Remote Sensing, 10*, 1767.

Kumar, T.K. (1975). Multicollinearity in Regression Analysis on JSTOR. *The Review of Economics and Statistics, 57*, 365-366.

Labate, D., Ceccherini, M., Cisbani, A., De Cosmo, V., Galeazzi, C., Giunti, L., Melozzi, M., Pieraccini, S., and Stagi, M. (2009). The PRISMA payload optomechanical design, a high performance instrument for a new hyperspectral mission. *Acta Astronautica, 65*, 1429-1436.

Lázaro-Gredilla, M., Titsias, M.K., Verrelst, J., and Camps-Valls, G. (2013). Retrieval of Biophysical Parameters With Heteroscedastic Gaussian Processes. *IEEE Geoscience and Remote Sensing Letters, 11*, 838-842.

Lee, C.M., Cable, M.L., Hook, S.J., Green, R.O., Ustin, S.L., Mandl, D.J., and Middleton, E.M. (2015). An introduction to the NASA Hyperspectral InfraRed Imager (HyspIRI) mission and preparatory activities. *Remote Sensing of Environment, 167*, 6-19.

Li, L., Ren, T., Ma, Y., Wei, Q., Wang, S., Li, X., Cong, R., Liu, S., and Lu, J. (2016). Evaluating chlorophyll density in winter oilseed rape (Brassica napus L.) using canopy hyperspectral red-edge parameters. *Computers and Electronics in Agriculture, 126*, 21-31.

Liang, S. (2007). Recent developments in estimating land surface biogeophysical variables from optical remote sensing. *Progress in Physical Geography: Earth and Environment, 31*, 501-516.

Lichtenthaler, H.K. and Buschmann, C. (2001). Chlorophylls and Carotenoids: Measurement and Characterization by UV-VIS Spectroscopy. *Current Protocols in Food Analytical Chemistry, 1*, F4.3.1-F4.3.8.

Lillesaeter, O. (1982). Spectral reflectance of partly transmitting leaves: Laboratory measurements and mathematical modeling. *Remote Sensing of Environment, 12*, 247-254.

Locherer, M., Hank, T., Danner, M., and Mauser, W. (2015). Retrieval of Seasonal Leaf Area Index from Simulated EnMAP Data through Optimized LUT-Based Inversion of the PROSAIL Model. *Remote Sensing, 7*, 10321-10346.

Loizzo, R., Daraio, M., Guarini, R., Longo, F., Lorusso, R., Dini, L., and Lopinto, E. (2019). Prisma Mission Status and Perspective. *IGARSS 2019 - 2019 IEEE International Geoscience and Remote Sensing Symposium*, pp. 4503-4506.

Loizzo, R., Guarini, R., Longo, F., Scopa, T., Formaro, R., Facchinetti, C., and Varacalli, G. (2018). Prisma: The Italian Hyperspectral Mission. *IGARSS 2018 - 2018 IEEE International Geoscience and Remote Sensing Symposium*, pp. 175-178.

Lu, D. (2006). The potential and challenge of remote sensing-based biomass estimation. *International Journal of Remote Sensing, 27*, 1297-1328.

Ma, S., He, F., Tian, D., Zou, D., Yan, Z., Yang, Y., Zhou, T., Huang, K., Shen, H., and Fang, J. (2018). Variations and determinants of carbon content in plants: a global synthesis. *Biogeosciences, 15*, 693-702.

Machwitz, M., Pieruschka, R., Berger, K., Schlerf, M., Aasen, H., Fahrner, S., Jiménez-Berni, J., Baret, F., and Rascher, U. (2021). Bridging the Gap Between Remote Sensing and Plant Phenotyping---and Opportunities for the Next Generation of Sustainable Agriculture. *Frontiers in Plant Science, 0*.

Malenovský, Z., Ufer, C., Lhotakova, Z., Clevers, J.G.P.W., Schaepman, M.E., Albrechtova, J., and Cudlín, P. (2006). A new hyperspectral index for chlorophyll estimation of a forest canopy: Area under curve normalised to maximal band depth between 650-725 nm. *EARSeL eProceedings 5 (2006) 2, 5*.

Mariotto, I., Thenkabail, P.S., Huete, A., Slonecker, E.T., and Platonov, A. (2013). Hyperspectral versus multispectral crop-productivity modeling and type discrimination for the HyspIRI mission. *Remote Sensing of Environment, 139*, 291-305.

Mateo-Sanchis, A., Piles, M., Amorós-López, J., Muñoz-Marí, J., Adsuara, J.E., Moreno-Martínez, i.a.e.A.f., and Camps-Valls, G. (2021). Learning main drivers of crop progress and failure in Europe with interpretable machine learning. *International Journal of Applied Earth Observation and Geoinformation, 104*, 102574.

Mauser, W., Bach, H., Hank, T., Zabel, F., and Putzenlechner, B. (2012). How spectroscopy from space will support world agriculture. *2012 IEEE International Geoscience and Remote Sensing Symposium*, pp. 7321-7324.

Mauser, W., Klepper, G., Zabel, F., Delzeit, R., Hank, T., Putzenlechner, B., and Calzadilla, A. (2015). Global biomass production potentials exceed expected future demand without the need for cropland expansion. *Nature Communications, 6*, 8946.

Meier, U. (2018). Growth stages of mono- and dicotyledonous plants: BBCH Monograph. Open Agrar Repositorium. Quedlinburg, Germany.

Merzlyak, M.N., Gitelson, A.A., Chivkunova, O.B., and Rakitin, V.Y. (1999). Non-destructive optical detection of pigment changes during leaf senescence and fruit ripening. *Physiologia Plantarum, 106*, 135-141.

Morata, M., Siegmann, B., Morcillo-Pallarés, P., Rivera-Caicedo, J.P., and Verrelst, J. (2021). Emulation of Sun-Induced Fluorescence from Radiance Data Recorded by the HyPlant Airborne Imaging Spectrometer. *Remote Sensing, 13*, 4368.

Mulla, D.J. (2013). Twenty five years of remote sensing in precision agriculture: Key advances and remaining knowledge gaps. *Biosystems Engineering, 114*, 358-371.

Mutanga, O., Skidmore, A.K., Kumar, L., and Ferwerda, J. (2005). Estimating tropical pasture quality at canopy level using band depth analysis with continuum removal in the visible domain. *International Journal of Remote Sensing, 26*, 1093-1108.

National Academies of Sciences, E., and Medicine, (2018). Thriving on Our Changing Planet: A Decadal Strategy for Earth Observation from Space. The National Academics Press. Washington, DC, USA.

Newton, J.E. and Blackman, G.E. (1970). The Penetration of Solar Radiation through Leaf Canopies of Different Structure. *Annals of Botany, 34*, 329-348.

Nieke, J. and Rast, M. (2018a). Towards the Copernicus Hyperspectral Imaging Mission For The Environment (CHIME). *IGARSS 2018 - 2018 IEEE International Geoscience and Remote Sensing Symposium*, pp. 157-159.

Nieke, J. and Rast, M. (2018b). Towards the Copernicus Hyperspectral Imaging Mission For The Environment (CHIME). *IGGARS 2018*, pp. 157-159. Valencia.

Nieke, J. and Rast, M. (2019). Status: Copernicus Hyperspectral Imaging Mission For The Environment (CHIME). In IGARSS 2019 - 2019 IEEE International Geoscience and Remote Sensing Symposium, pp. 4609-4611. IEEE.

Oppelt, N. and Mauser, W. (2004). Hyperspectral monitoring of physiological parameters of wheat during a vegetation period using AVIS data. *International Journal of Remote Sensing, 25*, 145-159.

Pascual-Venteo, A.B., Portalés, E., Berger, K., Garcia, J.L., Pérez-Suay, A., Rivera-Caicedo, J.P., and Verrelst, J. (2022). Prototyping Crop Traits Retrieval Models for CHIME: Dimensionality Reduction Strategies applied to PRISMA Data. *Remote Sensing, 14*, 2448.

Pasolli, E., Melgani, F., Alajlan, N., and Bazi, Y. (2012). Active Learning Methods for Biophysical Parameter Estimation. *IEEE Transactions on Geoscience and Remote Sensing, 50*, 4071-4084.

Pasqualotto, N., Delegido, J., Van Wittenberghe, S., Verrelst, J., Rivera, J.P., and Moreno, J. (2018). Retrieval of canopy water content of different crop types with two new hyperspectral indices: Water Absorption Area Index and Depth Water Index. *International Journal of Applied Earth Observation and Geoinformation, 67*, 69-78.

Paustian, K., Larson, E., Kent, J., Marx, E., and Swan, A. (2019). Soil C Sequestration as a Biological Negative Emission Strategy. *Frontiers in Climate, 0*.

Peñuelas, J., Filella, I., Biel, C., Serrano, L., and Savé, R. (1993). The reflectance at the 950–970 nm region as an indicator of plant water status. *International Journal of Remote Sensing, 14*, 1887-1905.

Peñuelas, J., Pinol, J., Ogaya, R., and Filella, I. (1997). Estimation of plant water concentration by the reflectance Water Index WI (R900/R970). *International Journal of Remote Sensing, 18*, 2869-2875.

Pipia, L., Amin, E., Belda, S., Salinero-Delgado, M., and Verrelst, J. (2021). Green LAI Mapping and Cloud Gap-Filling Using Gaussian Process Regression in Google Earth Engine. *Remote Sensing, 13*, 403.

Rasmussen, C.E. and Williams, C.K.I. (2006). Gaussian Processes for Machine Learning. MIT Press. Cambridge, MA, USA.

Richter, K., Hank, T.B., Mauser, W., and Atzberger, C. (2012). Derivation of biophysical variables from Earth observation data: validation and statistical measures. *Journal of Applied Remote Sensing, 6*, 23.

Richter, K., Rischbeck, P., Eitzinger, J., Schneider, W., Suppan, F., and Weihs, P. (2008). Plant growth monitoring and potential drought risk assessment by means of Earth observation data. *International Journal of Remote Sensing, 29*, 4943-4960.

Rivera-Caicedo, J.P., Verrelst, J., Muñoz-Marí, J., Camps-Valls, G., and Moreno, J. (2017). Hyperspectral dimensionality reduction for biophysical variable statistical retrieval. *ISPRS Journal of Photogrammetry and Remote Sensing, 132*, 88-101.

Running, S.W. and Gower, S. (1991). FOREST-BGC, A general model of forest ecosystem processes for regional applications. II. Dynamic carbon allocation and nitrogen budgets. *Tree Physiology, 9*, 147-160.

Running, S.W. and Nemani, R.R. (1991). Regional hydrologic and carbon balance responses of forests resulting from potential climate change. *Climatic Change, 19*, 349-368.

Salinero-Delgado, M., Estévez, J., Pipia, L., Belda, S., Berger, K., Paredes Gómez, V., and Verrelst, J. (2021). Monitoring Cropland Phenology on Google Earth Engine Using Gaussian Process Regression. *Remote Sensing, 14*, 146.

Schaepman, M.E. (2019). Presentation. Towards a Global Spectroscopy - Key Messages to Integrating Disparate, Heterogeneous Space-Time-Spectroscopy Data. ESA Workshop on International Cooperation in Spaceborne Imaging Spectroscopy, 9 - 11 July, ESA-ESRIN, Frascati, Italy. https://nikal.eventsair.com/NikalWebsitePortal/hyperspectral-2019/website. Online: Accessed 26th August, 2022.

Schaepman, M.E., Koetz, B., Schaepman-Strub, G., and Itten, K.I. (2005). Spectrodirectional remote sensing for the improved estimation of biophysical and -chemical variables: two case studies. *International Journal of Applied Earth Observation and Geoinformation, 6*, 271-282.

Schlerf, M., Atzberger, C., Hill, J., Buddenbaum, H., Werner, W., and Schüler, G. (2010). Retrieval of chlorophyll and nitrogen in Norway spruce (Picea abies L. Karst.) using imaging spectroscopy. *International Journal of Applied Earth Observation and Geoinformation, 12*, 17-26.

Scott, D. (2015). Multivariate density estimation: Theory, practice, and visualization: Second edition. John Wiley & Sons, Ltd. Chichester, England, UK.

Serrano, L., Ustin, S.L., Roberts, D.A., Gamon, J.A., and Peñuelas, J. (2000). Deriving Water Content of Chaparral Vegetation from AVIRIS Data. *Remote Sensing of Environment, 74*, 570-581.

Settles, B. (2009). Active Learning Literature Survey. University of Wisconsin--Madison. .

Sims, D.A. and Gamon, J.A. (2002). Relationships between leaf pigment content and spectral reflectance across a wide range of species, leaf structures and developmental stages. *Remote Sensing of Environment, 81*, 337-354.

Sims, D.A. and Gamon, J.A. (2003). Estimation of vegetation water content and photosynthetic tissue area from spectral reflectance: a comparison of indices based on liquid water and chlorophyll absorption features. *Remote Sensing of Environment, 84*, 526-537.

Stigka, E.K., Paravantis, J.A., and Mihalakakou, G.K. (2014). Social acceptance of renewable energy sources: A review of contingent valuation applications. *Renewable & Sustainable Energy Reviews, 32*, 100-106.

Stimson, H.C., Breshears, D.D., Ustin, S.L., and Kefauver, S.C. (2005). Spectral sensing of foliar water conditions in two co-occurring conifer species: Pinus edulis and Juniperus monosperma. *Remote Sensing of Environment, 96*, 108-118.

Svendsen, D., Morales-Álvarez, P., Ruescas, A.B., Molina, A., and Camps-Valls, G. (2020). Deep Gaussian processes for biogeophysical parameter retrieval and model inversion. *ISPRS Journal of Photogrammetry and Remote Sensing, 166*, 68-81.

Tagliabue, G., Boschetti, M., Bramati, G., Candiani, G., Colombo, R., Nutini, F., Pompilio, L., Rivera-Caicedo, J.P., Rossi, M., Rossini, M., Verrelst, J., and Panigada, C. (2022). Hybrid retrieval of crop traits from multi-temporal PRISMA hyperspectral imagery. *ISPRS Journal of Photogrammetry and Remote Sensing, 187*, 362-377.

Thenkabail, P.S., Mariotto, I., Gumma, M.K., Middleton, E.M., Landis, D.R., and Huemmrich, K.F. (2013). Selection of hyperspectral narrowbands (HNBs) and composition of hyperspectral twoband vegetation indices (HVIs) for biophysical characterization and discrimination of crop types using field reflectance and Hyperion/EO-1 data. *IEEE Journal of Selected Topics in Applied Earth Observations and Remote Sensing, 6*, 427-439.

Thompson, D.R., Gao, B.-C., Green, R.O., Roberts, D.A., Dennison, P.E., and Lundeen, S.R. (2015). Atmospheric correction for global mapping spectroscopy: ATREM advances for the HyspIRI preparatory campaign. *Remote Sensing of Environment, 167*, 64-77.

Transon, J., d'Andrimont, R., Maugnard, A., and Defourny, P. (2018). Survey of Hyperspectral Earth Observation Applications from Space in the Sentinel-2 Context. *Remote Sensing, 10*, 157.

Trombetti, M., Riaño, D., Rubio, M.A., Cheng, Y.B., and Ustin, S.L. (2008). Multi-temporal vegetation canopy water content retrieval and interpretation using artificial neural networks for the continental USA. *Remote Sensing of Environment, 112*, 203-215.

Tucker, C.J. (1980). Remote sensing of leaf water content in the near infrared. *Remote Sensing of Environment, 10*, 23-32.

UN (2022). World Population Prospects 2022: Summary of Results. United Nations Department of Economic and Social Affairs, Population Division. UN DESA/POP/2022/TR/NO. 3. New York, NY, USA.

Upreti, D., Huang, W., Kong, W., Pascucci, S., Pignatti, S., Zhou, X., Ye, H., and Casa, R. (2019). A Comparison of Hybrid Machine Learning Algorithms for the Retrieval of Wheat Biophysical Variables from Sentinel-2. *Remote Sensing, 11*, 481.

Ustin, S.L. and Gamon, J.A. (2010). Remote sensing of plant functional types. *New Phytologist, 186*, 795-816.

Ustin, S.L. and Middleton, E.M. (2021). Current and near-term advances in Earth observation for ecological applications. *Ecological Processes, 10*, 1-57.

Ustin, S.L., Riaño, D., and Hunt, E.R. (2012). Estimating canopy water content from spectroscopy. *Israel Journal of Plant Sciences, 60*, 9-23.

Ustin, S.L., Roberts, D.A., Pinzón, J., Jacquemoud, S., Gardner, M., Scheer, G., Castañeda, C.M., and Palacios-Orueta, A. (1998). Estimating Canopy Water Content of Chaparral Shrubs Using Optical Methods. *Remote Sensing of Environment, 65*, 280-291.

van der Linden, S., Rabe, A., Held, M., Jakimow, B., Leitão, P., Okujeni, A., Schwieder, M., Suess, S., and Hostert, P. (2015). The EnMAP-Box—A Toolbox and Application Programming Interface for EnMAP Data Processing. *Remote Sensing, 7*, 11249.

van Dijk, M., Morley, T., Rau, M.L., and Saghai, Y. (2021). A meta-analysis of projected global food demand and population at risk of hunger for the period 2010–2050. *Nature Food, 2*, 494-501.

Vapnik, V., Golowich, S.E., and Smola, A. (1996). Support vector method for function approximation, regression estimation and signal processing. *Proceedings of the 9th International Conference on Neural Information Processing Systems* pp. 281–287. MIT Press. Denver, Colorado.

Verhoef, W. (1984). Light scattering by leaf layers with application to canopy reflectance modeling: The SAIL model. *Remote Sensing of Environment, 16*, 125-141.

Verhoef, W. and Bach, H. (2007). Coupled soil–leaf-canopy and atmosphere radiative transfer modeling to simulate hyperspectral multi-angular surface reflectance and TOA radiance data. *Remote Sensing of Environment, 109*, 166-182.

Verrelst, J., Alonso, L., Camps-Valls, G., Delegido, J., and Moreno, J. (2011). Retrieval of Vegetation Biophysical Parameters Using Gaussian Process Techniques. *IEEE Transactions on Geoscience and Remote Sensing, 50*, 1832-1843.

Verrelst, J., Berger, K., and Rivera-Caicedo, J.P. (2020). Intelligent sampling for vegetation nitrogen mapping based on hybrid machine learning algorithms. *IEEE Geoscience and Remote Sensing Letters, in press*.

Verrelst, J., Camps-Valls, G., Muñoz-Marí, J., Rivera, J.P., Veroustraete, F., Clevers, J.G.P.W., and Moreno, J. (2015a). Optical remote sensing and the retrieval of terrestrial vegetation bio-geophysical properties – A review. *ISPRS Journal of Photogrammetry and Remote Sensing, 108*, 273-290.

Verrelst, J., Camps-Valls, G., Muñoz-Marí, J., Rivera, J.P., Veroustraete, F., Clevers, J.G.P.W., and Moreno, J. (2015b). Optical remote sensing and the retrieval of terrestrial vegetation bio-geophysical properties A review. *ISPRS Journal of Photogrammetry and Remote Sensing, 108*, 273-290.

Verrelst, J., De Grave, C., Amin, E., Reyes, P., Morata, M., Portales, E., Belda, S., Tagliabue, G., Panigada, C., Boschetti, M., Candiani, G., Segl, K., Guillasso, S., Berger, K., Wocher, M., Hank, T., Rascher, U., and Isola, C. (2021a). Prototyping vegetation traits models in the context of the hyperspectral CHIME mission preparation. *IEEE International Geoscience and Remote Sensing Symposium, IGARSS*. Brussels, Belgium.

Verrelst, J., Dethier, S., Rivera, J.P., Munoz-Mari, J., Camps-Valls, G., and Moreno, J. (2016a). Active Learning Methods for Efficient Hybrid Biophysical Variable Retrieval. *IEEE Geoscience and Remote Sensing Letters, 13*, 1012-1016.

Verrelst, J., Malenovský, Z., Van der Tol, C., Camps-Valls, G., Gastellu-Etchegorry, J.-P., Lewis, P., North, P., and Moreno, J. (2019). Quantifying Vegetation Biophysical Variables from Imaging Spectroscopy Data: A Review on Retrieval Methods. *Surveys in Geophysics, 40*, 589-629.

Verrelst, J., Rivera-Caicedo, J.P., Reyes-Muñoz, P., Morata, M., Amin, E., Tagliabue, G., Panigada, C., Hank, T., and Berger, K. (2021b). Mapping landscape canopy nitrogen content from space using PRISMA data. *ISPRS Journal of Photogrammetry and Remote Sensing, 178*, 382-395.

Verrelst, J., Rivera, J.P., Gitelson, A., Delegido, J., Moreno, J., and Camps-Valls, G. (2016b). Spectral band selection for vegetation properties retrieval using Gaussian processes regression. *International Journal of Applied Earth Observation and Geoinformation, 52*, 554-567.

Verrelst, J., Rivera, J.P., Leonenko, G., Alonso, L., and Moreno, J. (2013a). Optimizing LUT-Based RTM Inversion for Semiautomatic Mapping of Crop Biophysical Parameters from Sentinel-2 and -3 Data: Role of Cost Functions. *IEEE Transactions on Geoscience and Remote Sensing, 52*, 257-269.

Verrelst, J., Rivera, J.P., Moreno, J., and Camps-Valls, G. (2013b). Gaussian processes uncertainty estimates in experimental Sentinel-2 LAI and leaf chlorophyll content retrieval. *ISPRS Journal of Photogrammetry and Remote Sensing, 86*, 157-167.

Verrelst, J., Romijn, E., and Kooistra, L. (2012). Mapping Vegetation Density in a Heterogeneous River Floodplain Ecosystem Using Pointable CHRIS/PROBA Data. *Remote Sensing, 4*, 2866-2889.

Vohland, M. (2008). Using imaging and non-imaging spectroradiometer data for the remote detection of vegetation water content. *Journal of Applied Remote Sensing, 2*, 13.

Vohland, M., Mader, S., and Dorigo, W. (2010). Applying different inversion techniques to retrieve stand variables of summer barley with PROSPECT+SAIL. *International Journal of Applied Earth Observation and Geoinformation, 12*, 71-80.

Vuolo, F., Dini, L., and D'Urso, G. (2008). Retrieval of Leaf Area Index from CHRIS/PROBA data: an analysis of the directional and spectral information content. *International Journal of Remote Sensing, 29*, 5063-5072.

Wang, J., Shen, C., Liu, N., Jin, X., Fan, X., Dong, C., and Xu, Y. (2017a). Non-Destructive Evaluation of the Leaf Nitrogen Concentration by In-Field Visible/Near-Infrared Spectroscopy in Pear Orchards. *Sensors, 17*, 538.

Wang, Z., Skidmore, A.K., Darvishzadeh, R., and Wang, T. (2018). Mapping forest canopy nitrogen content by inversion of coupled leaf-canopy radiative transfer models from airborne hyperspectral imagery. *Agricultural and Forest Meteorology, 253-254*, 247-260.

Wang, Z., Skidmore, A.K., Wang, T., Darvishzadeh, R., Heiden, U., Heurich, M., Latifi, H., and Hearne, J. (2017b). Canopy foliar nitrogen retrieved from airborne hyperspectral imagery by correcting for canopy structure effects. *International Journal of Applied Earth Observation and Geoinformation, 54*, 84-94.

Weiss, M., Baret, F., Myneni, R.B., Pragnère, A., and Knyazikhin, Y. (2000). Investigation of a model inversion technique to estimate canopy biophysical variables from spectral and directional reflectance data. *Agronomie, 20*, 3-22.

Weiss, M., Jacob, F., and Duveiller, G. (2020). Remote sensing for agricultural applications: A meta-review. *Remote Sensing of Environment, 236*, 111402.

Welker, C.M., Balasubramanian, V.K., Petti, C., Rai, K.M., DeBolt, S., and Mendu, V. (2015). Engineering Plant Biomass Lignin Content and Composition for Biofuels and Bioproducts. *Energies, 8*, 7654-7676.

Wocher, M., Berger, K., Danner, M., Mauser, W., and Hank, T. (2018). Physically-Based Retrieval of Canopy Equivalent Water Thickness Using Hyperspectral Data. *Remote Sensing, 10*, 1924.

Wocher, M., Berger, K., Danner, M., Mauser, W., and Hank, T. (2020). RTM-based dynamic absorption integrals for the retrieval of biochemical vegetation traits. *International Journal of Applied Earth Observation and Geoinformation, 93*, 102219.

Wold, S., Esbensen, K., and Geladi, P. (1987). Principal component analysis. *Chemometrics and Intelligent Laboratory Systems, 2*, 37-52.

Yebra, M. and Chuvieco, E. (2009). Linking ecological information and radiative transfer models to estimate fuel moisture content in the Mediterranean region of Spain: Solving the ill-posed inverse problem. *Remote Sensing of Environment, 113*, 2403-2411.

Yi, Q., Wang, F., Bao, A., and Jiapaer, G. (2014). Leaf and canopy water content estimation in cotton using hyperspectral indices and radiative transfer models. *International Journal of Applied Earth Observation and Geoinformation, 33*, 67-75.

Yilmaz, M.T., Hunt, E.R., and Jackson, T.J. (2008). Remote sensing of vegetation water content from equivalent water thickness using satellite imagery. *Remote Sensing of Environment, 112*, 2514-2522.

Yoder, B.J. and Pettigrew-Crosby, R.E. (1995). Predicting nitrogen and chlorophyll content and concentrations from reflectance spectra (400–2500 nm) at leaf and canopy scales. *Remote Sensing of Environment, 53*, 199-211.

Zarco-Tejada, P.J., Rueda, C.A., and Ustin, S.L. (2003). Water content estimation in vegetation with MODIS reflectance data and model inversion methods. *Remote Sensing of Environment, 85*, 109-124.

Zeng, Y., Hao, D., Huete, A., Dechant, B., Berry, J., Chen, J.M., Joiner, J., Frankenberg, C., Bond-Lamberty, B., Ryu, Y., Xiao, J., Asrar, G.R., and Chen, M. (2022). Optical vegetation indices for monitoring terrestrial ecosystems globally. *Nature Reviews Earth & Environment, 3*, 477-493.

Zhang, J. and Zhang, X. (2019). The thermochemical conversion of biomass into biofuels. In Biomass, Biopolymer-Based Materials, and Bioenergy, pp. 327-368. Woodhead Publishing. Buckingham, England, UK.

Zhang, Q., Li, Q., and Zhang, G. (2011). Scattering Impact Analysis and Correction for Leaf Biochemical Parameter Estimation Using Vis-NIR Spectroscopy. *Spectroscopy, 26*, 28.

Zhou, K., Cheng, T., Zhu, Y., Cao, W., Ustin, S.L., Zheng, H., Yao, X., and Tian, Y. (2018). Assessing the Impact of Spatial Resolution on the Estimation of Leaf Nitrogen Concentration Over the Full Season of Paddy Rice Using Near-Surface Imaging Spectroscopy Data. *Frontiers in Plant Science, 9*.

Zou, X., Hernandez Clemente, R., Tammeorg, P., Lizarazo, C., Stoddard, F., Mäkelä, P., Pellikka, P., and Mõttus, M. (2015). Retrieval of leaf chlorophyll content in field crops using narrow-band indices: effects of leaf area index and leaf mean tilt angle. *International Journal of Remote Sensing, 36*, 6031-6055.

Appendix

APPENDIX A: Author's Tools in the EnMAP-Box Agricultural Applications

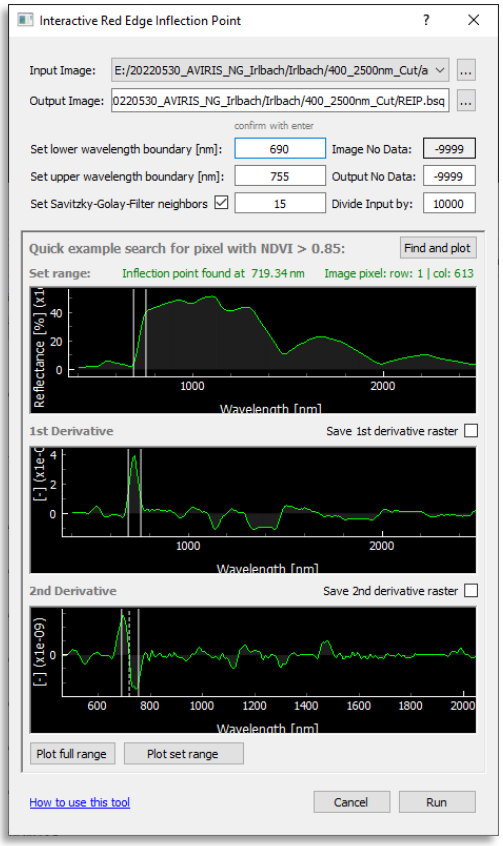

Appendix A.1: The Interactive Red Edge Inflection Point (iREIP) tool. The user can optimize the REIP detection by an example vegetation spectrum from the image before image processing. It also allows the saving of 1st and 2nd spectral derivatives.

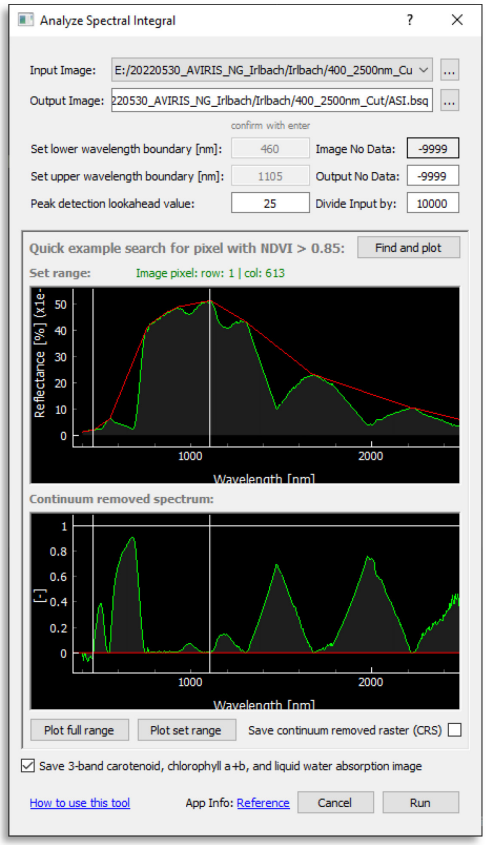

Appendix A.2: The Analyze Spectral Integral (ASI) tool. The user can select wavelength boundaries manually for integral calculation or use "Save 3-band"-mode for automatic separation of C_{ab}, C_{ex}, and C_w absorption ranges.

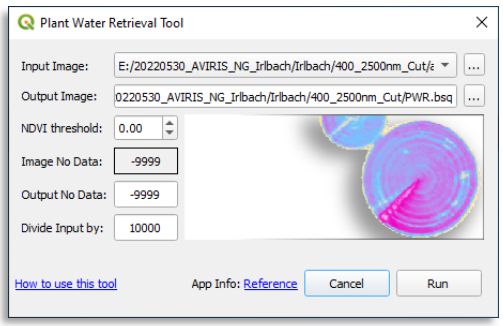

Appendix A.3: The Plant Water Retrieval (PWR) tool. It applies the retrieval method presented in paper I to extract the optically active water layer from the 970 nm water absorption feature.